VERSION 0.6: March 5, 2003

Analysis Note for $\phi \rightarrow K^+K^-$

D. Mukhopadhyay and D. Pal

Weizmann Institute for Sciences

M. Muniruzzaman and R. Seto

University of California at Riverside

C. Maguire
Vanderbilt University

Known Missing Pieces

1) Pair MC acceptance section 4 is not yet complete. Should be completed by March 9–10.

2) Embedded eps figures on single Kaon yields in section 6 are not readable except by Windows machines (??). The same is true for the Appendix section G, which also needs more text description.

3) The ϕ line shape analysis section 8 has not been started, pending completion of the yield sections.

4) The summary section 9 is not yet written. Appendix section D for extra run–by–run efficiency plots is not yet (may not be) developed

5) The EMCal single kaon MC acceptance is not finished; getting adjusted to new code flux.

Contents

List of Figures

List of Tables

1 Introduction

This Analysis Note describes the procedures used to derive the obtain the yield $dN/dy\,dm_t$ for the $\phi \rightarrow K^+K-$ signal in the Run2 PHENIX data for $Au + Au$. The yield analysis has been confined to the East Arm data for which the Drift Chamber active acceptance in Run2 was better and for which we are more certain of the momentum calibration by virtue of having the previous calibration studies based on identified mass measurements using the TOF subsystem. In the East Arm there are three means of studying the $\phi \rightarrow K^+K^-$ signal

a) Using only the TOF PID information for both sign kaons

b) Using the EMCal PID for one kaon and TOF PID for the other kaon

c) Using only the EMCal PID for both kaons. The EMCal is restricted to the to PbSc sectors (E2 and E3) in the East Arm. We have not yet explored the possibility of using the PbGl for kaon particle ID. Since the PbGl is behind to TOF, it would serve to cover that part of the azimuth not seen in TOF.

Because the better time resolution of the TOF subsystem allows one to go to higher kaon particle momentum than for the EMCal subsystem (2 GeV/c compared to 1 GeV/c), the TOF–TOF pairs will extend out to higher pair transverse mass m_T. However, given the narrow aperture of the TOF, the overall acceptance is small and diminishes at low transverse mass. The TOF-TOF pairs account for about 25% of the total signal observed in the East Arm.

The TOF–EMCal pairs account for about half the observed signal. With one kaon in the TOF ranging out to 2 GeV/c and the other in the EMCal going up to 1 GeV/c,the pair m_T limit of the TOF–EMCal pairs is less than that of the TOF-TOF pairs. However, with the broader opening angle, the TOF–EMCal pairs have better acceptance at lower m_T.

It follows that the EMCal–EMCal pairs account for the smallest fraction of the yield, and encompass the least range in pair m_T. However, these pairs will also serve to augment the data yield at lowest m_T where the TOF-TOF acceptance is smallest.

In many of the aspects of the data reduction we have carried out two independent sets of analysis. The real data yield analysis has been done separately by the groups at WIS and at UCR. Interim discrepancies between the two groups were identified and resolved. Similarly the Monte Carlo acceptance analysis for the ϕ were carried out first by the WIS group, and then repeated independently at Vanderbilt with consistent results. We will show some of the comparisons, or simply mention that both sets of analysis agree with one another. Finally, our crosschecking includes an analysis of the inclusive kaon spectra to compare to the work of the Hadron PWG.

2 Data Selection

2.1 Run and Global Event Selection

We are using the CNT nanoDSTs produced for Run2 in pass 3, the standard pass for the Au+Au analyses. Initially we also looked at the special HWG nanoDSTs. The HWG nanoDSTS do not contain the EMCal information, and so are not suitable for the analysis of the complete ϕ signal available in the East Arm. There is a also nanoDST subtlety between the HWG and the CNT nanoDSTs. For a track association to the TOF subsystem the HWG nanoDSTs do not require a PC3 match or an EMCal match. The CNT nanoDSTs do require either a PC3 or an EMCal track match for a track to be stored. This distinction results a few percent greater efficiency for pairs into the TOF-TOF as analyzed with the HWG as compared to the CNT nanoDSTs.

We used a standard set of good run selection criteria: full field, no major Drift Chamber Quality Assurance faults, no large scale PC HV dropouts. More recently we have pared down the run list another 20% by just using the run set selected by the hadron PWG. The use of this common run set facilitated the comparison of the inclusive kaon spectra between our analysis and their analysis. A list of the runs in use is given in Appendix A.

Within the accepted set of runs we required the typical global event trigger requirements:

a) Events satisfied the *IsMinBias* trigger condition of the *PHTrig* class

b) Events were within ± 30 cm Z vertex as determined by the BBC

c) Events had a centrality-by-the clock value between 0 and 93%

The final number of events in our sample was about 20M min bias triggers corresponding to 93% of the minimum bias cross section, the normal number taken for the BBC efficiency.

2.2 Tracking Cuts

Tracking cuts are applied on single tracks first, and then on track pairs.

2.2.1 Single Track cuts

The following single track cuts were imposed

1) Dch/PC1 Tracklets
   a)) Highest Drift Chamber quality only (31 or 63)
   b)) Drift Chamber/PC1 *zed* value ± 75 cm (fiducial cut)
2) Track associations to TOF
   a) Energy loss in TOF greater than 2 MeV

b) Track projection match within 3σ (actually $tofsdphi^2 + tofsdz^2 < 9.0$)

c) Kaon particle ID value *IsKaon* from -2 to $+2$

d) Particle momentum from 0.2 to 2.0 GeV/c [*CFM: Do we really go down to 200 MeV/c ??*]

3) Track associations in EMCal

a) Particle Momentum from 0.3 to 1.0 GeV/c

b) PC3 track match within 3σ (actually $pc3sdphi^2 + pc3sdz^2 < 9.0$) [*CFM: Do we require 3σ on EMCal association too ??*]

c) Renormalized EMCal mass (see Appendix B)

2.2.2 Track Pair Cuts

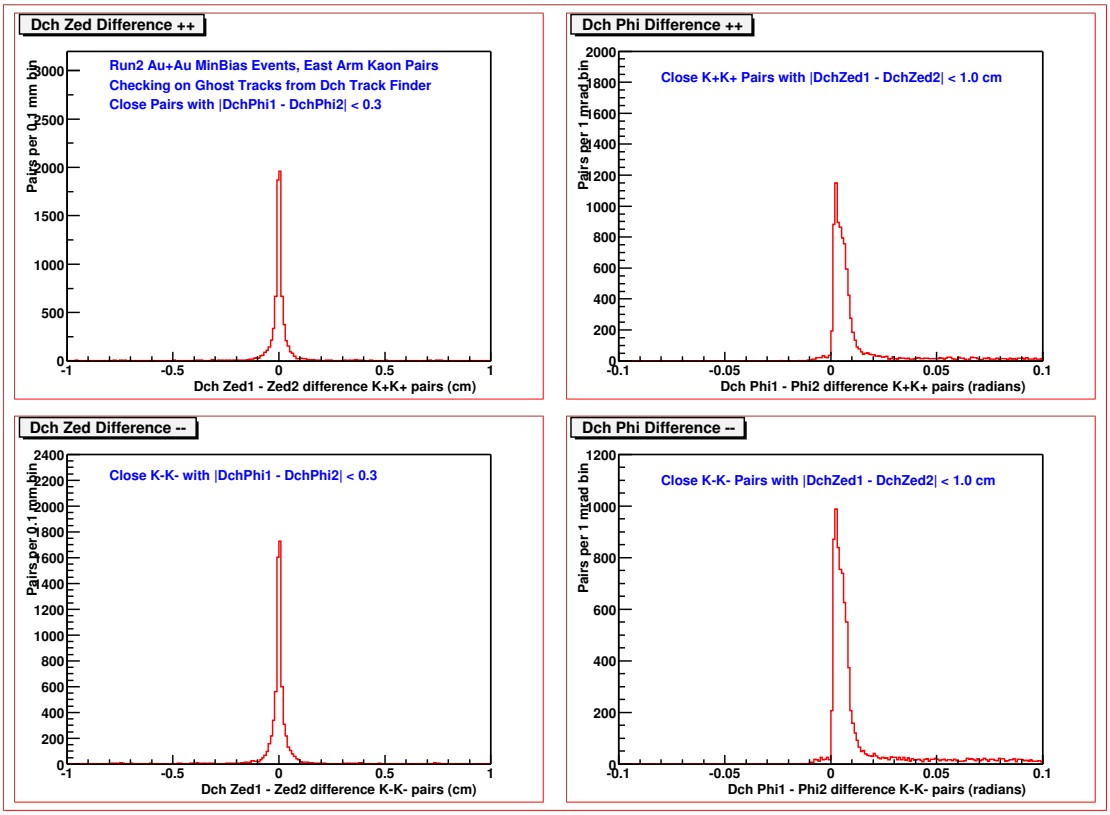

Figure 1: Determination of the Drift Chamber Ghost pair criteria. The separation distances in the *DchZed* and the *DchPhi* track parameters are plotted for same sign tracks in close proximity.

There are two sets of track pair cuts used in this analysis. The first set is for the *Drift Chamber Ghost Tracks*. The "ghosts" are Dch/PC1 tracklets which are believed to share most but not all

the same wire plane hits in the Drift Chamber, and are associated with the same PC1 cluster. As such the ghosts will have the same apparent charge sign, and their exit Dch exit coordinates *DchZed* and *DchPhi* will be very close[1]. The Drift Chamber Ghost criteria used in this analysis are:

a) The *DchZed* values are within 2 mm

b) The *DchPhi* values are within 0.03 radians

If there are two same sign Dch/PC1 tracklets which meet the above two criteria, then a random choice is made to discard one of these and keep the other. The above criteria were suggested to the *phenix-off-l* list on November 9, 2002[2]. The numerical *DchZed* and *DchPhi* limits are derived by looking at their respective spectra as shown in Fig. 1. These variables can also be correlated with each other in a two-dimensional histogram to indicate that these limits are sufficient.

The other set of pair cuts used in this analysis are for the so-called "intruder"' pairs. Intruder pairs are opposite sign tracks initially identified as kaons which are found to cause a spurious mass peak at approximately 1.06 GeV in the TOF-TOF or EMCal-EMCal signals, but never in the TOF-EMCal signals. It has been determined that these false mass peaks arise because of an artifact of the two particle tracks sharing the same time hit, either in EMCal or in TOF. Such a sharing would not be possible with a TOF-EMCal pair. Since tracks sharing the same time hit most probably have a bad time parameter, it has been decided to reject both members of the pair. In the TOF system, tracks sharing the same slat number in a given event are rejected. In the EMCal, because clusters are an amalgam of different tower contributions, there is no single integer detector element index to indicate a shared hit. Rather, if two tracks are found to be in the same sector, and have the same energy and time information, then time sharing is assumed for the two tracks.

The Drift Chamber ghost pair rejection cuts are made **before** the intruder pair cuts are considered. The Drift Chamber ghost pairs have a high probability of having the sharing the same time element, as can be expected for ghost tracks in the Dch/PC1 region being projected to the outer tracking subsystems.

A more detailed explanation of the intruder phenomenon is shown in Appendix C.

2.3 Data Binning

The following centrality bins were used for the different subsystem combinations:

a) TOF–TOF in 0–10%, 10–20%, 20–40%, 40–60%, 60–93%

b) TOF-EMCal in 0–10%, 10–40%, 40–92%

c) EMCal–EMCal in 0–10%, 10–40%, 40–92%

[1] It would also be useful to determine if the Dch/PC1 ghosts projected to the same PC3, TOF, and/or EMCal associations, but the required information for that check is not available on the nanoDSTs.

[2] https://www.phenix.bnl.gov/phenix/WWW/p/lists/phenix-off-l/msg10123.html

The following transverse mass m_T bins were used (GeV/c):

a) TOF–TOF in 1.4 ± 0.2, 1.7 ± 0.1, 1.9 ± 0.1, 2.1 ± 0.1, 2.3 ± 0.1, 2.5 ± 0.1, 2.7 ± 0.1, 2.9 ± 0.1, 3.5 ± 0.4

b) TOF–EMCal in 1.25 ± 0.15, 1.5 ± 0.1, 1.7 ± 0.1, 1.9 ± 0.1, 2.1 ± 0.1, 2.6 ± 0.4

c) EMCal–EMCal in 1.25 ± 0.15, 1.5 ± 0.1, 1.7 ± 0.1, 1.9 ± 0.1, 2.15 ± 0.15

3 Pair Signal Generation

The pair signal was generated in the following manner. All opposite sign tracks passing the cut criteria in a given event for subsystem pair (TOF–TOF, TOF–EMCal, or EMCal–EMCal) were evaluated for their invariant mass. This process results in a true pairs signal riding above a large combinatoric background. Additionaly, the same sign spectra were generated for all same sign pairs in the event In turn, the combinatoric background was calculated according to the method of AN116. Kaons from different events were sorted into discrete Z vertex and centrality bins. Same sign and opposite sign spectra were generated for the mixed events. The normalization R of the opposite sign, mixed event background to the same event opposite sign spectrum was accomplished using the square of the ratio of the product of the like sign pairs.

$$R = \sqrt{\frac{N_{++}^{\text{same}} N_{--}^{\text{same}}}{N_{++}^{\text{mixed}} N_{--}^{\text{mixed}}}}$$

The normalization factor was cross checked by reproducing the like sign yield in the same event event analysis. [Will include these results in tables, ≈ 0.005 precision in the normalization]. In the AN116 normalization procedure, the mixed event kaon particles are stored into sets of centrality and Z–vertex bins in order to approximate the required statistical distributions of the samples. In this analysis, Z–bins of 4 cm and centrality bins in 5% increments were used for the combinatoric normalization.

We show below the opposite sign spectra and same sign spectra for TOF-TOF, East-East and TOF-East combinations for minimum bias data. We also show the table of the predicted N_{++} and N_{--} pairs as compared with the measured N_{++} and N_{--} pairs, as a function of centrality bin.

3.1 TOF-TOF

The integral predicted and measured like and unlike sign spectra for the TOF-TOF combination is given in Table 1.

The minimum bias like and unlike sign spectra and subtracted stectra are shown in Fig (2) through Fig (6).

3.2 EAST-EAST

The integral predicted and measured like and unlike sign spectra for the EAST-EAST combination is given in Table 2.

The minimum bias like and unlike sign spectra and subtracted stectra are shown in Fig (8) through Fig (12).

Table 1: The integral predicted and measured like and unlike sign spectra for the TOF-TOF

cent	N_{+-}^{same}	N_{++}^{same}	N_{--}^{same}	N_{+-}^{mix}	N_{++}^{mix}	N_{--}^{mix}	$\frac{N_{+-}^{\text{same}}}{N_{+-}^{\text{mix}}}$	$\frac{N_{++}^{\text{same}}}{N_{++}^{\text{mix}}}$	$\frac{N_{--}^{\text{same}}}{N_{--}^{\text{mix}}}$	R
0 - 10	130310	73362	56968	129295.0	73304.4	57472.6	1.0079	1.0008	0.9912	0.9920
10 - 20	70311	39483	30642	69565.5	39465.6	30819.6	1.0107	1.0004	0.9942	0.9947
20 - 30	33193	18685	14403	32809.8	18779.8	14499.6	1.0117	0.9950	0.9933	0.9883
30 - 40	14817	8123	6238	14236.8	8122.1	6284.9	1.0408	1.0001	0.9925	0.9927
40 - 50	5513	2979	2306	5242.0	3002.6	2317.3	1.0517	0.9921	0.9951	0.9873
50 - 60	1743	880	715	1586.4	919.5	691.0	1.0987	0.9570	1.0348	0.9903
60 - 70	437	207	193	399.8	229.8	177.2	1.0932	0.9007	1.0893	0.9811
70 - 80	103	33	37	69.9	42.4	33.7	1.4738	0.7779	1.0994	0.8553
80 - 90	36	8	5	12.6	7.5	5.7	2.8	1.0722	0.8753	0.9385
mb	256463	143760	111507	253221	143868	112307	1.0128	0.9992	0.9929	0.9921
0 - 10	130310	73362	56968	129295	73304.4	57472.6	1.0079	1.0008	0.9912	0.9920
10 - 40	118321	66291	51283	116612	66364.6	51605.2	1.0147	0.9989	0.9938	0.9927
40 - 92	7832	4107	3256	7313.7	4202.71	3225.8	1.0709	0.9772	1.0094	0.9864

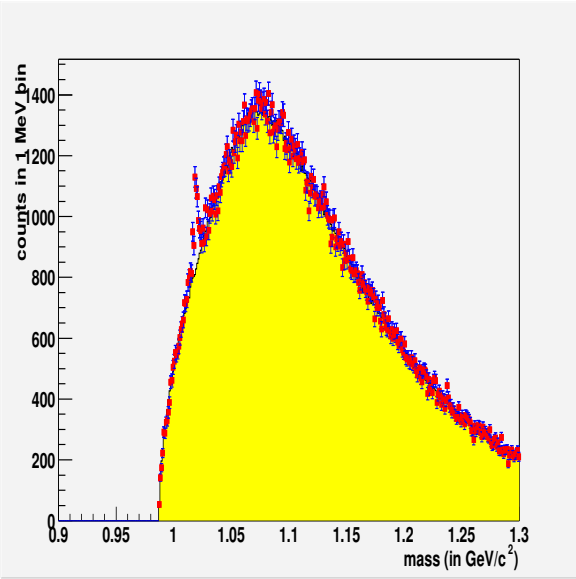

Figure 2: Unlike sign signal and combinatoric mass spectra in TOF-TOF for minimum bias events

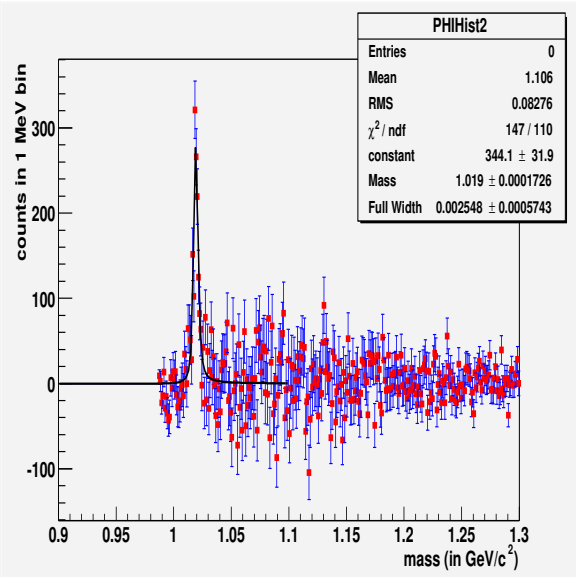

Figure 3: Invariant Mass Spectra in TOF-TOF for minimum bias events

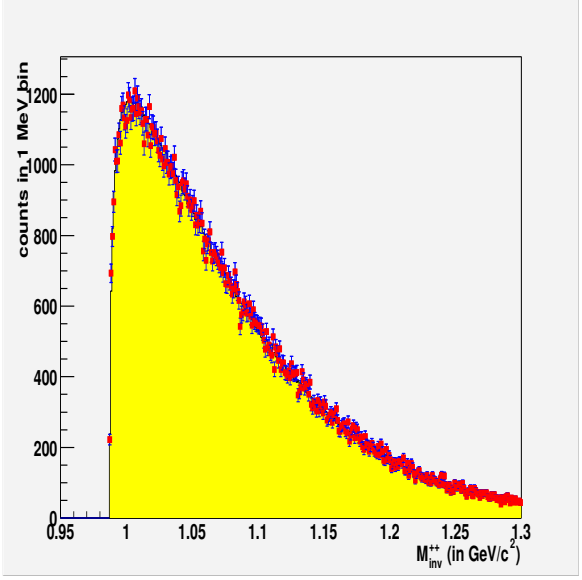

Figure 4: Measured and predicted ++ sign spectra in TOF-TOF for minimum bias events

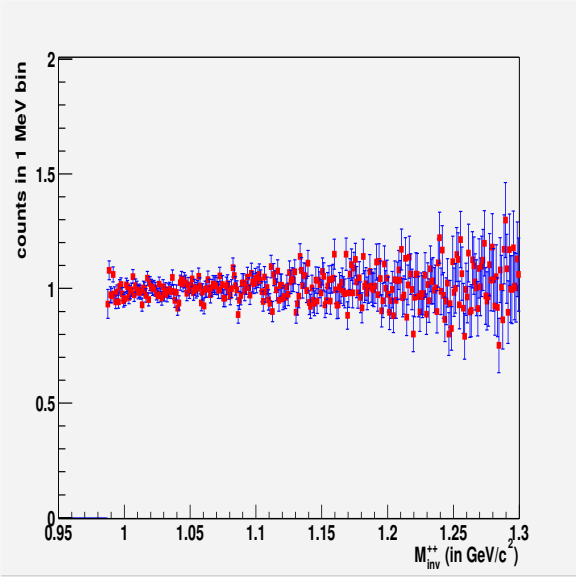

Figure 5: Ratio of measured and predicted ++ sign spectraI in TOF-TOF for minimum bias events

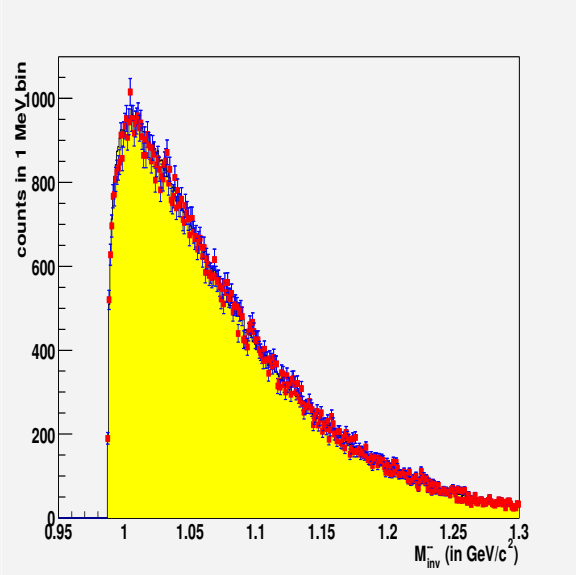

Figure 6: Measured and predicted – sign spectra in TOF-TOF for minimum bias events

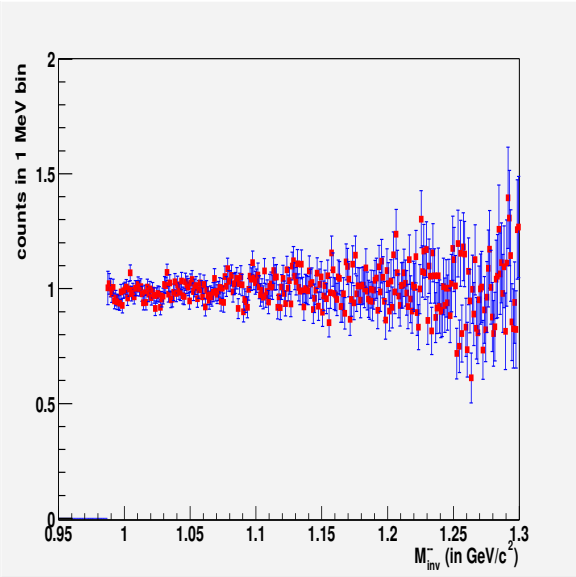

Figure 7: Ratio of measured and predicted – sign spectraI in TOF-TOF for minimum bias events

Table 2: The integral predicted and measured like and unlike sign spectra for the EAST-EAST

cent	N_{+-}^{same}	N_{++}^{same}	N_{--}^{same}	N_{+-}^{mix}	N_{++}^{mix}	N_{--}^{mix}	$\frac{N_{+-}^{\text{same}}}{N_{+-}^{\text{mix}}}$	$\frac{N_{++}^{\text{same}}}{N_{++}^{\text{mix}}}$	$\frac{N_{--}^{\text{same}}}{N_{--}^{\text{mix}}}$	R
0 - 10	111963	43802	70477	111122	43961.7	70296	1.0076	0.9964	1.0026	0.9989
10 - 20	61041	23633	38825	60582.2	23783.5	38649.9	1.0076	0.9937	1.0045	0.9982
20 - 30	30201	11492	18787	29387.1	11593.8	18697.8	1.0277	0.9912	1.0048	0.9959
30 - 40	13370	4963	8467	12964.8	5024.7	8320.5	1.0313	0.9877	1.0176	1.0051
40 - 50	5374	2014	3353	5197.3	2025.8	3358.5	1.0340	0.9942	0.9984	0.9926
50 - 60	1734	603	1088	1620.0	638.7	1028.2	1.0704	0.9441	1.0582	0.9990
60 - 70	475	191	275	458.4	179.5	299.9	1.0363	1.0643	0.9169	0.9758
70 - 80	101	33	52	82.8	33.2	53.0	1.2191	0.9946	0.9812	0.9759
80 - 90	37	10	19	27.6	9.5	18.4	1.3421	1.0577	1.0338	1.0935
mb	224296	86741	141343	221452	87258.8	140719	1.0128	0.9941	1.0044	0.9985
0 - 10	111963	43802	70477	111122	43961.7	70296	1.0076	0.9964	1.0026	0.9989
10 - 40	104612	40088	66079	102936	40402.2	65670.1	1.0163	0.9922	1.0062	0.9984

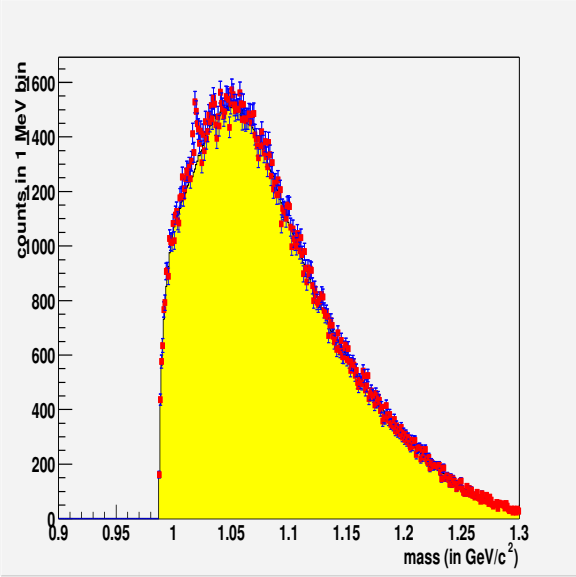

Figure 8: Unlike sign signal and combinatoric mass spectra in EAST-EAST for minimum bias events

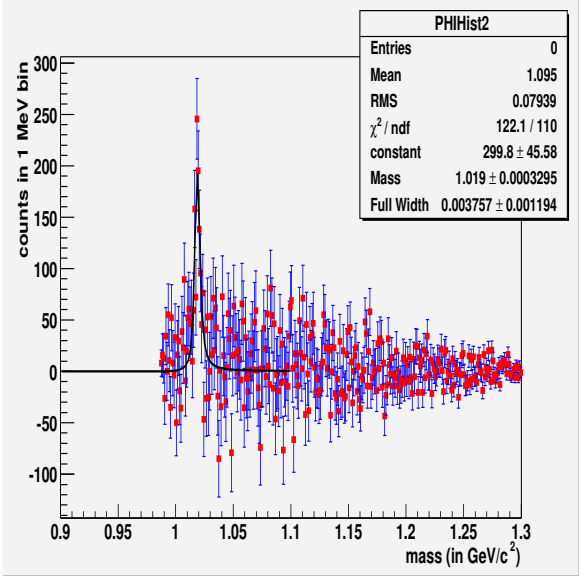

Figure 9: Invariant Mass Spectra in EAST-EAST for minimum bias events

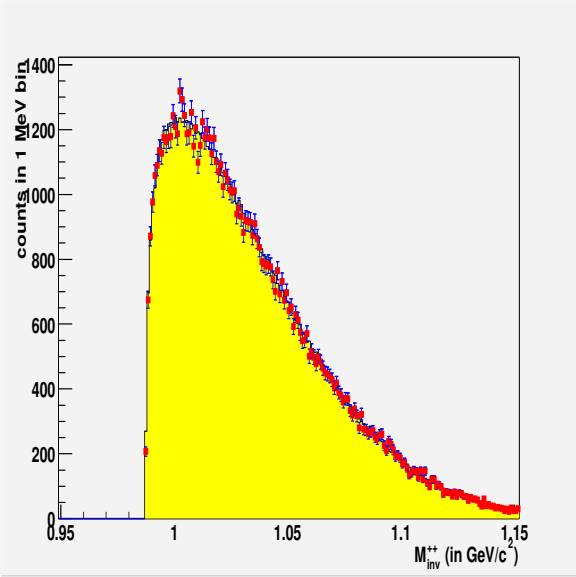

Figure 10: Measured and predicted ++ sign spectra in EAST-EAST for minimum bias events

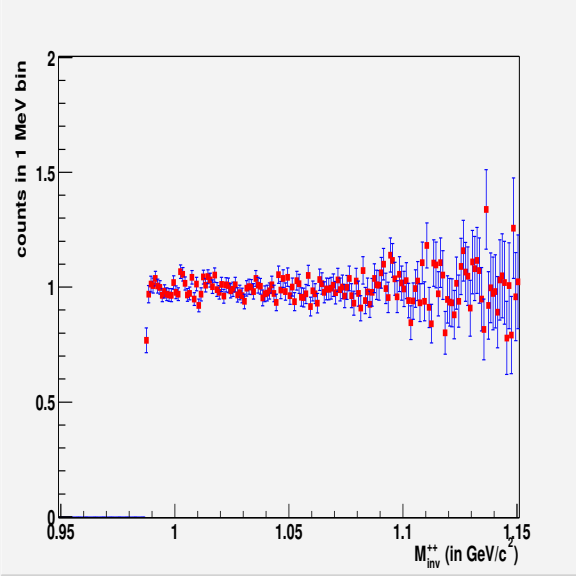

Figure 11: Ratio of measured and predicted ++ sign spectraI in EAST-EAST for minimum bias events

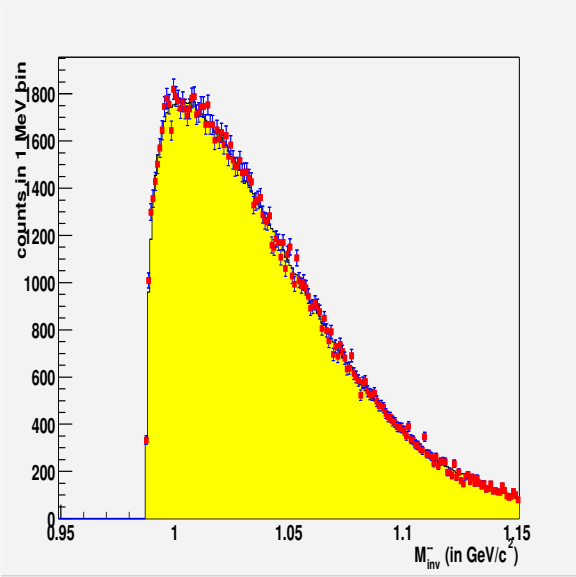

Figure 12: Measured and predicted – sign spectra in EAST-EAST for minimum bias events

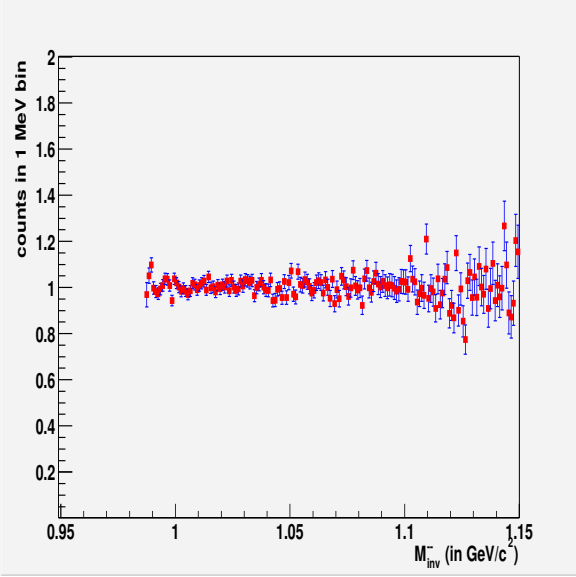

Figure 13: Ratio of measured and predicted – sign spectraI in EAST-EAST for minimum bias events

Table 3: The integral predicted and measured like and unlike sign spectra for the TOF-EAST

cent	$N_{+-}^{\rm same}$	$N_{++}^{\rm same}$	$N_{--}^{\rm same}$	$N_{+-}^{\rm mix}$	$N_{++}^{\rm mix}$	$N_{--}^{\rm mix}$	$\frac{N_{+-}^{\rm same}}{N_{+-}^{\rm mix}}$	$\frac{N_{++}^{\rm same}}{N_{++}^{\rm mix}}$	$\frac{N_{--}^{\rm same}}{N_{--}^{\rm mix}}$	R
0 - 10	245241	117000	127291	244074	117585	128065	1.0048	0.9950	0.9940	0.9890
10 - 20	132590	63024	69386	132257	63481.5	69665.1	1.0025	0.9928	0.9960	0.9888
20 - 30	64365	30127	33128	63183.8	30283.7	33159.9	1.0187	0.9948	0.9990	0.9939
30 - 40	27842	13059	14693	27703.9	13124.5	14679.7	1.0050	0.9950	1.0009	0.9959
40 - 50	10854	4981	5651	10610.9	5048.2	5697.8	1.0229	0.9867	0.9918	0.9786
50 - 60	3483	1481	1800	3265.5	1556.1	1731.8	1.0666	0.9518	1.0394	0.9892
60 - 70	947	398	468	863.2	398.3	464.4	1.0971	0.9991	1.0077	1.0068
70 - 80	213	66	89	153.3	71.4	83.3	1.3896	0.9241	1.0681	0.9870
80 - 90	63	18	24	41.6	18.7	24.5	1.5155	0.9625	0.9796	0.9428
mb	485598	230154	252530	482165	231585	253565	1.0071	0.9938	0.9959	0.9898
0 - 10	245241	117000	127291	244074	117585	128065	1.0048	0.9950	0.9940	0.9890
10 - 40	224797	106210	117207	223146	106893	117505	1.0074	0.9936	0.9975	0.9911
40 - 92	15560	6944	8032	14936.4	7095.2	8002.0	1.0418	0.9787	1.0038	0.9824

3.3 TOF-EAST

The integral predicted and measured like and unlike sign spectra for the TOF-EAST combination is given in Table 3.

The minimum bias like and unlike sign spectra and subtracted stectra are shown in Fig (14) through Fig (18).

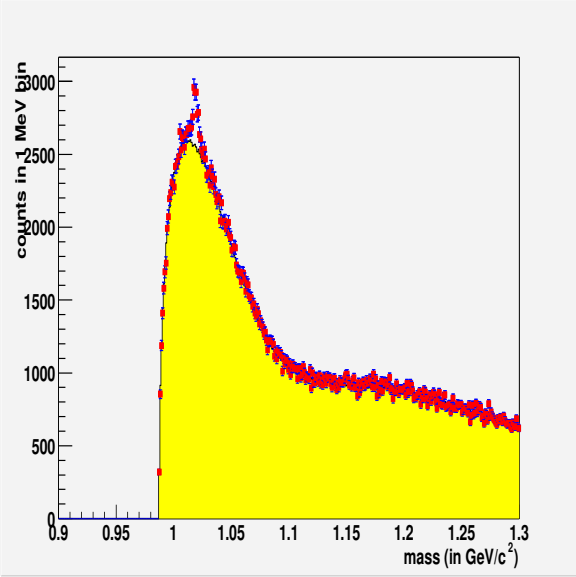

Figure 14: Unlike sign signal and combinatoric mass spectra in TOF-EAST for minimum bias events

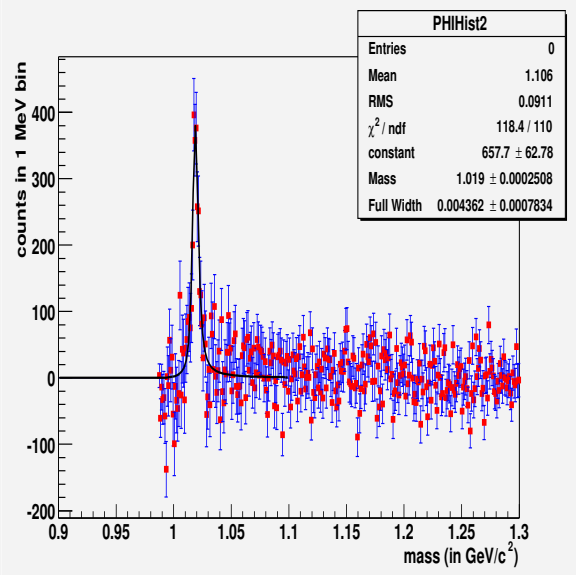

Figure 15: Invariant Mass Spectra in TOF-EAST for minimum bias events

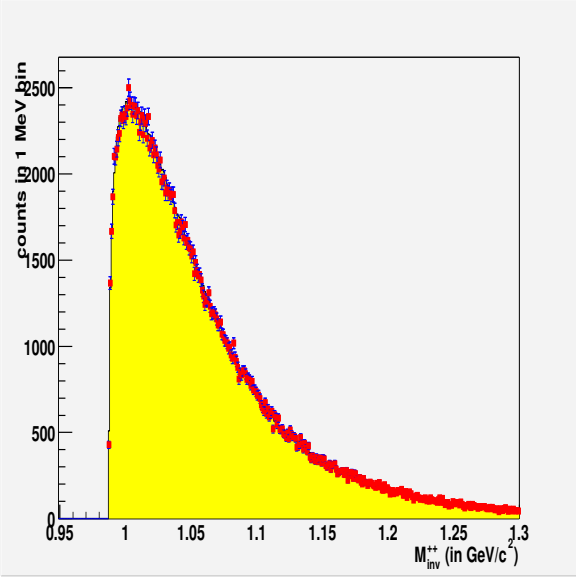

Figure 16: Measured and predicted ++ sign spectra in TOF-EAST for minimum bias events

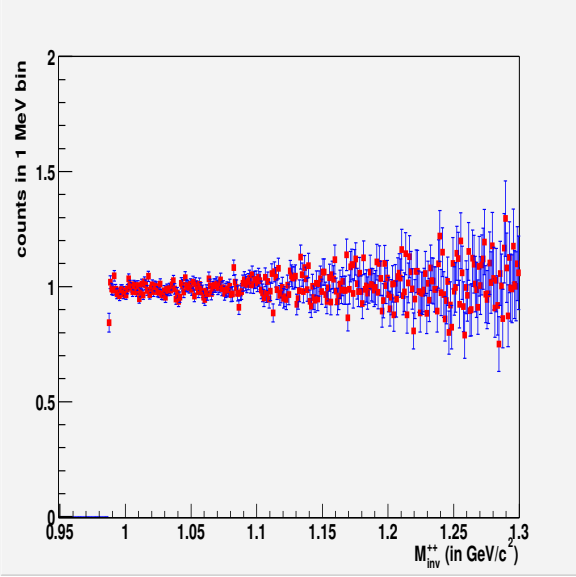

Figure 17: Ratio of measured and predicted ++ sign spectraI in TOF-EAST for minimum bias events

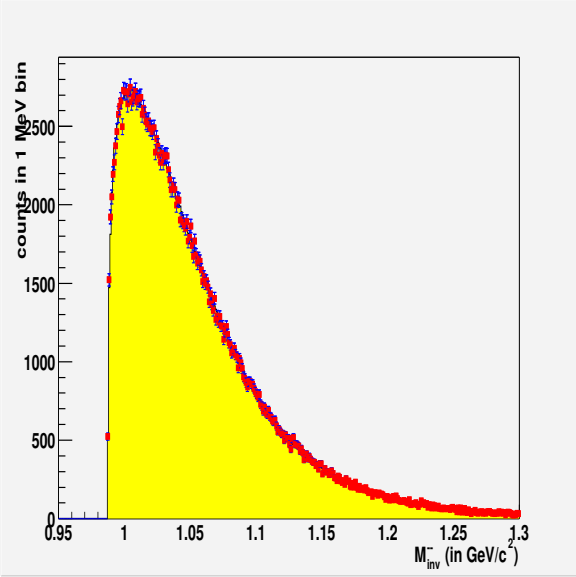

Figure 18: Measured and predicted – sign spectra in TOF-EAST for minimum bias events

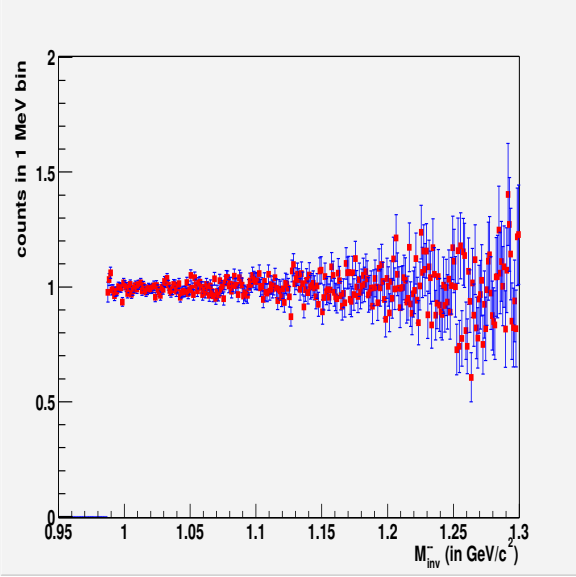

Figure 19: Ratio of measured and predicted – sign spectraI in TOF-EAST for minimum bias events

4 Monte Carlo Acceptance and Embedding Efficiency Calculations

4.1 MC for ϕ Pairs

We have processed single $\phi \rightarrow K^+K^-$ pair Monte Carlo events for 32.3 M for the PHENIX central arm.

We generated the events using the 'EXODUS' event generator taken from $CVSROOT with the following specifications:

a) flat rapidity distribution within $|y| \leq 0.6$ and uniform azimuthal angle, ϕ: 0 - 2π.

b) flat z-vertex distribution within $|z| < 30$ cm.

c) p_T distribution of the ϕ mesons according to:

$dN/dp_T = p_T \exp(\text{-}m_T/(t_{f_o} + \beta^2 m_\phi)$

with $t_{f_o} = 0.157$ GeV and $\beta = 0.4$, i.e, an effective slope of T = 0.320 GeV.

We decayed the ϕ mesons within EXODUS and stored the resulting outputs into ascii OSCAR file.

The invariant mass and m_T distribution of the input ϕ mesons reconstructed through K^+K^- channel is shown in Fig. 20 and Fig. 21 respectively.

The decay kaon pairs were passed through the Run2 version of PISA, and the events reconstructed with the detector response code and pattern recognition software in the PHOOL framework[3]. In order to speed up the event reconstruction process in PHOOL, initial cuts of *dchReqFlag* = 3 (at least 3 Drift Chamber wire plane hits),*pc1ReqFlag = 1* (at least one hit on PC1) and *forcedEMCalAccept* = 1 (at least 1 EMCal hit) were required of the PISA hits data stream before further processing would be done.

The detector response code included the effects of the dead channels in the Drift Chamber, the Pad Chambers, and the TOF.

4.2 Single pair MC results

The loss of $\phi \rightarrow K^+K^-$ pairs at various stages of MC simulation with TOF is shown in Table 4.

By knowing the number of thrown mesons at a given m_t bin, and comparing that to the number of meson reconstructed in that m_t bin, then the acceptance factor for the m_t bin could be derived. This has been done separately for the TOF–TOF, TOF–EMCal, and EMCal–EMCal pairs.

It is important to tabulate the several factors contributing to the loss of acceptance of the ϕ in simulation, in order that those numbers can be independently understood. For the present

[3]The particular library set used is described at https://www.phenix.bnl.gov/WWW/run02/DPM/qm02_MCsingle.

The simulated DST was generated with a Z-vertex smearing of 7 mm, and a Time-zero smearing of 40 ps to approximate the BBC performance. The before–smearing Z was taken from the PISA event header data structure.

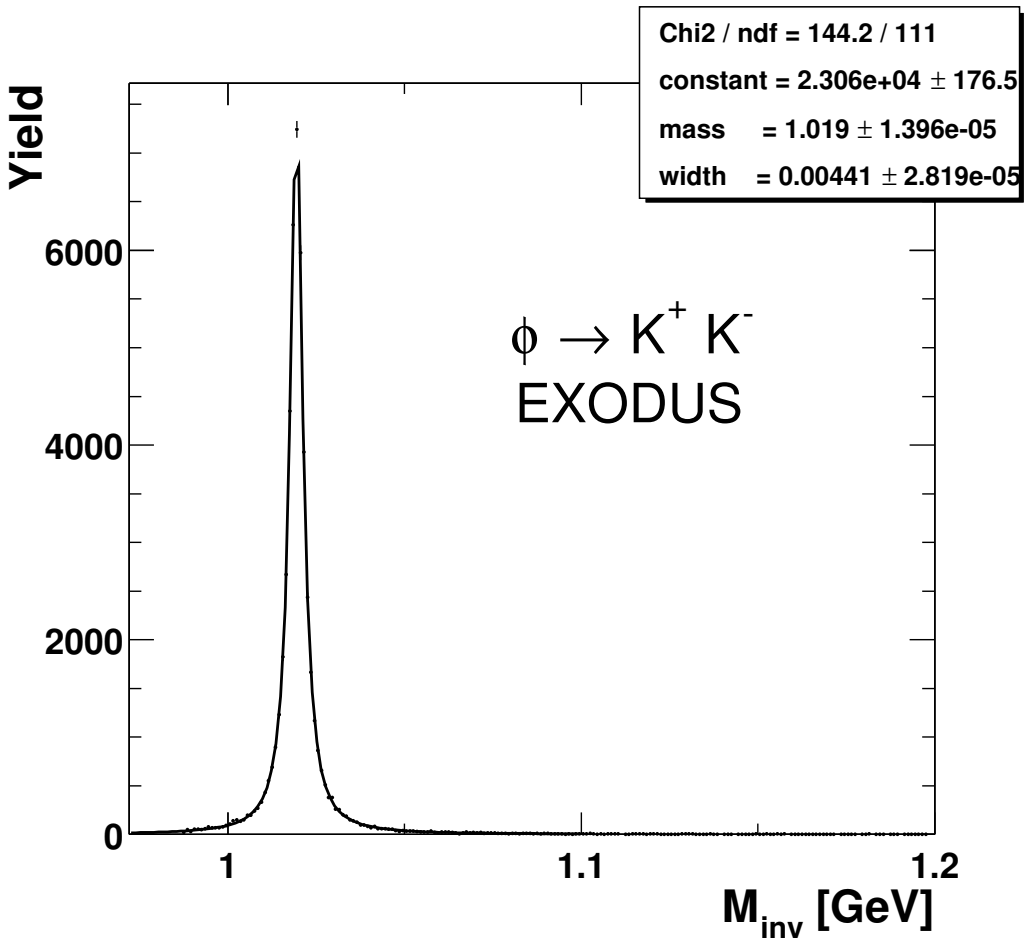

Figure 20: Invariant mass spectra of K^+K^- pairs from ϕ generated by EXODUS

simulation the acceptance losses for MC pairs is shown in Table 4.

4.3 Embedding Corrections

The centrality (occupancy) dependence of $\phi \rightarrow K^+K^-$ pair reconstruction was done by embedding single pairs into the real data. The single embedding efficiency has two parts, the efficiency of track reconstruction and the PID efficiency. The present embedding software (*offline/packages/embed*) considers the both.

We estimate the embedding efficiency factors for centrality bins 0 - 92% in step of 10% such that the effective yield from the raw data is

$$N_{\phi}^{eff} = \frac{\Sigma N_{\phi}^{raw}}{\epsilon_{K^+K^-}} \tag{1}$$

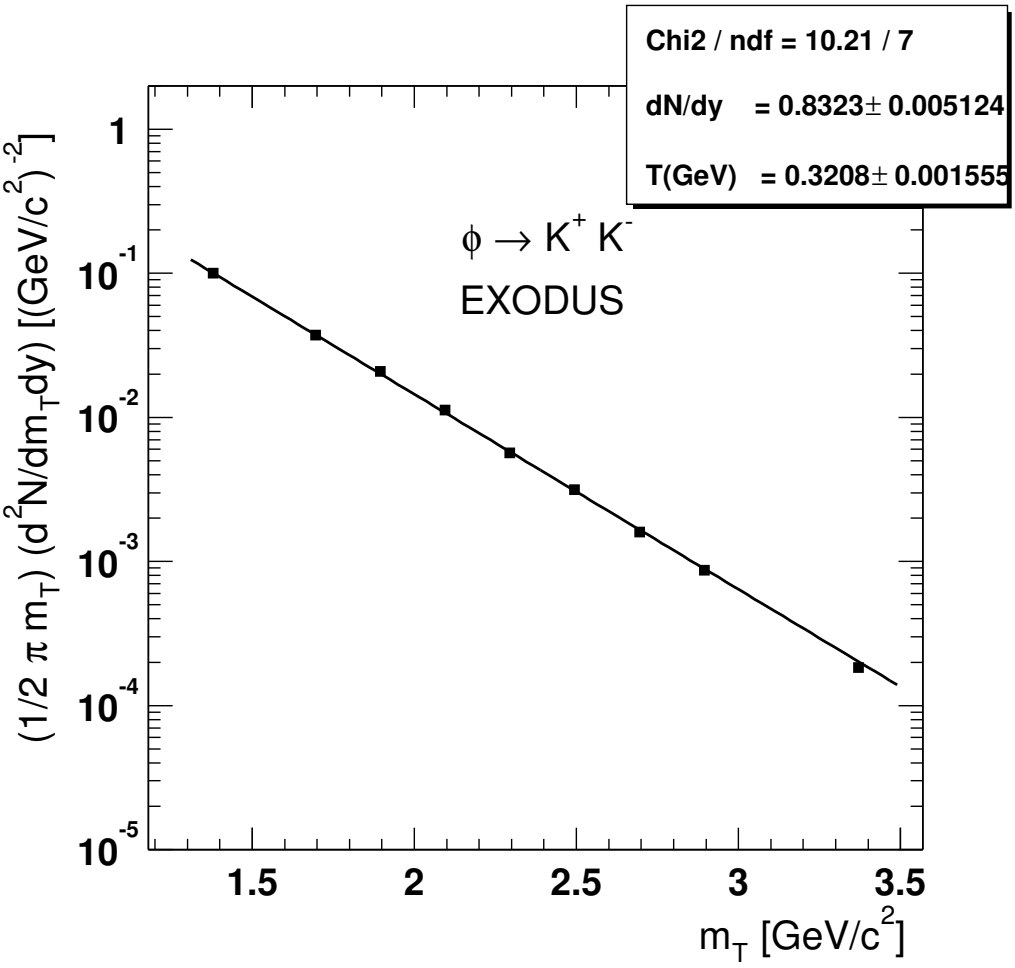

Figure 21: m_T spectra of $\phi \to K^+K^-$ pairs mesons generated by EXODUS

The results for single kaon and $\phi \to K^+K^-$ pairs at the TOF wall are presented in the Table 5.
The embedding results for PbSc (east) are shown in Table 6.
The embedding results for PbSc (east)(K^-) - TOF (K^+) are shown in Table 7.

4.4 Comparison of MC with data

4.5 Tuning of MC with data

Table 4: MC Acceptance Losses for the ϕ

Cut Condition	Number Surviving	Survival Fraction
Events with single TOF hit in PISA	9864	–
Events reconstructed on DST	6044	0.613
Events found on nanoDST	5666	0.937
3σ track match + 2σ PID cut	5186	0.915
Drift Chamber Quality cut 31 or 63	4580	0.883
Drift Chamber *DchZed* cut $\pm$75 cm	4537	0.991
Particle Momentum window 0.3 to 2.00 GeV/c	4321	0.952
$\pm$5 MeV mass cut	3172	0.73

Table 5: Embedding efficiencies for single kaons and kaon pairs from the ϕ mesons at TOF

Centrality (%)	$\epsilon^{emb}_{K^+}$	$\epsilon^{emb}_{K^-}$	$\epsilon^{emb}_{K^+} \times \epsilon^{emb}_{K^-}$	$\epsilon_{K^+K^-}$
0 - 92 (MB)	0.9379 ± 0.0016	0.9393 ± 0.0016	0.8810 ± 0.0022	0.9037 ± 0.008
0 - 10	0.8424 ± 0.003	0.8465 ± 0.003	0.7131 ± 0.0037	0.7549 ± 0.015
10 - 20	0.9015 ± 0.004	0.9014 ± 0.004	0.8126 ± 0.0056	0.8541 ± 0.022
20 - 30	0.9387 ± 0.005	0.9401 ± 0.005	0.8825 ± 0.007	0.8869 ± 0.028
30 - 40	0.9633 ± 0.006	0.9603 ± 0.006	0.9250 ± 0.008	0.9246 ± 0.032
40 - 50	0.9787 ± 0.005	0.9789 ± 0.005	0.9580 ± 0.007	0.9753 ± 0.026
50 - 60	0.9859 ± 0.005	0.9878 ± 0.005	0.9739 ± 0.007	0.9742 ± 0.025
60 - 70	0.9936 ± 0.005	0.9942 ± 0.006	0.9878 ± 0.008	0.9850 ± 0.029
70 - 80	0.9978 ± 0.006	0.9985 ± 0.006	0.9963 ± 0.009	1.000 ± 0.033
80 - 92	0.9976 ± 0.006	0.9989 ± 0.006	0.9965 ± 0.009	0.9955 ± 0.033

Table 6: Embedding efficiencies for single kaons and kaon pairs from the ϕ mesons at PbSc (east)

Centrality (%)	$\epsilon^{emb}_{K^+}$	$\epsilon^{emb}_{K^-}$	$\epsilon^{emb}_{K^+} \times \epsilon^{emb}_{K^-}$	$\epsilon_{K^+K^-}$
0 - 92 (MB)	0.9239 ± 0.004	0.9312 ± 0.004	0.8603 ± 0.005	0.8619 ± 0.018
0 - 10	0.8067 ± 0.007	0.8205 ± 0.007	0.6619 ± 0.008	0.6590 ± 0.030
10 - 20	0.8817 ± 0.010	0.8945 ± 0.010	0.7887 ± 0.012	0.8022 ± 0.055
20 - 30	0.9214 ± 0.013	0.9303 ± 0.013	0.8572 ± 0.017	0.8497 ± 0.061
30 - 40	0.9423 ± 0.013	0.9558 ± 0.015	0.9007 ± 0.019	0.8616 ± 0.068
40 - 50	0.9717 ± 0.011	0.9765 ± 0.012	0.9569 ± 0.016	0.9231 ± 0.057
50 - 60	0.9825 ± 0.011	0.9855 ± 0.011	0.9683 ± 0.015	0.9667 ± 0.059
60 - 70	0.9914 ± 0.013	0.9948 ± 0.014	0.9863 ± 0.019	0.9804 ± 0.068
70 - 80	0.9964 ± 0.015	0.9934 ± 0.015	0.9898 ± 0.021	0.9825 ± 0.075
80 - 92	0.9998 ± 0.014	0.9962 ± 0.015	0.9960 ± 0.021	1.0000 ± 0.07551

Table 7: Embedding efficiencies for single kaons and kaon pairs from the ϕ mesons with TOF (K^+) - East (K^-) combination.

Centrality (%)	$\epsilon^{emb}_{K^+}$	$\epsilon^{emb}_{K^-}$	$\epsilon^{emb}_{K^+} \times \epsilon^{emb}_{K^-}$	$\epsilon_{K^+K^-}$
MB (0 - 92)	0.9306 ± 0.004	0.9227 ± 0.004	0.8620 ± 0.005	0.8746 ± 0.018
0 - 10	0.8471 ± 0.008	0.8143 ± 0.007	0.6898 ± 0.009	0.7116 ± 0.029
10 - 20	0.8956 ± 0.012	0.8794 ± 0.011	0.7876 ± 0.014	0.8252 ± 0.047
20 - 30	0.9393 ± 0.015	0.9259 ± 0.014	0.8698 ± 0.019	0.8725 ± 0.061
30 - 40	0.9567 ± 0.017	0.9557 ± 0.016	0.9143 ± 0.022	0.9103 ± 0.073
40 - 50	0.9728 ± 0.013	0.9677 ± 0.012	0.9414 ± 0.017	0.9422 ± 0.057
50 - 60	0.9805 ± 0.013	0.9794 ± 0.012	0.9603 ± 0.017	0.9628 ± 0.056
60 - 70	0.9879 ± 0.016	0.9958 ± 0.015	0.9838 ± 0.022	0.9695 ± 0.069
70 - 80	0.9911 ± 0.018	0.9951 ± 0.017	0.9862 ± 0.025	1.0000 ± 0.080
80 - 92	0.9906 ± 0.017	0.9945 ± 0.016	0.9851 ± 0.023	0.9834 ± 0.070

5 Run-by-run Efficiency Corrections

The entire analysis is done for DC + PC1 + TOF/ PbSc (EAST) tracks using the CNT nDST files. Also, the production of CNT requires each track to have a 5σ match with PC3 or EMCal. The run-by-run dead area variations of these subsystems influences the ϕ yields. The dead areas in the subsystems may have different effects on the positive and negative kaons with different momenta. This initiates us to calculate the run-by-run efficiency for K^+K^- pairs for different subsystem combinations, like, TOF-TOF, TOF - East, East - East and all east. This is measured over all selected runs.

5.1 Method

The outline of the run-by-run efficiency calculation is described below.

The run "31464" was found to be a "good" run from the point of view of drift chamber dead area compared to the other runs. So, the effieciency of this run was taken as 1 and the efficiencies for the other runs are calculated with respect to it.

We calculated the numbers $A_{K^+} = N_{K^+}/$ event and $A_{K^-} = N_{K^-}/$ event for each run for different centrality and momentum bins.

Using the above numbers, we calculated the K_+ and K^- efficiencies of each run with respect to the run 31464 as:

$$\epsilon_{K^+} = \frac{A_{K^+}^{31464}}{A_{K^+}} \tag{2}$$

$$\epsilon_{K^-} = \frac{A_{K^-}^{31464}}{A_{K^-}} \tag{3}$$

Finally, we computed an average of $\epsilon_{K^{+/-}}$ weighted over the number of events (in each run) as:

$$< \epsilon_{K^+} >= \frac{\Sigma \epsilon_{K^+}^{run} \times N_{event}^{run}}{\Sigma N_{event}^{i}} \tag{4}$$

$$< \epsilon_{K^-} >= \frac{\Sigma \epsilon_{K^-}^{run} \times N_{event}^{run}}{\Sigma N_{event}^{i}} \tag{5}$$

The summation was carried out over all runs.

We call it as the average run-by-run efficiency for the single kaons. The pair efficiency is calculated by simply taking the product of the single efficiencies as:

$$< \epsilon_{K^+K^-} >=< \epsilon_{K^+} > \times < \epsilon_{K^-} > \tag{6}$$

5.2 Results for TOF

The run-by-run efficiency for positive and negative kaons as a function of the number of participant (centrality) are shown in the Fig. 22. The minimum bias efficiencies are also indicated by dotted lines. In either case, we did not observe any centrality dependence of run-by-run kaon efficiency.

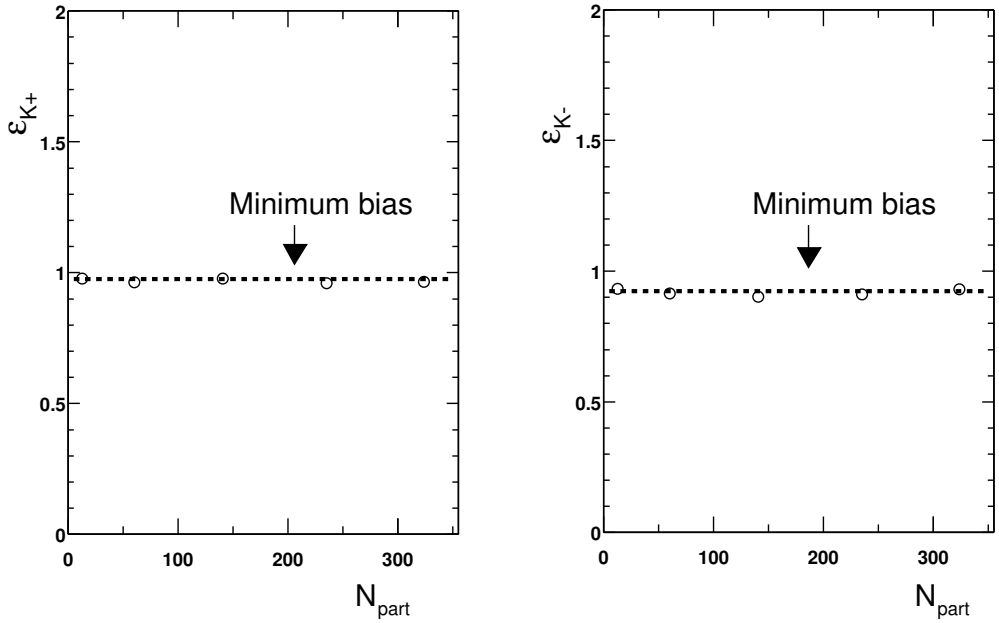

Figure 22: Run-by-run efficiency for K^+ (left) and K^- (right) as a function of the number of participants (centrality). The dotted line in each plot indicates the minimum bias efficiency

The above study is done for the kaons integrated over all momentum bins.

In order to investigate the momentum dependence of run-by-run variation, we plotted run-by-run efficiency as a function of the kaon momenta in Fig. 23. The figure shows that the run-by-run efficiency of the kaons are constant within $\pm$ 3%.

Since there is no centrality and/or momentum dependence, we use the minimum bias run-by-run efficiencies for K^+ and K^- which are $0.976255 \pm 8.12052e-05$ and $0.924427 \pm 7.38575e-05$ respectively. Accordingly, the run-by-run pair efficiency is the product of the singles, i.e., $0.9024 \pm 1.097e-04$.

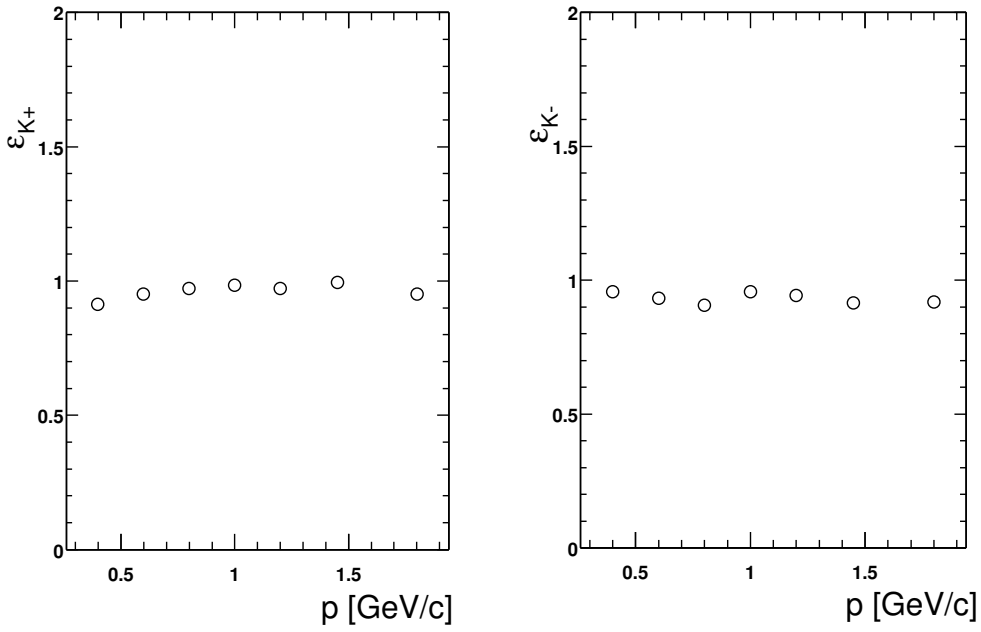

Figure 23: Run-by-run efficiency for K^+ (left) and K^- (right) as a function of the kaon momenta.

5.3 Results for PbSc east

5.4 Results for TOF-PbSc east

5.5 Results for all east

6 Single Kaon Analysis

Before presenting the results of the $\phi \rightarrow K^+K-$ analysis we show first the results of an inclusive kaon analysis. The inclusive kaon analysis is based on exactly the same single track and pair track cuts described previously in the Tracking Cuts subsection 2.2 for the pairs analysis. The $\frac{1}{2\pi\, m_T}\frac{d^2N}{dm_T\, dy}$ for this inclusive kaon yield will be compared with that obtained independently by the Hadron PWG in its separate analysis. The Hadron PWG uses much tighter particle cuts with about a factor of 1.6–2.0 less acceptance than we can afford for the pairs analysis. A comparison of the PPG016 MC correction factors and those of the Hadron PWG are shown in Appendix E. In the comparison it is seen that for the K^+ yield, the PPG016 acceptance factor is approximately a factor of 2.0 larger than is the Hadron PWG acceptance factor, independent of momentum. Similarly, the PPG016 acceptance factor is approximately a factor of 1.7 larger. The different ratios as a function of charge sign is likely due to the different fiducial cuts made in the two acceptance calculations for the relatively narrow aperture TOF subsystem.

Table 8: Comparison of Inclusive Kaon dN/dy and T Extracted by Two Different PHENIX Analyses

Centrality	K^+				K^-			
%	dN/dy[a]	dN/dy[b]	T[a]	T[b]	dN/dy[a]	dN/dy[b]	T[a]	T[b]
0–5	46.36	46.58	0.286	0.292	43.43	43.58	0.289	0.300
5–10	37.96	37.67	0.287	0.294	35.87	35.00	0.289	0.302
10–15	32.01	31.62	0.283	0.293	29.55	29.54	0.287	0.300
15–20	26.53	26.49	0.283	0.293	24.40	24.42	0.285	0.297
20–30	19.51	19.05	0.282	0.291	18.09	17.66	0.285	0.296
30–40	12.55	12.19	0.279	0.287	11.69	11.37	0.277	0.291
40–50	7.59	7.42	0.269	0.281	7.00	6.89	0.271	0.285
50–60	4.21	4.06	0.260	0.272	3.91	3.74	0.260	0.278
60–70	2.06	1.97	0.250	0.267	1.90	1.84	0.251	0.270
70–90	0.83	0.79	0.236	0.260	0.81	0.75	0.237	0.261
80–93	0.43	0.28	0.227	0.255	0.41	0.27	0.226	0.251

[a] PPG016 analysis
[b] Hadron PWG analysis

When these two sets of acceptance factors are used in the extractions of the yields for the inclusive kaons, one obtains the results shown in Figs. 24, 25, 26 and 27. A comparison of the extracted $dN/dy\, dm_T$ and inverse slopes is given in Table 8.

As one can see there os agreement in all bins of centrality except the most peripheral bin. The inverse slopes found by our ppg are about 10-40 MeV larger. These differences are probably to be expected because we believe our looser cuts will allow in more background. This is being studied by using tigther cuts.

The agreement of our kaons spectra with that of the Hadron PWG gives us confidence that we are doing the following things correctly

a) acceptance of kaons (including pid/tracking etc)

b) single track embedding corrections. We note that the ghost pair and intruder pair rejectios are being taken into consideration here. (IS THIS CORRECT?)

c) run-by-run corrections

d) general run numerics of finding the correct number of triggers etc, and application of the relevant factors (e.g. $1/2\pi$) in the invariant yields.

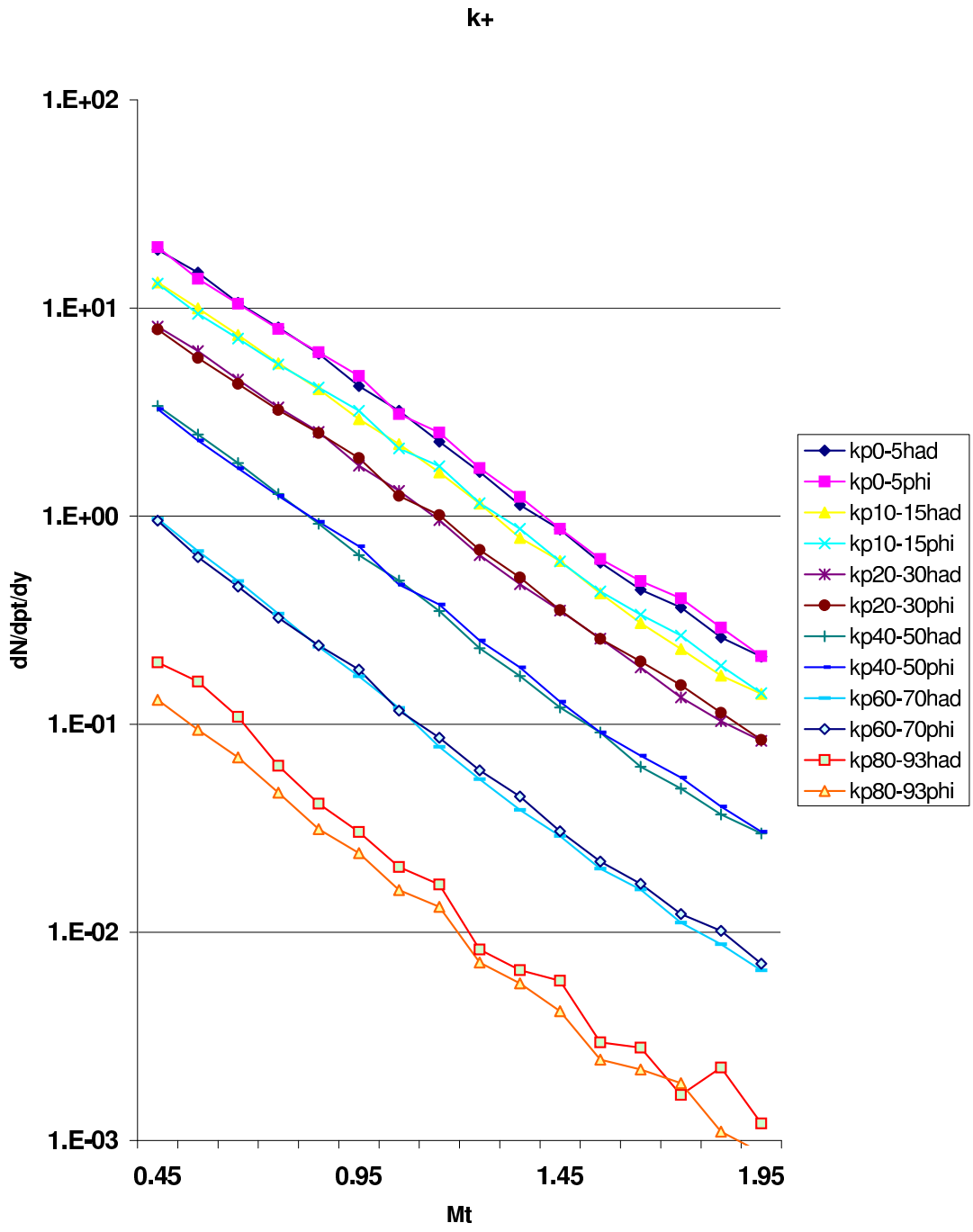

Figure 24: Comparison of the yields for K^+ as a function of centrality and transverse momentum, as determined by the PPG016 and the Hadron PWG. Odd bins in centrality. Points labeled as "had" come from the Hadron PWG. Points labeled "phi" are from this analysis.

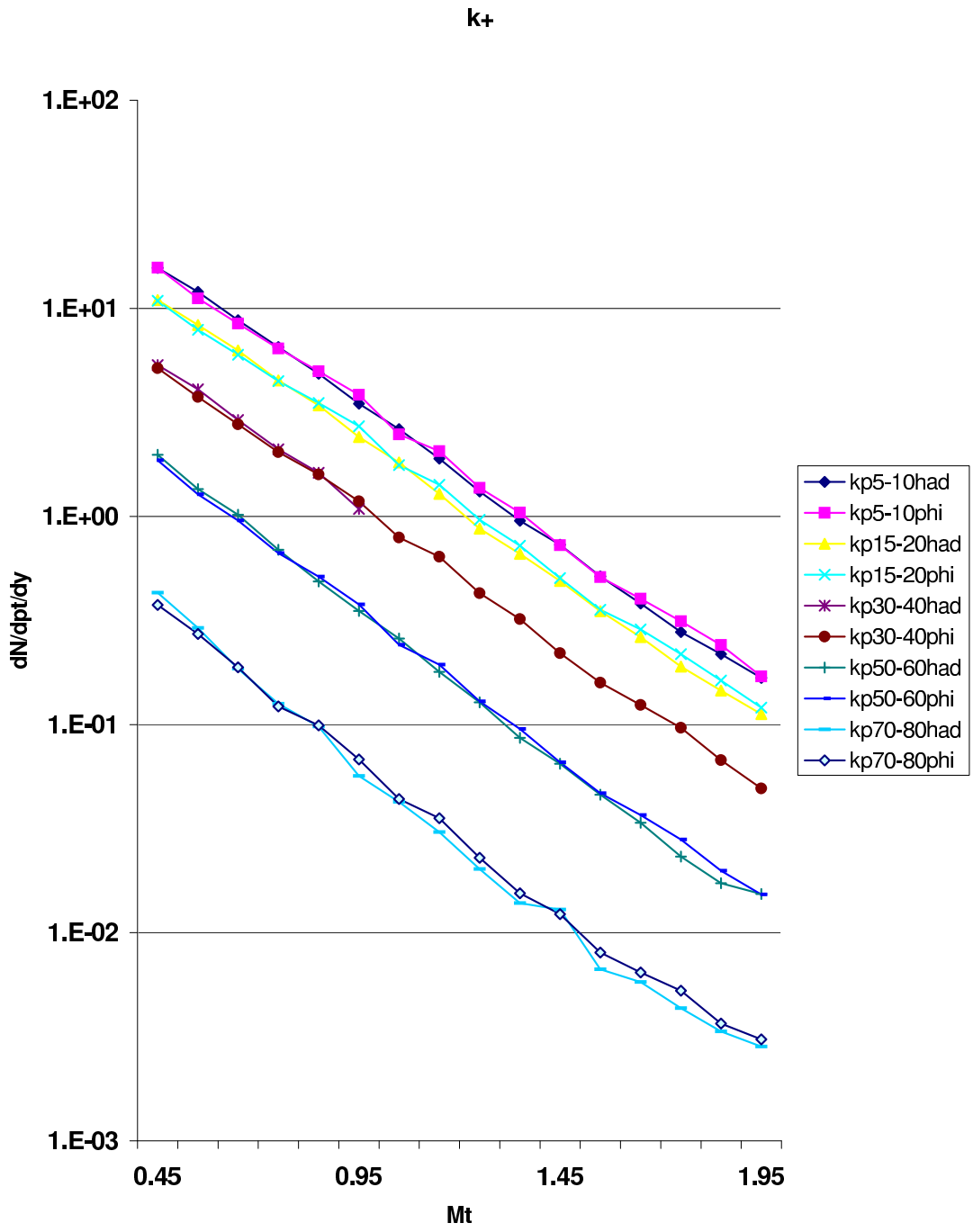

Figure 25: Same as Fig. 24 for even bins in centralality.

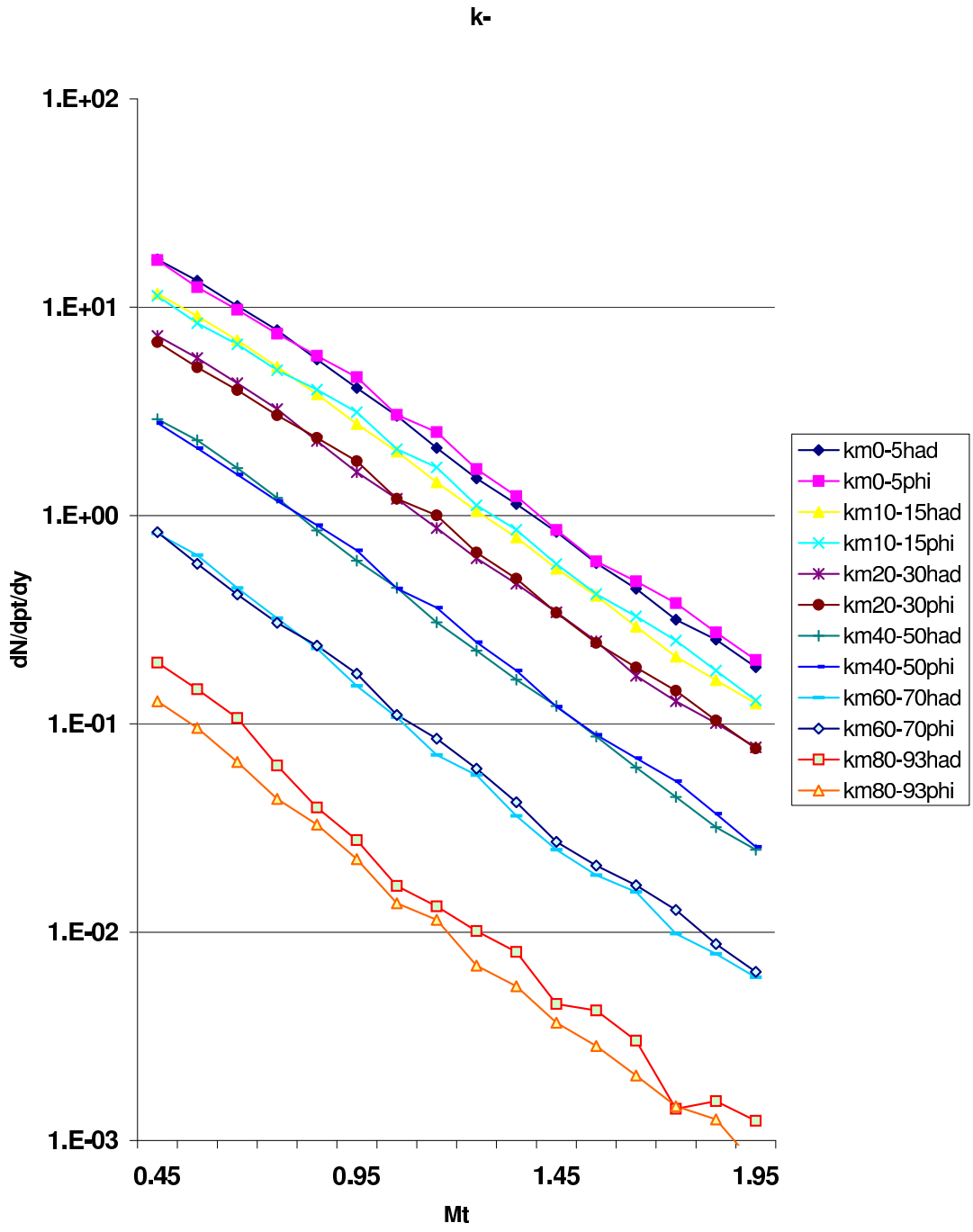

Figure 26: Comparison of the yields for K^- as a function of centrality and transverse momentum, as determined by the PPG016 and the Hadron PWG. Odd bins in centrality. Points labeled as "had" come from the Hadron PWG. Points labeled "phi" are from this analysis.

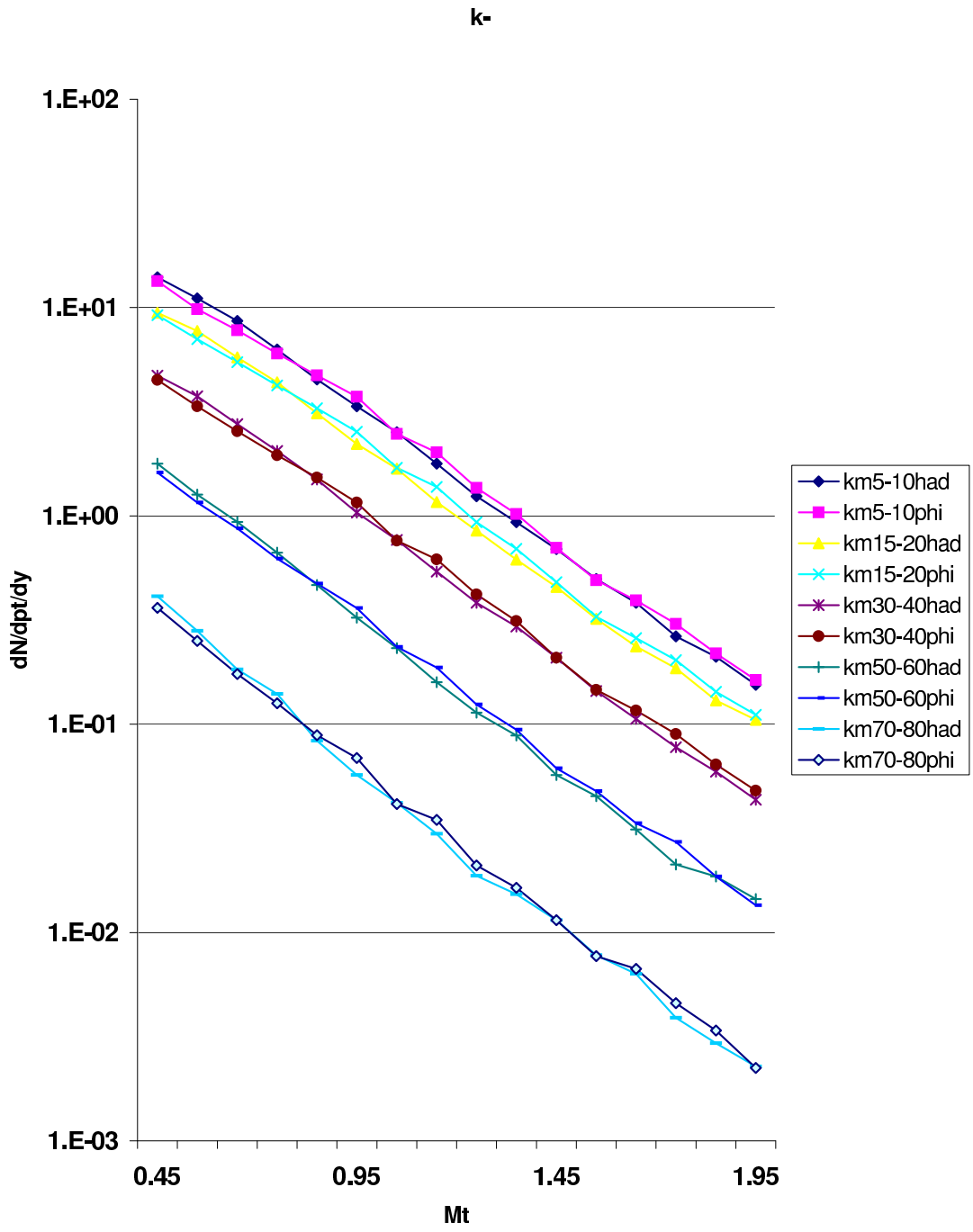

Figure 27: Same as Fig. 26 for even bins in centralality.

7 Analysis of the ϕ Yields

One of the two very important studies we aim to perform is the ϕ transverse mass distribution and extraction of ϕ yield and inverse slope parameters, the other being the mass centroid and width of ϕ. In both of these studies, we look for the centrality dependence of the the yield and inverse slope parameters in this section.

For the transverse mass distribution, we use the centralities and the m_T bins specified earlier. Examples of ϕ signals and combinatoric backgrounds can be found in Appendices H and I. While a fit was done using a relativistic Breit-Wigner convoluted with a Gaussian, however yields were obtained using counts over background in the range [1.014,1.024]

$$S = \mathrm{T} - \mathrm{B}, \tag{7}$$

where T is the number of counts from the real pairs, which contains signal and background, and B is the number of counts from the background pairs, normalized to $2\sqrt{N_{++}^{Real}.N_{--}^{Real}}$, in a given m_T window. The number of signals and backgrounds, together with the Monte-Carlo ϕ's are shown in Tables 19-21 in Appendix J.

The assignment of the error bars on the corrected yield are of importance. The errors are calculated in the following ways by the UCR and WIS groups.

7.1 UCR Approach

The error of the yield is estimated as $\sqrt{S+B}$, where S is the ϕ signal and B is the background. The reason behind this estimation of error is as follows. If we think of S as signal and B as background and T as the total then

$$T = S + B \tag{8}$$
$$S = T - B \tag{9}$$

Now we did the naive thing

$$\Delta S = \Delta T(+)\Delta B \tag{10}$$

where the (+) mean adding in quadrature *i.e.*

$$\Delta S = \sqrt{\Delta T^2 + \Delta B^2} = \sqrt{S + 2B} \tag{11}$$

Now we should really distinguish between the background under the signal and the background which we subtract. So let us write

$$T = S + B \tag{12}$$
$$S = T - B' \tag{13}$$

What is the error on B? Well it is the number of events under the ϕ peak in the particular measurement we have made so it goes like $\sqrt{B}$. What is the error in B' ? This is not a

measurement in the same sense. It comes from a mixed background (which for this argument can be of infinite statistics). We will assume we know the normalization exactly. We then know B' exactly - *i.e.* there is no error on it. We can prove this with the following thought experiment. B' the calculated error. We can then run an experiment in which we have no ϕ's and run in a million times to measure B'. We can then get B' to any accuracy we wish. Then the error becomes $\sqrt{S+B}$.

7.2 WIS Approach

For the errors

$$\delta(S) = \sqrt{(\delta T^2 + \delta B^2)}, \tag{14}$$

where

$$\delta B = 2\sqrt{(N_{++}^{Real}.N_{--}^{Real})}/N_{mix}^{total} = C * D \tag{15}$$

$$\delta(B)/B = \sqrt{([\delta(C)/C]^2 + [\delta(D)/D]^2)}. \tag{16}$$

where δB is computed by standard propagation of error technique.
The ϕ yield is calculated as in the Eq.(17).

$$\frac{1}{2\pi m_T}\frac{d^2N}{dm_T dy} = \frac{1}{2\pi m_T}\frac{N_\phi}{N_{evt}}\mathrm{CF}\frac{1}{\epsilon_{\mathrm{embed}}}\frac{1}{\mathrm{BR}}\frac{1}{\Delta \mathrm{m_T}}.\mathrm{Corrections} \tag{17}$$

where,

$$\begin{aligned} \mathrm{CF} &= \frac{MC_{thrown}}{MC_{accepted}} \\ \mathrm{Corrections} &= \epsilon_{run-by-run}.MC_{tune}.\Gamma_{tune} \\ MC_{tune} &= 1.03 \\ \Gamma_{tune} &= 1.06 \end{aligned}$$

MC_{thrown} and $MC_{accepted}$ are the number of Monte-Carlo particle thrown in each m_T bin and the number accepted in that bin. ϵ_{embed} is the embedding efficiency. $\epsilon_{run-by-run}$ is the run by run correction . BR is branching ratio of ϕ decaying into K^+K^- channel and is given by 0.49. Δm_T is the spread of the m_T bin. $\mathrm{MC_{tune}}$ is the correction between the various cuts made in the MC vs the data. Γ_{tune} is correction for the mass window originating from the Monte Carlo. The Monte Carlo is done for non-relativistic Breit-Wigner, but the real data follows relativistic Breit-Wigner. So a correction has to be made to account for this effect. The correction also depends on the mass window for signal extraction. We give these correction for different mass windows in Table 9.

7.3 Yield and Spectra

With the yield and the error of the yield calculated, we can plot the transverse mass distribution of ϕ. In Appendices H and Iwe show the m_T distributions for the most central $(0\% - 10\%)$, mid-central $(10\% - 40\%)$, peripheral $(40\% - 92\%)$. The error bars are statistical only. While plotting

Mass Window (GeV/c^2)	Yield fraction in Breit-Wigner	Yield fraction in Rel Breit-Wigner	Γ_{tune}
1.014 - 1.024	0.726	0.690	1.06
1.009 - 1.029	0.862	0.821	1.05
1.004 - 1.034	0.908	0.869	1.04

Table 9: Correction for Breit-Wigner to Relativistic Breit-Wigner of the Monte Carlo for Different Mass Windows

the m_T distribution, we took the effects of binning into account. The Reference[1] describes in details the effect of the bin size on the falling spectra. The center of the bin is shifted by the amount given in Eq.(18).

$$\overline{x}_0 = -\frac{b\Delta^2}{24} \tag{18}$$

where Δ is the full-width of the bin. The parameter b comes from the exponential $f(x) = A\exp(-bx)$.

The m_T spectra were fitted with an exponential function given in Eq.(19).

$$\frac{1}{2\pi m_T}\frac{d^2N}{dm_T dy} = \frac{dN/dy}{2\pi T(m_\phi + T)}\mathrm{e}^{-(m_T - m_\phi)/T} \tag{19}$$

While fitting, the parameter m_ϕ was kept fixed and the inverse slope parameter T and the the yield dN/dy were set free.

To find the shift $\overline{x}_0$, we need the parameter b. From Eq.(19) we see that $b = 1/T$. So we first fit the m_T distribution with no shift in the bin center. The fits gives us the value of T. We use this value in Eq.(18) to find the approximate shift. We then re-plot taking the bin shift into account and fit to get the value if T. The do a second iteration to calculate $\overline{x}_0$ using the latest value of T. We then re-plot and refit. We make this iteration over many times until the temperature shows no change.

Table 10: dN/dy and Temperatures for $\phi \to K^+K^-$ TOF–TOF Pairs Extracted in Two Analyses

Centrality %	UCR Analysis		WIS Analysis	
	dN/dy	T (MeV)	dN/dy	T (MeV)
0–10	2.4 ± 1.2	452 ± 78	2.3 ± 0.8	471 ± 66
10–40	1.78 ± 0.37	411 ± 29	1.61 ± 0.26	429 ± 26
40–92	0.23 ± 0.06	408 ± 40	0.23 ± 0.05	419 ± 32
min bias	0.92 ± 0.17	422 ± 26	0.93 ± 0.13	438 ± 23

The yields for the $\phi \to K^+K^-$ as a function of m_T and centrality class were analyzed first for the TOF–TOF pairs by both the UCR and the WIS groups. Their mass spectra, after combinatoric

background subtraction are shown completely in Appendix Sections H and I. The yields were fitted with the dN/dy and inverse slope ("Temperature") as two free parameters. A comparison of the extracted results between UCR and WIS for the TOF-TOF pairs is shown in Table 10. One can see that the two sets of analyses produce results which are in good agreement with each other in each of the centrality classes.

Table 11: dN/dy and T for $\phi \to K^+K^-$ in TOF-TOF, TOF-EMC, and EMC-EMC from UCR

Centrality	TOF–TOF		TOF–EMCal		EMCal–EMCal	
%	dN/dy	T (MeV)	dN/dy	T (MeV)	dN/dy	T (MeV)
0–10	2.4 ± 1.2	452 ± 78	3.7 ± 1.2	490 ± 200	3.5 ± 1.6	458 ± 354
10–40	1.78 ± 0.37	411 ± 29	1.9 ± 0.4	475 ± 110	2.2 ± 0.6	390 ± 136
40–92	0.23 ± 0.06	408 ± 40	0.35 ± 0.07	380 ± 68	0.36 ± 0.16	310 ± 121
minbias	0.92 ± 0.17	422 ± 26	1.12 ± 0.17	459 ± 78	1.17 ± 0.23	433 ± 130

Table 12: UCR average dN/dy and T for ϕ in TOF–TOF, TOF–EMC, EMC–EMC

Centrality	Weighted Average	
%	dN/dy	T (MeV)
0–10	3.15 ± 0.75	457 ± 71
10–40	1.90 ± 0.25	414 ± 27
40–92	0.29 ± 0.04	394 ± 33
min bias	1.05 ± 0.11	426 ± 24

The UCR group has also analyzed the yields for the case of one or both kaons being present in the EMCal subsystem. These result for dN/dy and T are shown in Table 11, with the weighted average values shown in Table 12. At present we do not have good embedding correction factors for the EMCal, so we are choosing the same embedding factors as for the TOF. In Table 11 one can see that the Temperature parameter is best determined for the TOF–TOF pairs, while it is only poorly determined for the EMCal–EMCal pairs. On the other hand, the yield parameter is better determined with the EMCal subsystem pairs, at least by measure of the ratio of the fit error to the extracted dN/dy value. The dN/dy values for the EMCal pairs are $\approx 50\%$ higher than for the TOF only pairs, although the fit uncertainties allow the results to overlap.

The weighted average values in Table 12 are valid if there are no systematic error changes between the different subsystem pairs.

References

[1] M.J.Tannenbaum, PHENIX Analysis Note AN062 (2001).

8 Analysis of the ϕ Centroid and Width

9 Summary

A List of Data Runs Used by PPG016

All of the analysis to be shown here is based on the so-called after-burned CNT nanoDSTs generated in mid-June 2002, and residing on the /phenix/data26 to /phenix/data29 disks. These include only the Au+Au runs at the present time. The complete Au+Au run list was pared down according to the following choices

1. Zero field, photon converter, and reverse field runs were eliminated, where the list of those runs is contained on the Run2 DPM WWW site.

2. Runs with problematic Drift Chamber or Drift Chamber plus Pad Chamber tracking performance have been listed at a WWW site put up by the Stony Brook Group. These runs were ignored.

3. The Pad Chamber group has examined every file segment of every Run, and come up with a "do not use at all" and a "discouraged use" list of Runs based on PC HV outages. We not to use the "discouraged use" files from the PC QA studies.

4. We examine our Run lists against Run lists used by other analyses in case we still are including some Runs which we should not for some reason. We especially compare with the HWG file lists for high-p_T analysis.

After applying all of the above conditions, we end up with 180 Runs, which we call the **Golden Runs**. There are 4775 file segments in the selected runs that we use for our analysis. The complete list of runs and files are given in Table 14. The number of events from the selected runs are given in Table 13.

Centrality	N_{evt}
0-10	2200687
10-20	2212313
20-30	2179573
30-40	2179038
40-50	2206354
50-60	2185476
60-70	2197392
70-80	2162280
80-92	2485953
Total	20009063

Table 13: Number of events in the data sample used by PPG016

Table 14: Number of file segments in runs used by PPG016

Run	Number of Segments
28163	44
28170	29
28199	16
28209	22
28212	7
28284	35
28286	23
28302	23
28447	26
28450	28
28485	41
28488	8
28490	5
28570	35
28573	13
28577	35
29116	4
29122	14
29146	22
29171	28
29178	25
29179	11
29183	54
29184	36
29185	25
29186	22
29515	18
29529	20
29531	51
29534	11
29536	63
29537	48
29561	16
29562	10
29563	40
29566	10
29987	58
30000	42
30001	42
30003	18
30007	69
30009	34

Run	Number of Segments
30019	8
30062	9
30069	12
30074	26
30087	5
30088	36
30143	6
30146	6
30148	46
30149	36
30158	25
30159	32
30193	40
30195	28
30196	44
30197	6
30329	6
30388	13
30631	8
30633	69
30642	34
30650	42
30807	30
30812	5
30813	8
30814	22
30816	56
30820	6
30911	49
30913	53
30916	67
30917	21
30920	42
31009	21
31013	32
31014	27
31021	34
31024	9
31025	32
31058	45
31060	17
31072	55
31075	25
31079	38

Run	Number of Segments
31140	6
31143	10
31145	18
31230	39
31232	31
31233	6
31239	36
31240	28
31243	41
31244	49
31249	17
31252	47
31254	22
31256	31
31460	8
31464	48
31500	9
31503	25
31520	22
31631	10
31637	8
31639	41
31814	38
31815	9
31824	22
31836	11
31837	25
31868	49
31870	36
32523	43
32524	25
32525	42
32526	47
32548	37
32549	17
32913	5
32914	7
32929	21
32934	23
32948	56
32949	44
33049	5
33050	25
33051	13
33055	5

Run	Number of Segments
33056	14
33064	6
33067	30
33068	6
33082	16
33083	14
33085	5
33098	15
33119	33
33123	31
33124	15
33149	25
33150	33
33161	25
33166	22
33168	17
33169	9
33299	30
33303	72
33309	40
33314	25
33321	6
33323	18
33327	6
33336	52
33337	26
33345	40
33392	6
33393	5
33460	10
33463	20
33468	13
33526	8
33535	25
33541	40
33542	62
33547	27
33550	21
33557	35
33577	14
33610	9
33611	16
33612	32
33693	20

B EMCal Mass Renormalization

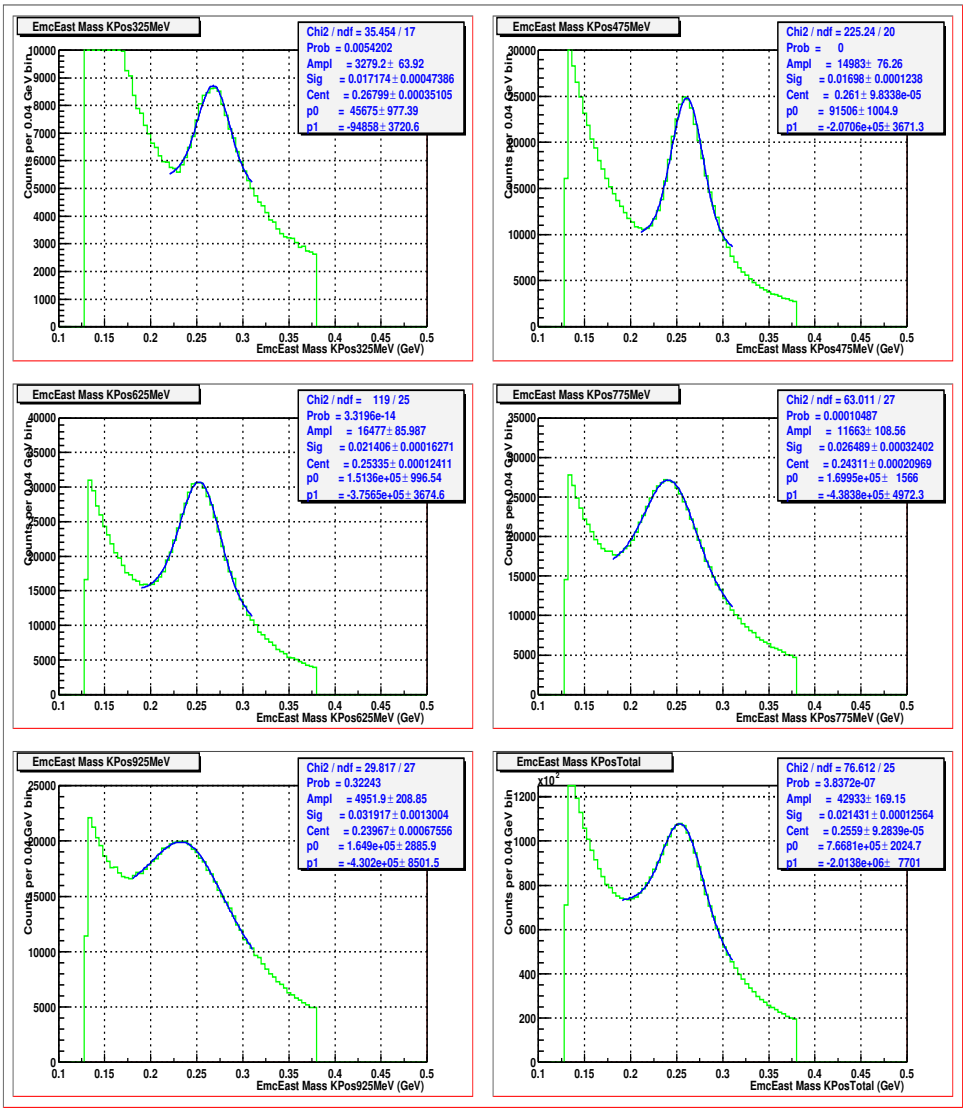

Figure 28: Partial mass-squared spectrum for positive particles deduced from the PHENIX East EMCal subsystem, before momentum–dependent corrections. The spectra are in bins of particle momentum from 325 to 1075 MeV, with bin widths of ±75 MeV. There are Gaussian peaks fitted on top of a linear + quadratic background in each case.

The CNT nanoDSTs contain the information about the EMCal clusters which are associated to a reconstructed track. These data include the time–of–flight to the cluster and the calculated path length to the cluster. Using these two pieces of EMCal information together with the momentum reconstruction value for the track enables one to derive the mass of the particle. According to Gabor David of the EMCal hardware group, the sectors E2 and E3 should have

approximately 400 ps time resolution for hadrons. Hence, one may expect to obtain useful K/π mass resolution up until about 1 GeV/c.

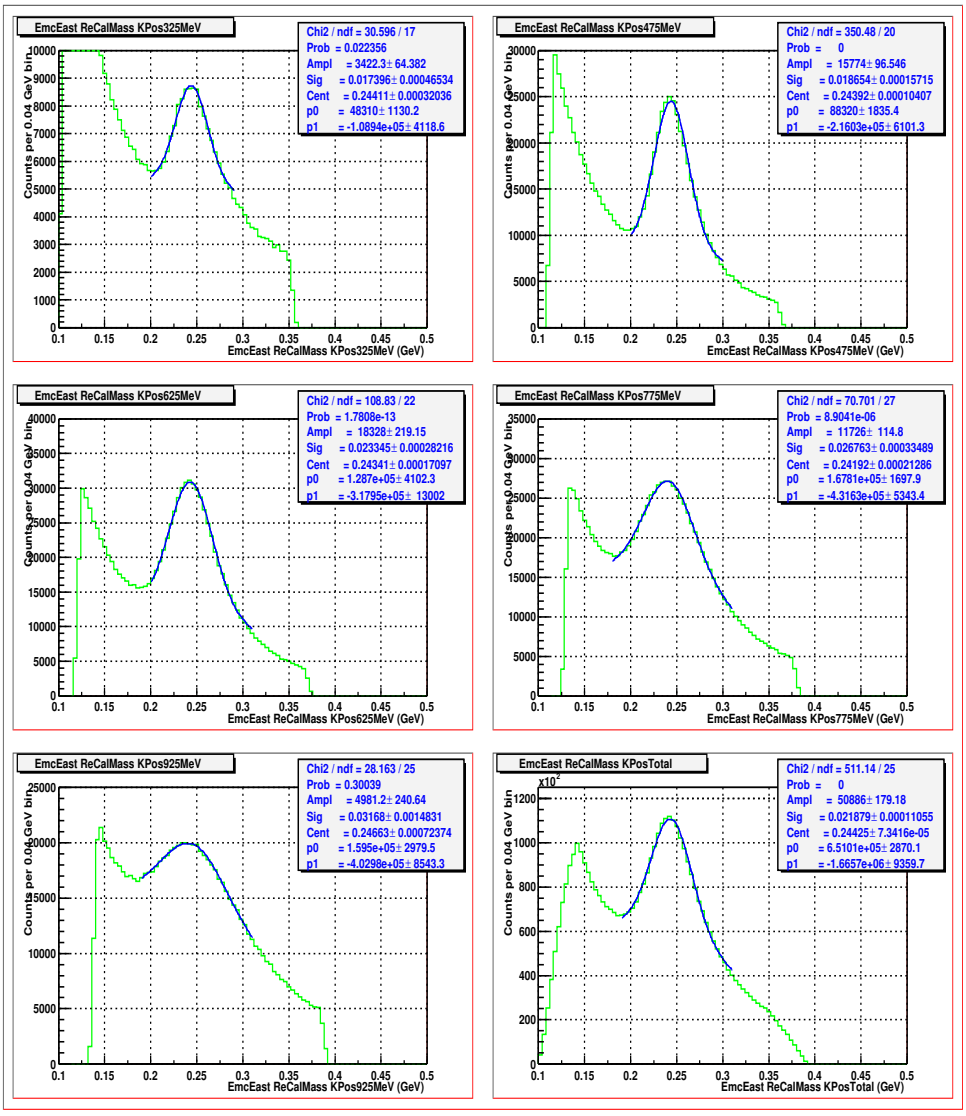

Figure 29: Partial mass-squared spectrum for positive particles deduced from the PHENIX East EMCal subsystem, after momentum–dependent corrections. The steep shoulder at low mass is from the pions.

An example of such a mass spectrum for positive particles is shown in Fig. 28. One normally plots the square of the mass since the mass value m is derived from the equation

$$m^2 = \frac{p^2(1-\beta^2)}{\beta^2}$$

where $\beta \equiv v/c$ is determined from the time-of-flight and the path length. The variable p is the particle momentum. Experimental resolution uncertainties could lead to the deduced β being

apparently greater than unity for some particle tracks, although this is not the case for kaons in PHENIX.

In Fig. 28 the mass-squared spectrum is plotted for six momentum bins ±75 MeV centered at 325 to 1075 MeV. Except for the last bin which appears more as a shoulder on the background tail from the lower mass pions, there are distinctive peaks in the other five momentum bins. However, it can be seen that the centroids of these peaks vary significantly as a function of momentum. This occurs because the timing calibration of the EMCal was not perfected prior to the production of the nanoDSTs. Therefore, for this analysis, we introduced a momentum dependent mass rescaling to compensate for the slight timing mis–calibration. The results of the improved mass-squared spectrum are shown in Fig. 28. With this renormalization of the mass spectrum, it is then possible to set tighter momentum dependent mass windows in order to tag the candidate kaon tracks with better signal-to-background probability. Based on the distinctive mass peaks shown in Fig. 28, particles with momentum between 300 and 1000 MeV/c are considered for particle identification in the EMCal in the $\phi \rightarrow K^+K^-$ analysis in PPG016.

Table 15: Momentum Dependence of the Kaon Mass–Squared Centroids from the EMCal

p (GeV/C)	K^+	K^-	Ratio K^+/K^-
0.325 ± 0.075	0.2680 ± 0.0004	0.2538 ± 0.0001	1.0559 ± 0.0016
0.475	0.2610 ± 0.0001	0.2522 ± 0.0001	1.0349 ± 0.0006
0.625	0.2534 ± 0.0001	0.2478 ± 0.0001	1.0226 ± 0.0006
0.775	0.2431 ± 0.0002	0.2413 ± 0.0002	1.0075 ± 0.0012
0.925	0.2397 ± 0.0007	0.2387 ± 0.0004	1.0042 ± 0.0034

The equivalent before–and–after mass spectra for the negative particles are shown in Fig. 30 and Fig. 31. The fitted centroids of the mass peaks are tabulated in Table 15. From these results one can observe an interesting systematic difference between the positive kaons and the negative kaons. The positive kaons have a greater centroid variation as compared to the negative kaons. Perhaps related to that, the negative kaon mass peaks in each momentum bin are slightly sharper than for the positive kaons. Such a systematic discrepancy cannot be explained by a simple time–zero offset which would apply equally to both charge signs.

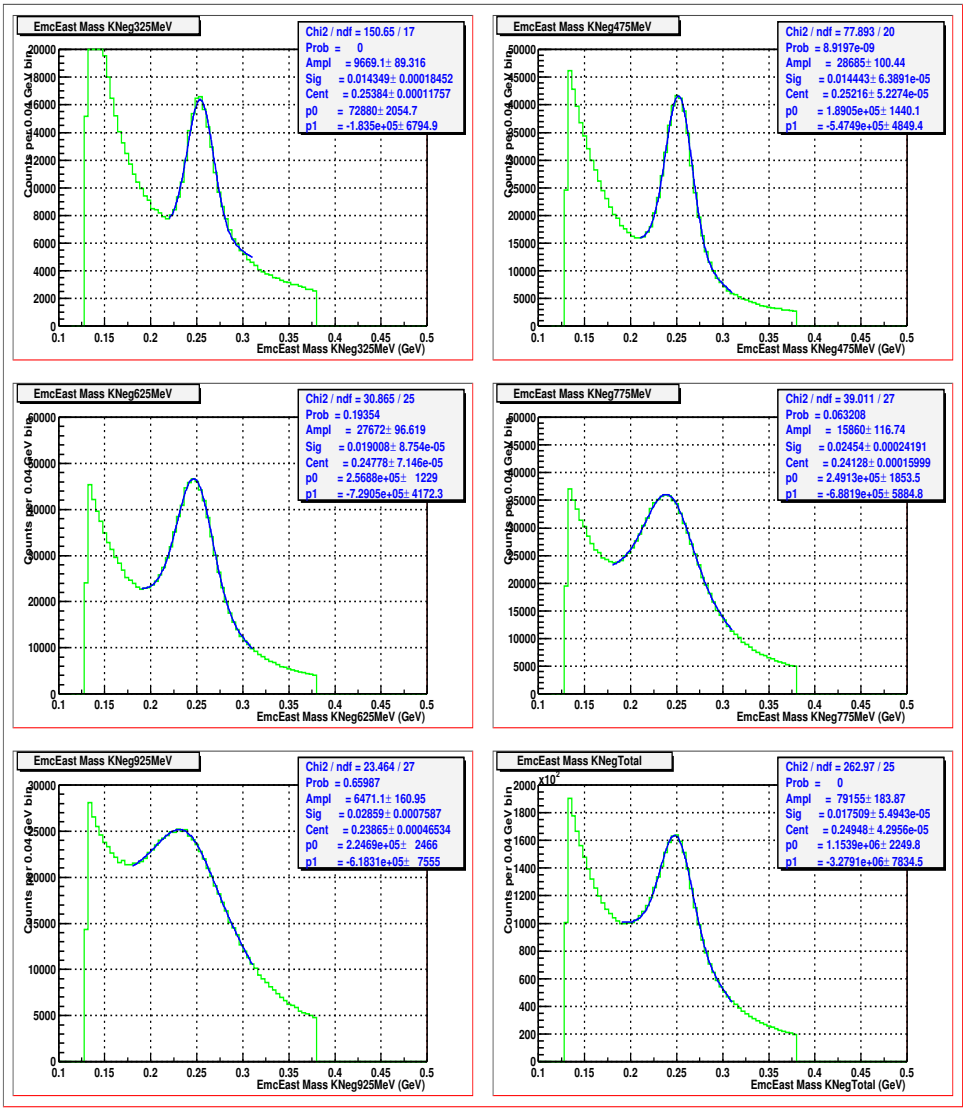

Figure 30: Partial mass-squared spectrum deduced for negative particles from the PHENIX East EMCal subsystem, before timing corrections. The spectra are in bins of particle momentum from 325 to 1075 MeV, with bin widths of ±75 MeV. There are Gaussian peaks fitted on top of a linear + quadratic background in each case.

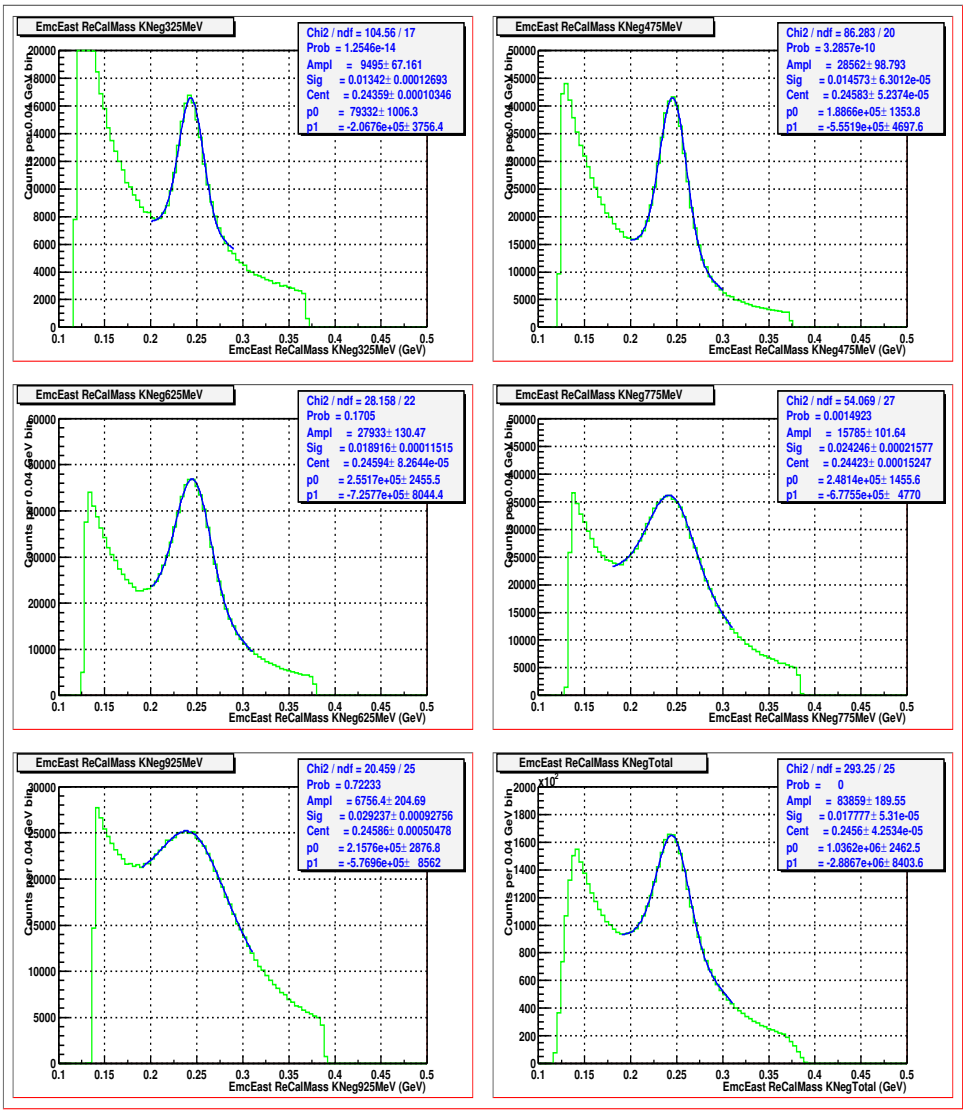

Figure 31: Partial mass-squared spectrum for negative particles deduced from the PHENIX East EMCal subsystem, after timing corrections. The spectra are in bins of particle momentum from 325 to 1075 MeV, with bin widths of ±75 MeV. There are Gaussian peaks fitted on top of a linear + quadratic background in each case.

C Explanation of the Intruder Peak

It was seen that there is a structure above the ϕ mass at around 1.06 GeV (see Reference[1]). The structure was initially thought as the K^0_S peak, where pions coming from $K^0_S \to \pi^+\pi^-$ decay were thought as identified as kaon in TOF. But the yield of the intruder is too large to be explained by the doubly misidentified pions.

Charles F. Maguire concentrated on this problem while doing the $\phi \to K^+K^-$ analysis. His works led to a hypothesis proposed in the Ligh/Heavy Working Group by Y. Akiba[2] to explain this intruder peak.

We enclose the hypothesis below.

1. In the intruder peak, let one of the two tracks be a real kaon. Let us call it $trk1$.
2. The other one ($trk2$) is a track of opposite charge that points to the same TOF hit or EMCAL cluster of $trk1$. Thus the timing information of $trk1$ and $trk2$ are the same.
3. Since TOF_{trk1} =TOF_{trk2}, mass_{trk1} is probably similar to mass_{trk2}. Thus if trk1 is a kaon, trk2 is also assigned as kaon.
4. The condition (2) means that, in the rest frame of the pair (trk1+trk2), the apparent decay momentum of trk1 and trk2 is similar and they should be about 200 MeV/c (the magnetic p_t kick of the Central Magnet). This kinematic condition can cause a peak in the effective mass of (trk1+trk2).

The hypothesis explains the following feature of the intruder

- The yield of intruder increases with centrality.
- There is little signal in TOF-EMC combination.
- The mass value is roughly correct. The expected mass peak position produced by this mechanism roughly is
$$M_{intruder} = 2\sqrt{M_k^2 + (p_t)^2_{kick}} \tag{20}$$
For kaon using $M_k = 493$ MeV and $(p_t)_{kick} = 200$ MeV, we have $M_{intruder} = 1.064$ GeV. Similarly for For proton, $M_{intruder}$ =1.918 GeV.

Charles F. Maguire tested the hypothesis and it indeed expelled the intruders. Following the hypothesis,

we use the following steps to eliminate the intruders.

- Impose the global cuts
  - -30cm<bbcz<30cm
  - 0<isminbias<93

- Consider tracks which have best Dch quality (31 or 63)
- Eliminate the drift chambers ghost tracks. The Dch ghosts are of the same charge and they are within $|\Delta zed| < 0.2$ and $|\Delta\phi| < 0.03$. One of the tracks of the pair that satisfies condition to be ghost is rejected randomly.
- Tracks that survive the ghost rejection are subject to the intruder rejection. To reject intruders in TOF we do the following:
  - identify tracks in TOF. We use a 3σ radius matching at TOF (tofsdphi*tofsdphi + tofsdz*tofsdz < 9)
  - compare the slat of the tracks. If there are two hits on a slat in an event, the timing information of the tracks are bad, and they show up as intruders. So if the slat of two tracks are same (slat1==slat2), both of them are rejected.

  To reject intruders in EMCal we do the following:
  - identify tracks in EMCal. We use a 3σ radius matching at EMCl (emcsdphi*emcsdphi + emcsdz*emcsdz < 9)
  - compare the sectors, energies and time of flight of the tracks. If two tracks in the same EMC sector have same energy and same time (sect1==sect2 && ecorr1==ecorr2 && temc1==temc2), both of them are rejected.

References

[1] M. Muniruzzaman and R. Seto, PHENIX Analysis Note AN153 (2002).

[2] Y. Akiba, Collaboration wide Communication, 12 September 2002.

D Tables and Plots for the Run Efficiency Corrections

E Tables and Plots for Single Kaon Yield Analysis

Table 16: Comparison Monte Carlo Correction Factors for Single K^+

p_T (GeV/C)	PPG016 CF K^+	Hadron PWG CF K^+	K^+ Ratio (Hadron PWG/PPG016)
0.45	230 ± 19	461 ± 10	2.01 ± 0.17
0.55	145 ± 10	304 ± 6	2.09 ± 0.15
0.65	114 ± 7	234 ± 4	2.05 ± 0.14
0.75	97 ± 6	199 ± 3	2.04 ± 0.13
0.85	91 ± 6	183 ± 3	2.01 ± 0.13
0.95	88 ± 4	163 ± 3	1.86 ± 0.12
1.05	73 ± 4	156 ± 3	2.13 ± 0.13
1.15	76 ± 4	143 ± 3	1.87 ± 0.11
1.25	67 ± 4	131 ± 2	1.96 ± 0.12
1.35	65 ± 4	123 ± 2	1.88 ± 0.11
1.45	60 ± 3	122 ± 2	2.05 ± 0.11
1.55	56 ± 3	116 ± 2	2.08 ± 0.12
1.65	58 ± 3	112 ± 2	1.94 ± 0.11
1.75	59 ± 3	111 ± 2	1.89 ± 0.11
1.85	55 ± 3	105 ± 2	2.12 ± 0.11

Table 17: Comparison Monte Carlo Correction Factors for Single K^-

p_T (GeV/C)	PPG016 CF K^-	Hadron PWG CF K^-	K^- Ratio (Hadron PWG/PPG016)
0.45	261 ± 21	408 ± 8	1.57 ± 0.13
0.55	170 ± 12	274 ± 5	1.62 ± 0.12
0.65	144 ± 10	210 ± 4	1.46 ± 0.11
0.75	114 ± 7	176 ± 3	1.53 ± 0.10
0.85	101 ± 6	153 ± 3	1.52 ± 0.10
0.95	80 ± 4	139 ± 3	1.81 ± 0.11
1.05	82 ± 5	132 ± 2	1.61 ± 0.10
1.15	65 ± 3	118 ± 2	1.82 ± 0.10
1.25	71 ± 4	113 ± 2	1.59 ± 0.10
1.35	70 ± 4	111 ± 2	1.59 ± 0.09
1.45	68 ± 4	109 ± 2	1.61 ± 0.09
1.55	58 ± 3	104 ± 2	1.79 ± 0.10
1.65	57 ± 3	101 ± 2	1.77 ± 0.10
1.75	55 ± 3	96 ± 2	1.75 ± 0.10
1.85	53 ± 3	95 ± 2	1.79 ± 0.10

F Tables and Plots for the ϕ Yield Analysis

G First Comparison of STAR and PHENIX results

An comparison was made between the TOF-TOF data, early versions of the EMC-TOF and EMC-EMC data and the STAR data. Several important caveats to this comparison show be made here. The first is that the data including the EMC has uses the embedding efficiencies which were derived for the TOF. The correct embedding efficiencies will be available soon and these comparisons will be updated. Star data made available to us via the plots shown at QM2002 are simply lifted from the plots (no tables are available), hence error bars are estimates. The actual plots from STAR are show in figure 32. Since the analysis using the TOF is the most mature, this data is shown first in comparison to STAR Figs. 33. One can clearly see that the data from PHENIX is lower and shows a larger slope. This is shown more explicitly in and Figs. 34 and table 18. One of the obvious questions is whether or not there is a problem with our low pt data since the acceptance of the TOF drops sharply. Using the EMCAL we can cover this range. Figs. 35, 36, and 37 show now the data including the EMCAL-TOF data and the EMCAL-EMCAL data. Since the embedding efficiency is not included correctly, it is too early to draw any strong conclusions, however it appears that the EMCAL-TOF data with its larger acceptance at low pt has a somewhat larger yield than the data from the TOF alone. This would then cause the inverse slope to drop thereby increasing the dN/dy.

Table 18: dN/dy and Temperatures for $\phi \to K^+K^-$ TOF-TOF Pairs Extracted in Two Analyses

Centrality	STAR Analysis		PHENIX-TOF Analysis	
$Npart$	dN/dy	T (MeV)	dN/dy	T (MeV)
28	0.46 ± 0.04	340 ± 13	0.26 ± 0.06	378 ± 30
94	1.54 ± 0.12	370 ± 12	0.93 ± 0.17	404 ± 25
201	4.15 ± 0.26	340 ± 16	2.05 ± 0.39	410 ± 26
325	6.60 ± 0.57	330 ± 18	2.38 ± 0.83	452 ± 55

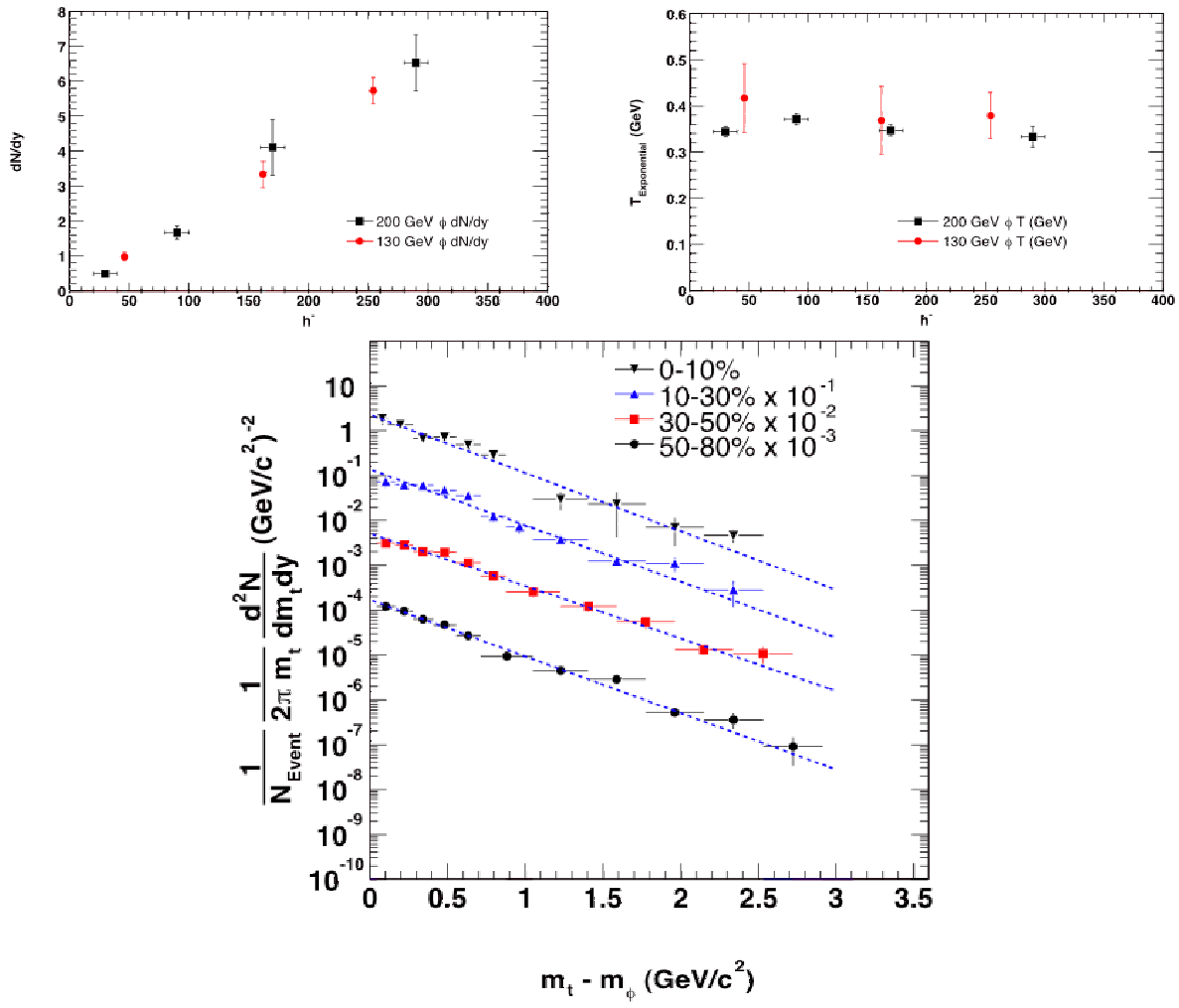

Figure 32: STAR data for reference

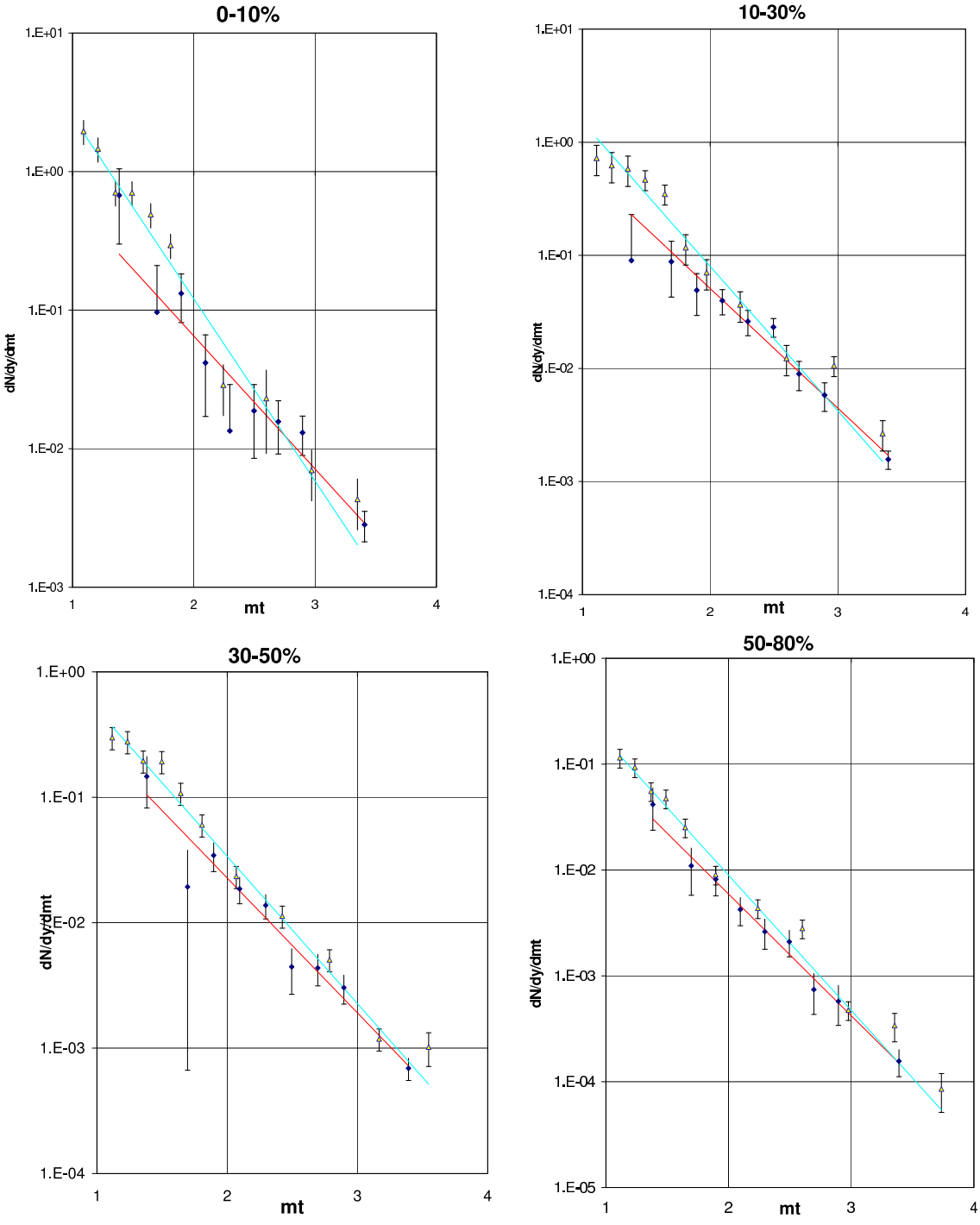

Figure 33: Comparison of STAR data to PHENIX TOF data. PHENIX data is indicated in red, STAR in blue.

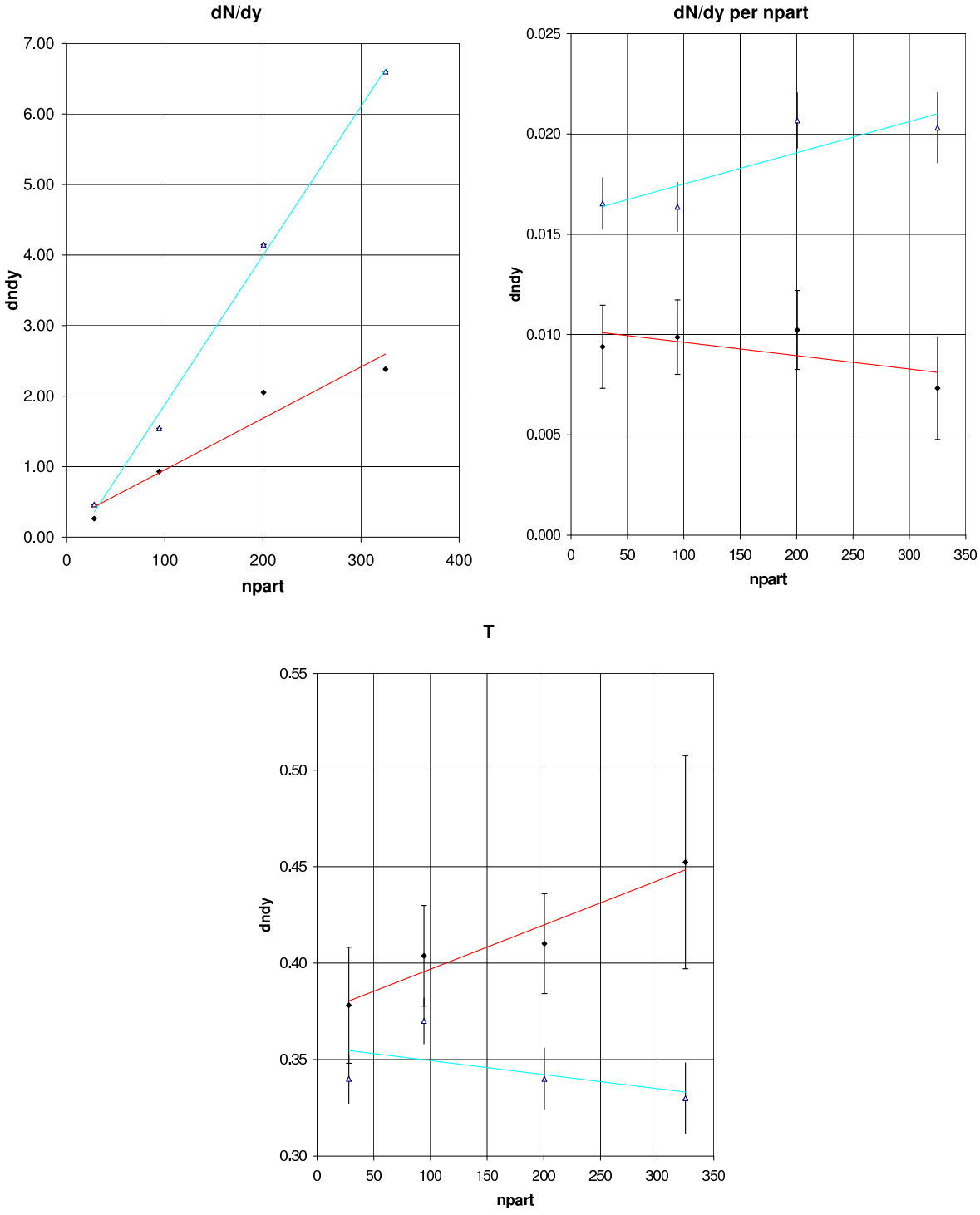

Figure 34: Comparison of derived values for STAR and PHENIX TOF. PHENIX data is indicated in red, STAR in blue.

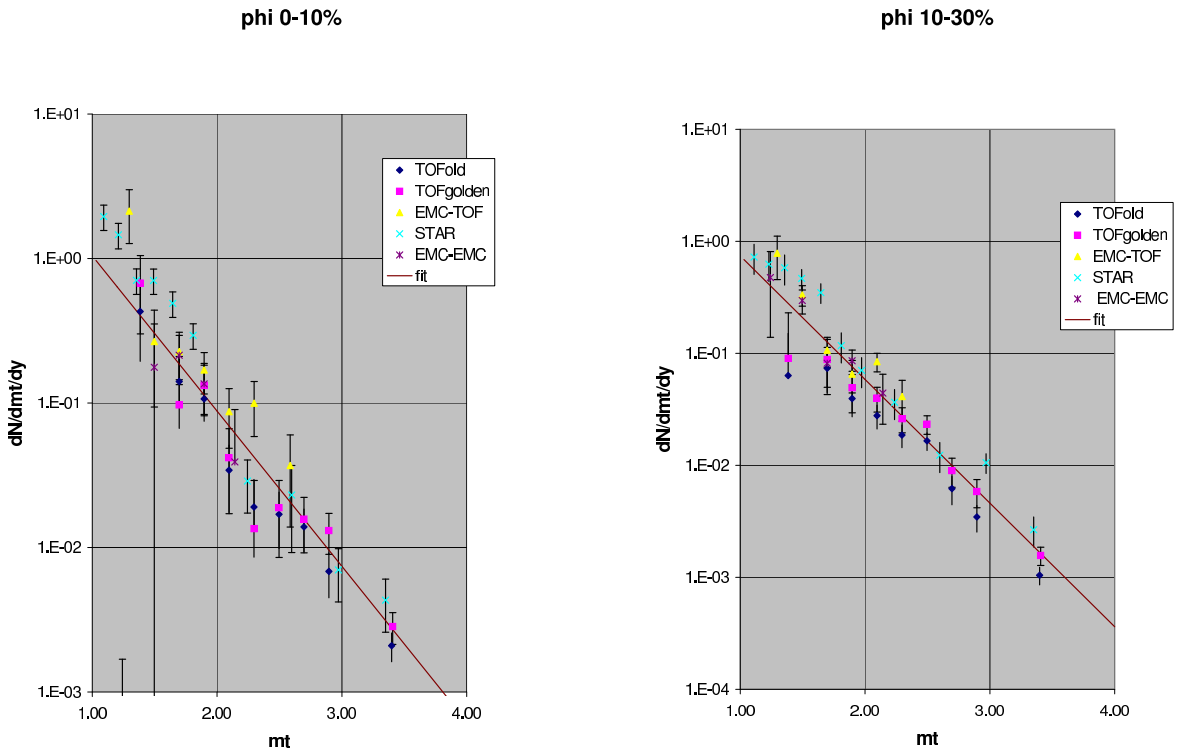

Figure 35: Comparison of ϕ yeilds between STAR data, and PHENIX TOF-TOF, EMC-TOF, and EMC-EMC data. PHENIX yields shown are from the UCR group. STAR yields are from QM 2002 slides.

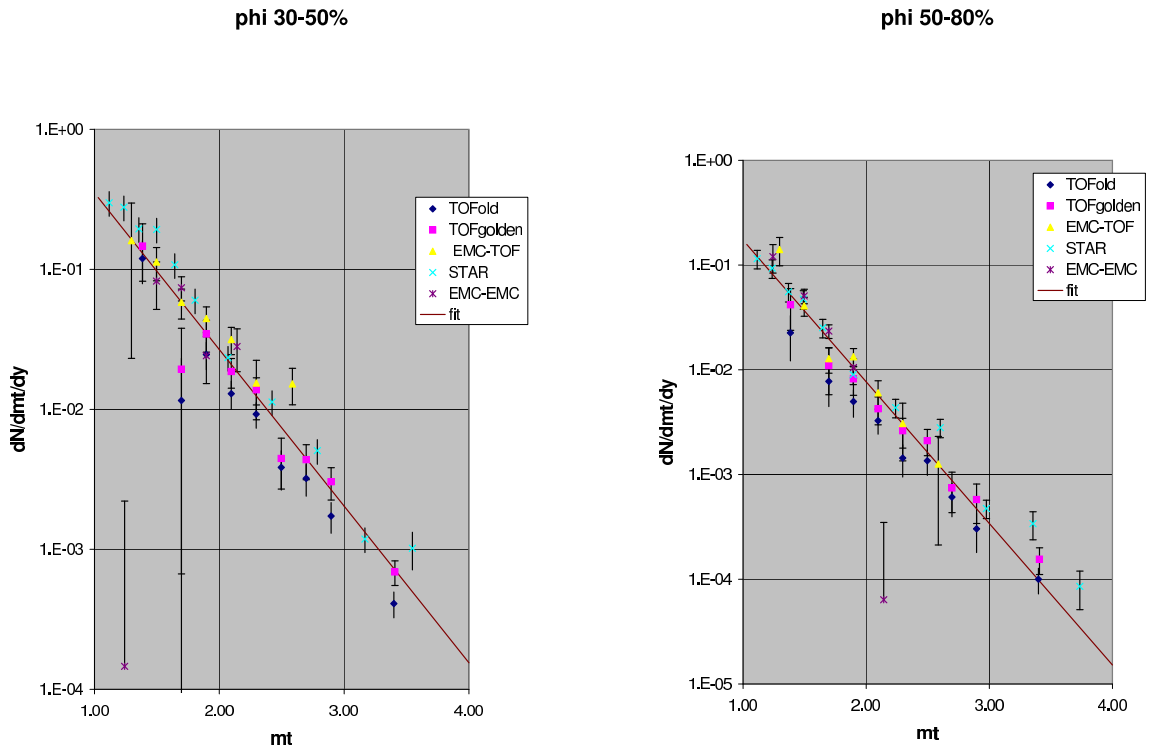

Figure 36: Comparison of ϕ yeilds between STAR data, and PHENIX TOF-TOF, EMC-TOF, and EMC-EMC data. PHENIX yields shown are from the UCR group. STAR yields are from QM 2002 slides.

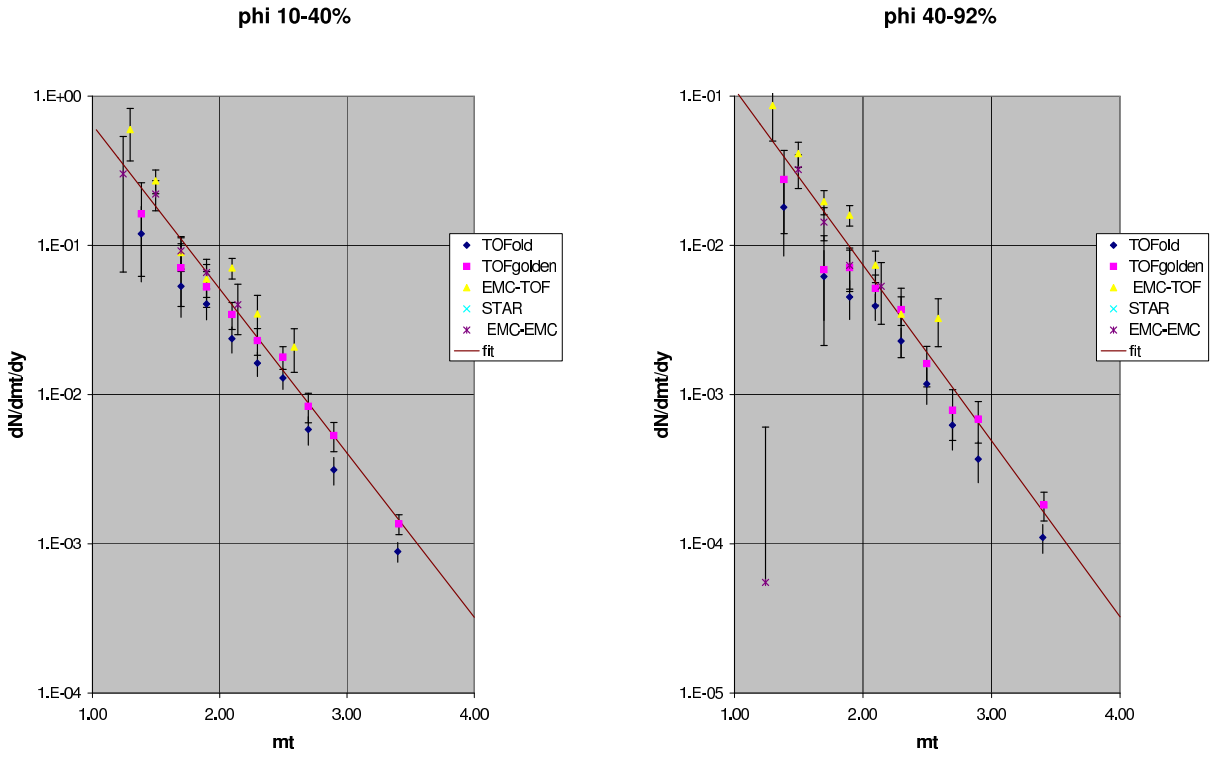

Figure 37: Comparison of ϕ yields - PHENIX centrality binning.

H Analysis Results for the ϕ from the UCR group

H.1 Invariant mass spectra for TOF–TOF pairs analyzed by UCR

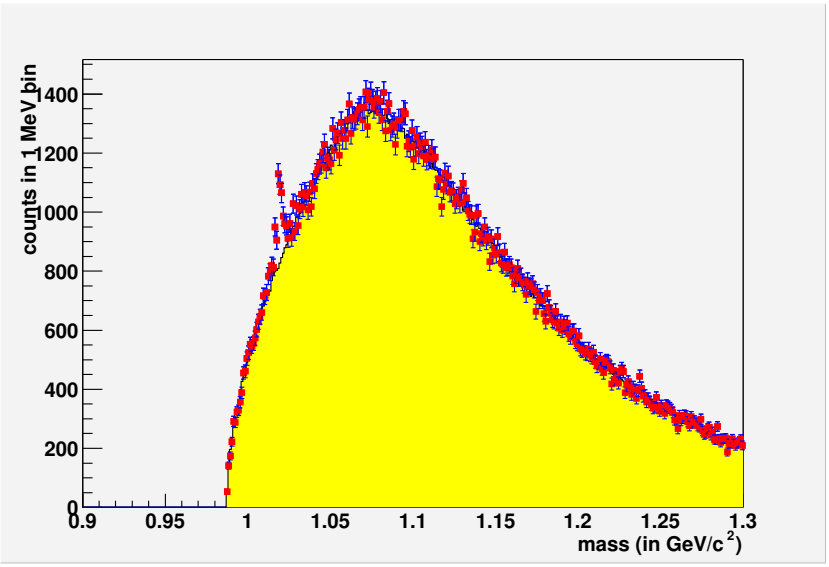

Figure 38: Signal and Combinatoric mass spectra in TOF–TOF extracted by the UCR group for the minimum bias events

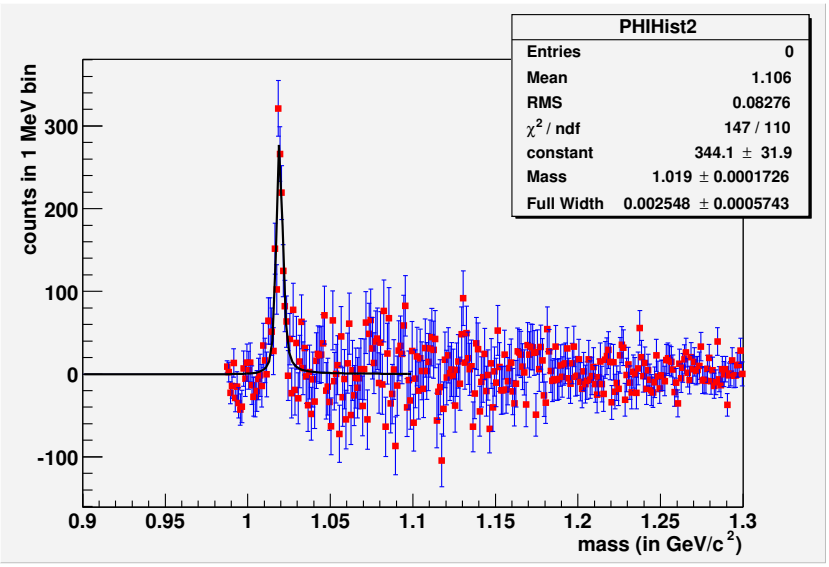

Figure 39: Invariant mass spectra in TOF–TOF extracted by the UCR group for the mininum bias events

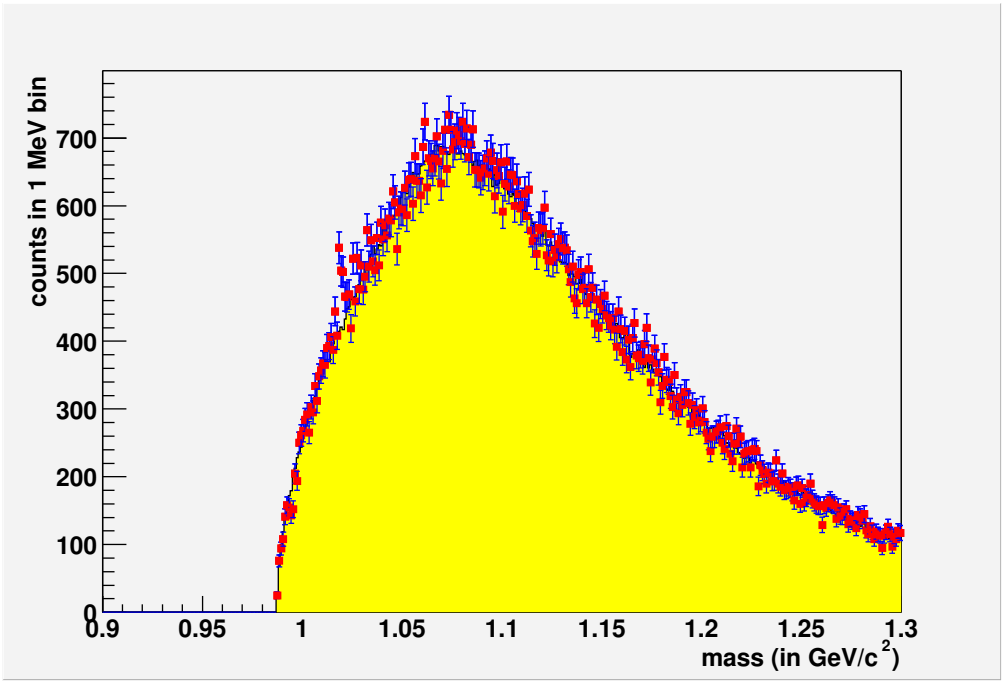

Figure 40: Signal and Combinatoric mass spectra in TOF–TOF extracted by the UCR group for the 0–10% centrality class

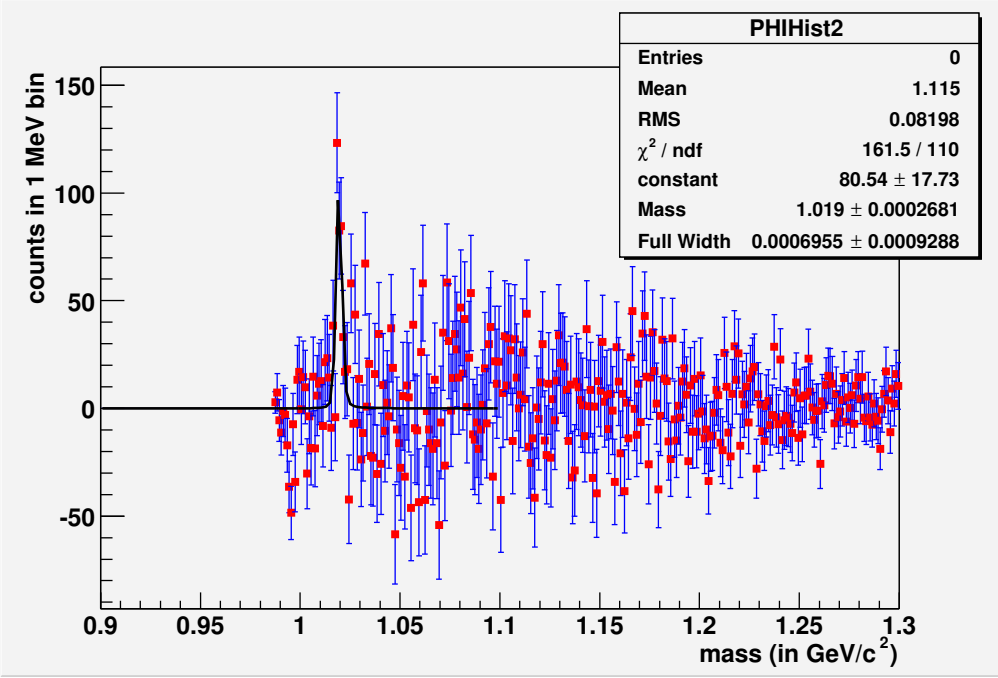

Figure 41: Invariant mass spectra in TOF–TOF extracted by the UCR group for the 0–10% centrality class

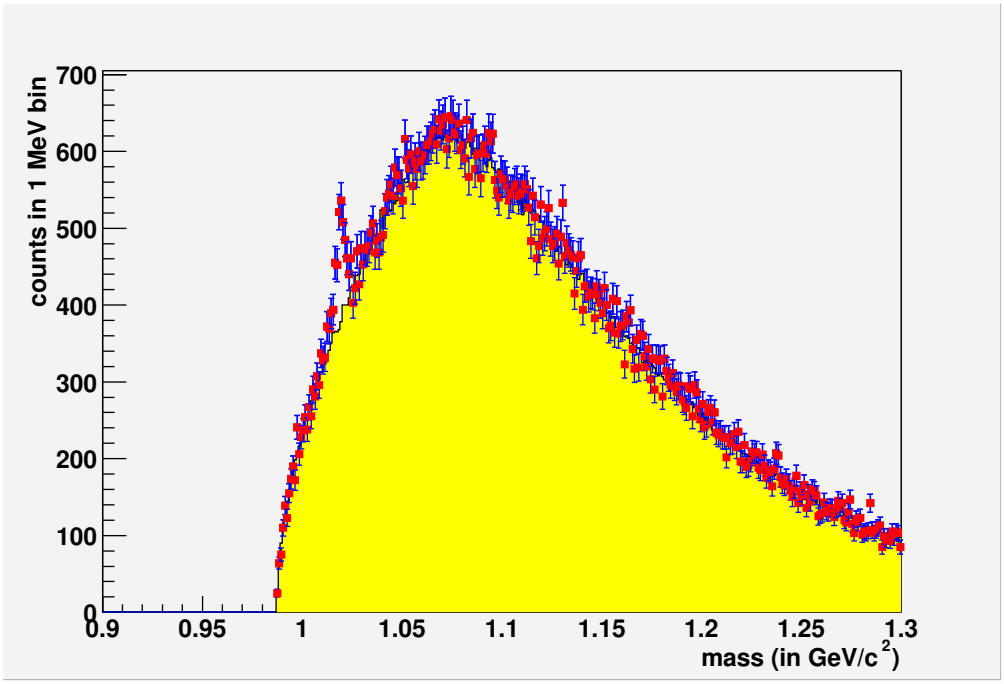

Figure 42: Signal and Combinatoric mass spectra in TOF–TOF extracted by the UCR group for the 10–40% centrality class

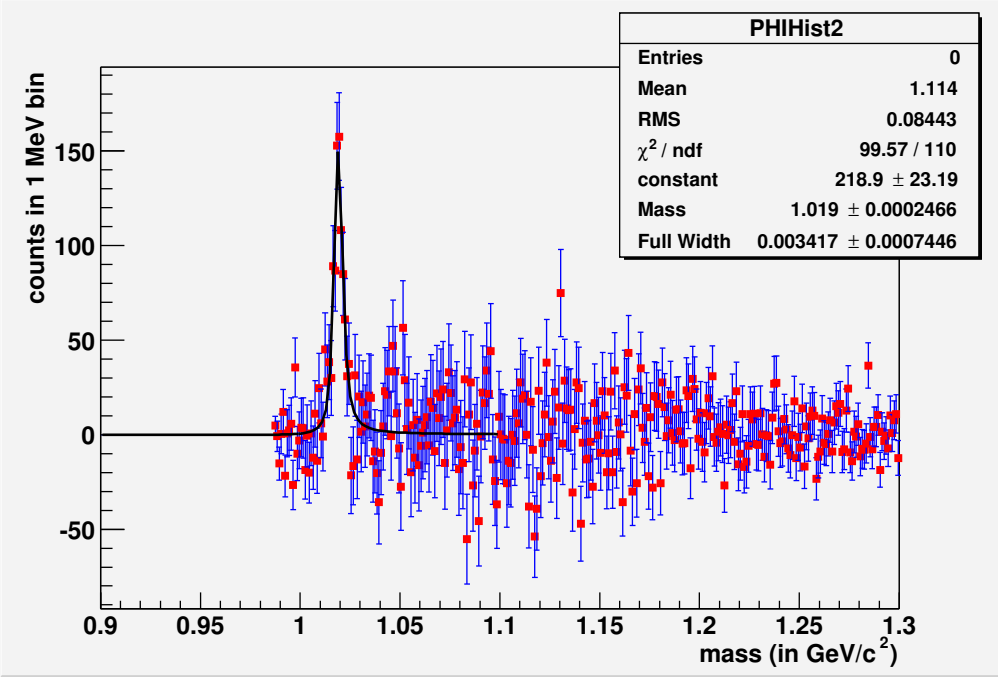

Figure 43: Invariant mass spectra in TOF–TOF extracted by the UCR group for the 10–40% centrality class

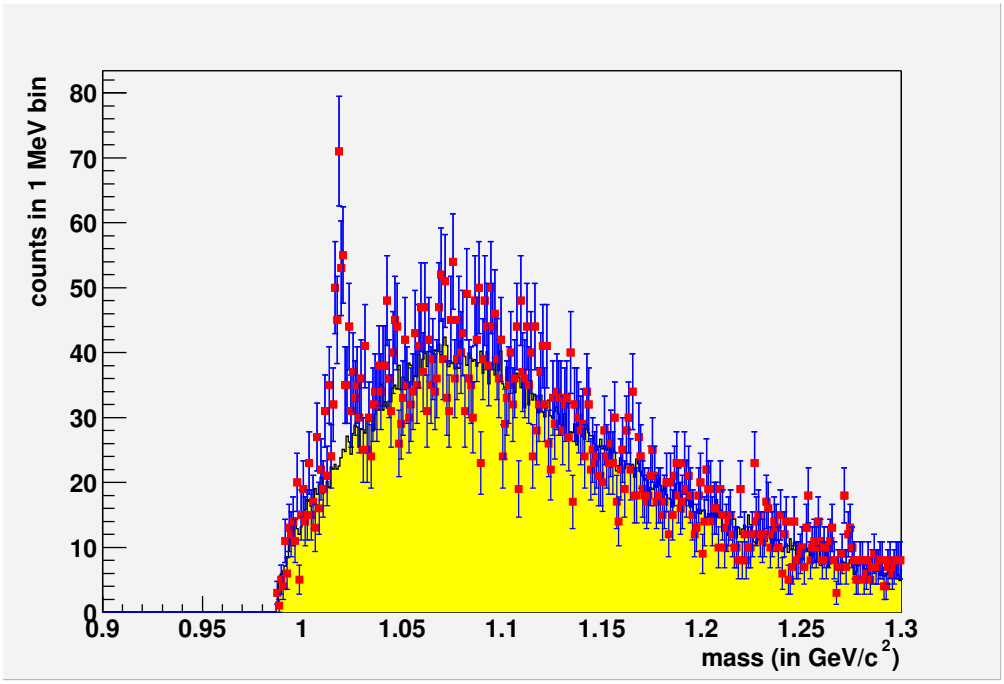

Figure 44: Signal and Combinatoric mass spectra in TOF–TOF extracted by the UCR group for the 40–92% centrality class

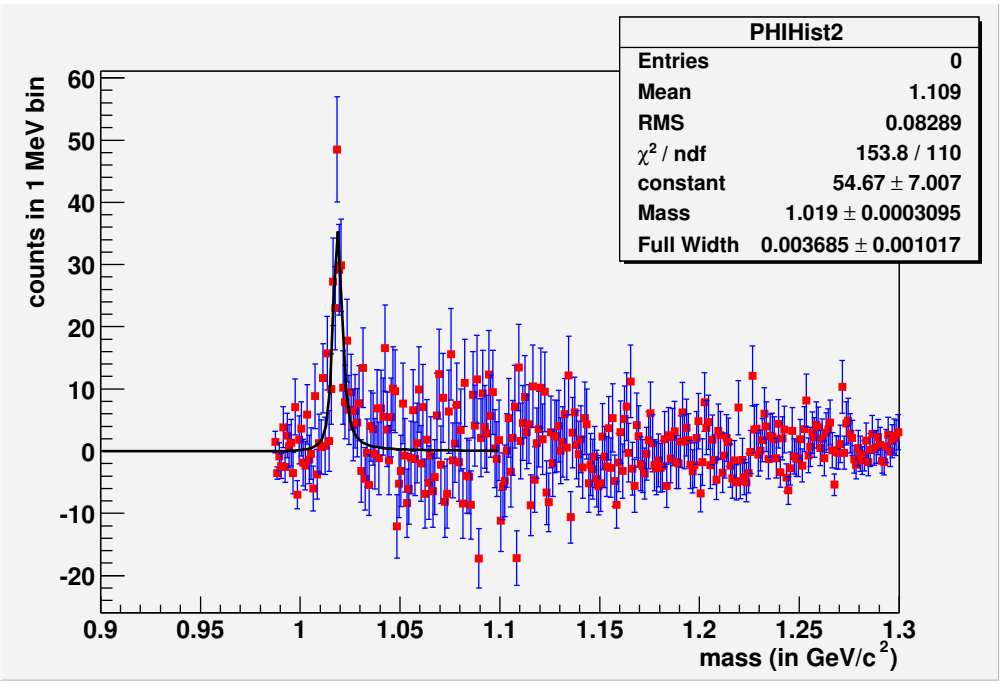

Figure 45: Invariant mass spectra in TOF–TOF extracted by the UCR group for the 40–92% centrality class

H.2 Yield $dN/dy\,dm_T$ for TOF–TOF pairs analyzed by UCR

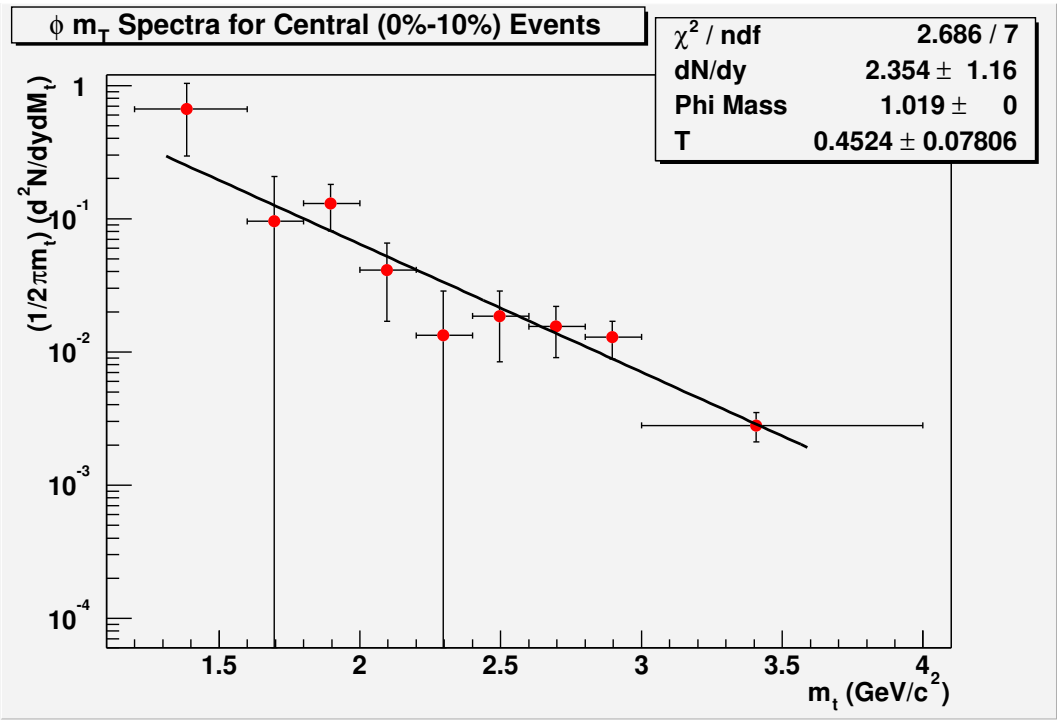

Figure 46: Yield in TOF–TOF extracted by the UCR group for the 0–10% centrality class

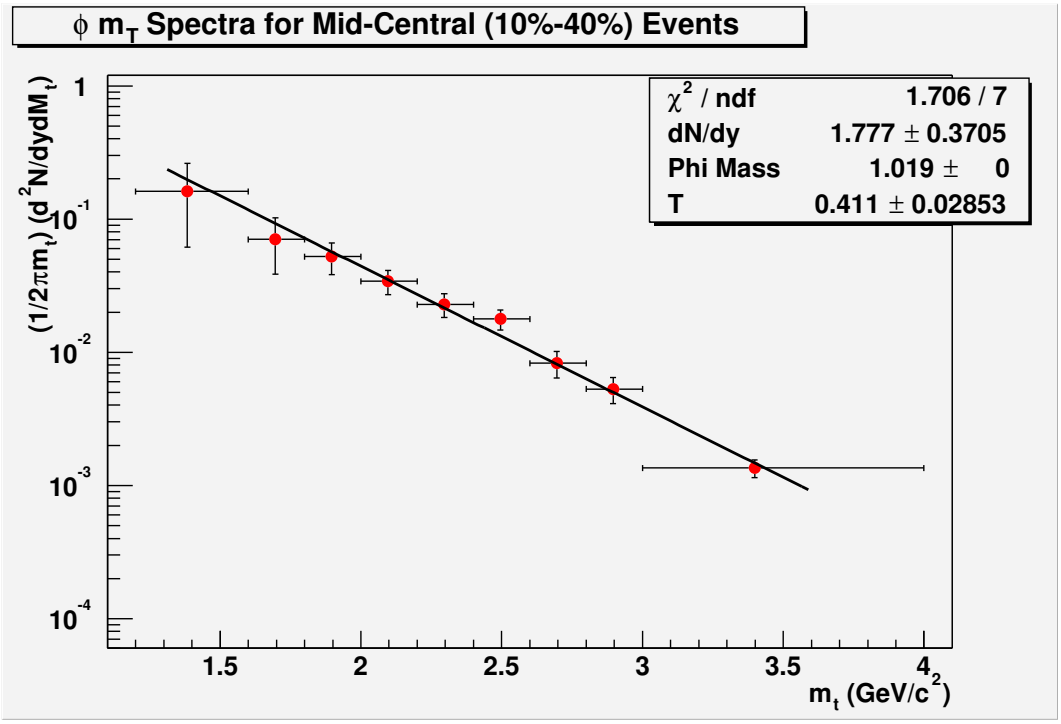

Figure 47: Yield in TOF–TOF extracted by the UCR group for the 10–40% centrality class

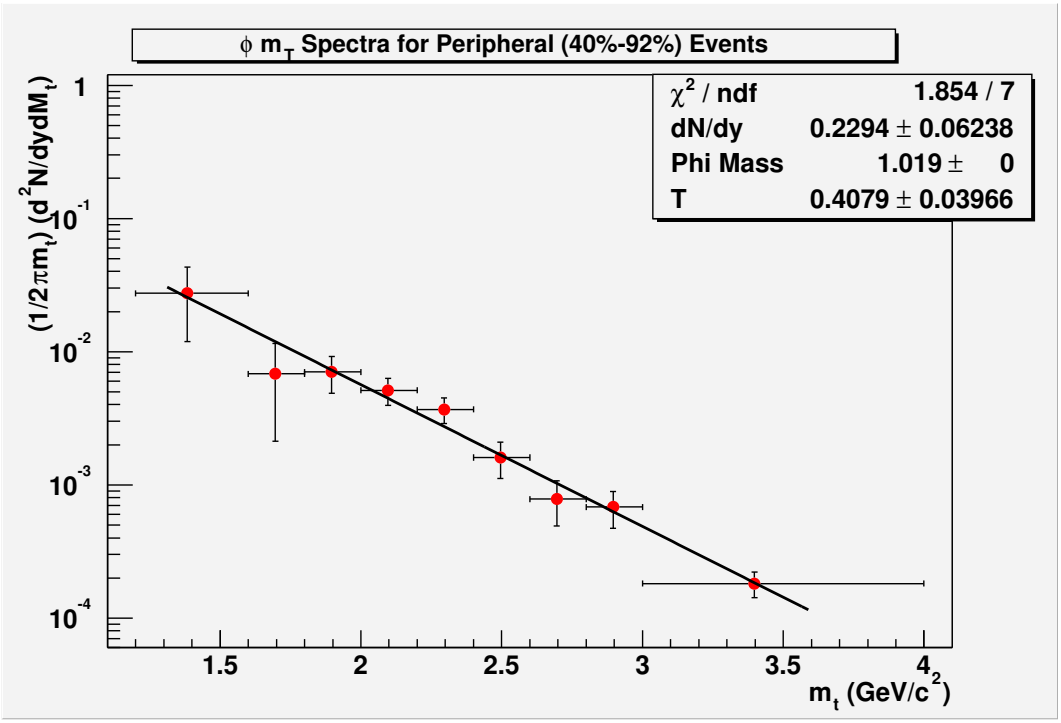

Figure 48: Yield in TOF–TOF extracted by the UCR group for the 40–92% centrality class

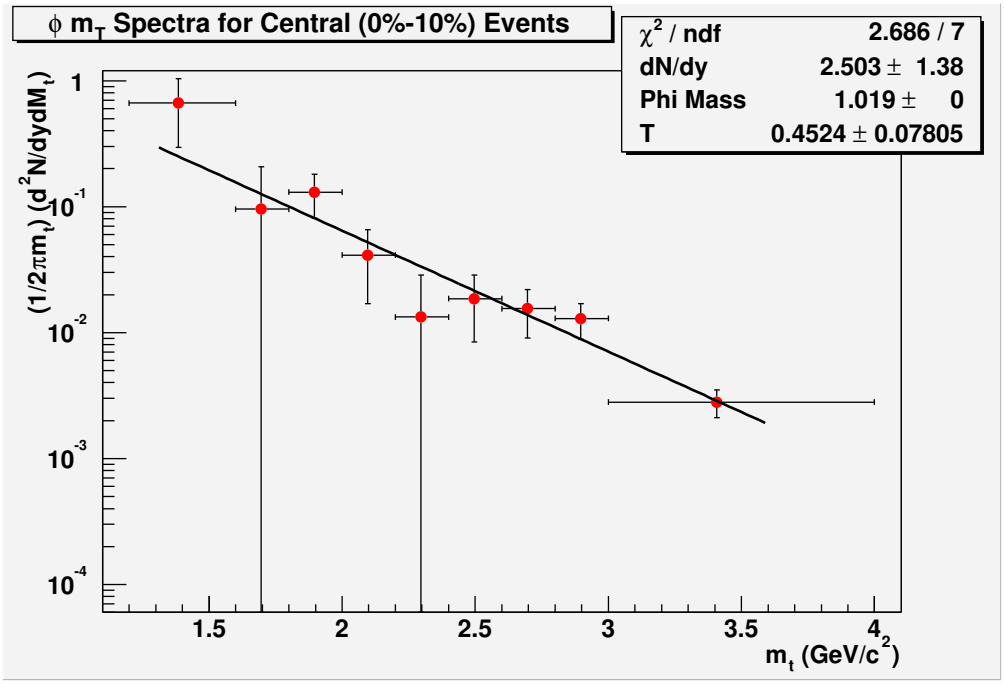

Figure 49: Yield in TOF–TOF extracted with Boltzmann shape by the UCR group for the 0–10% centrality class

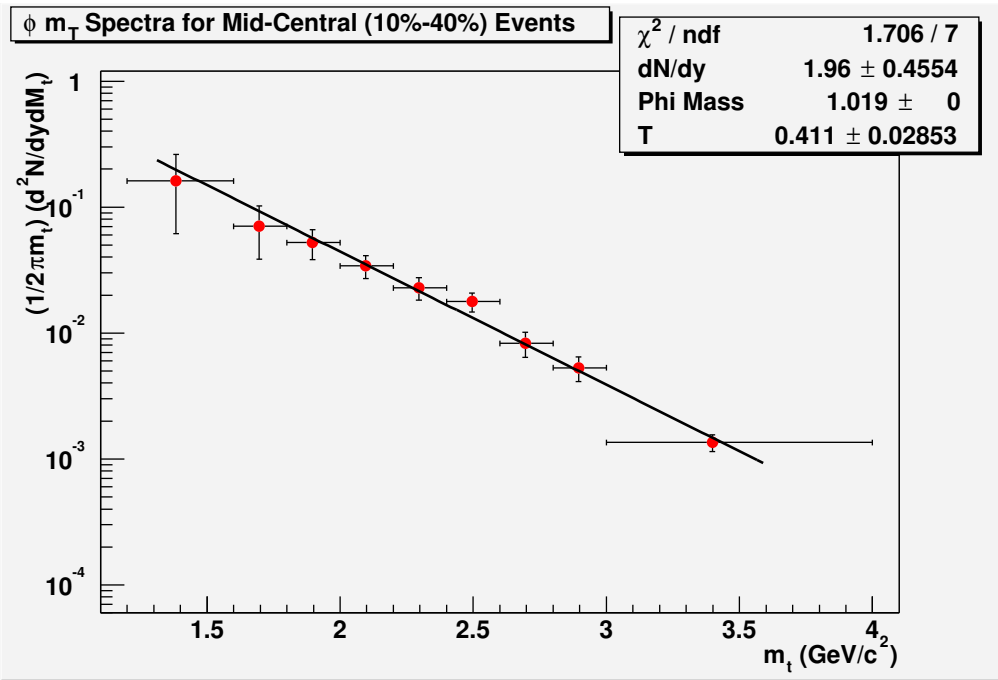

Figure 50: Yield in TOF–TOF extracted with Boltzmann shape by the UCR group for the 10–40% centrality class

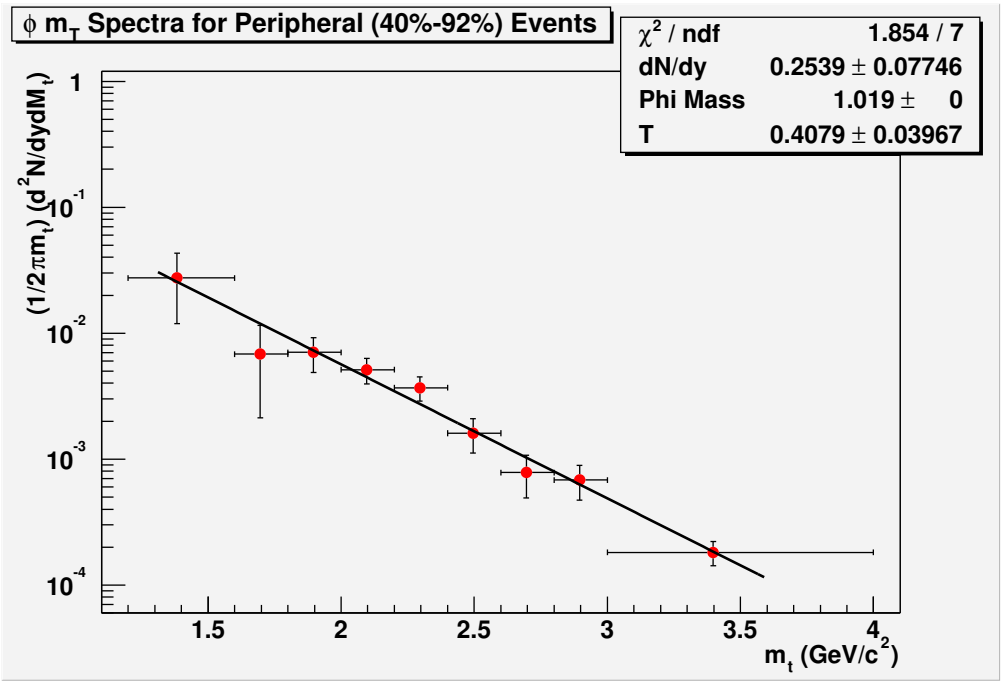

Figure 51: Yield in TOF–TOF extracted with Boltzmann shape by the UCR group for the 40–92% centrality class

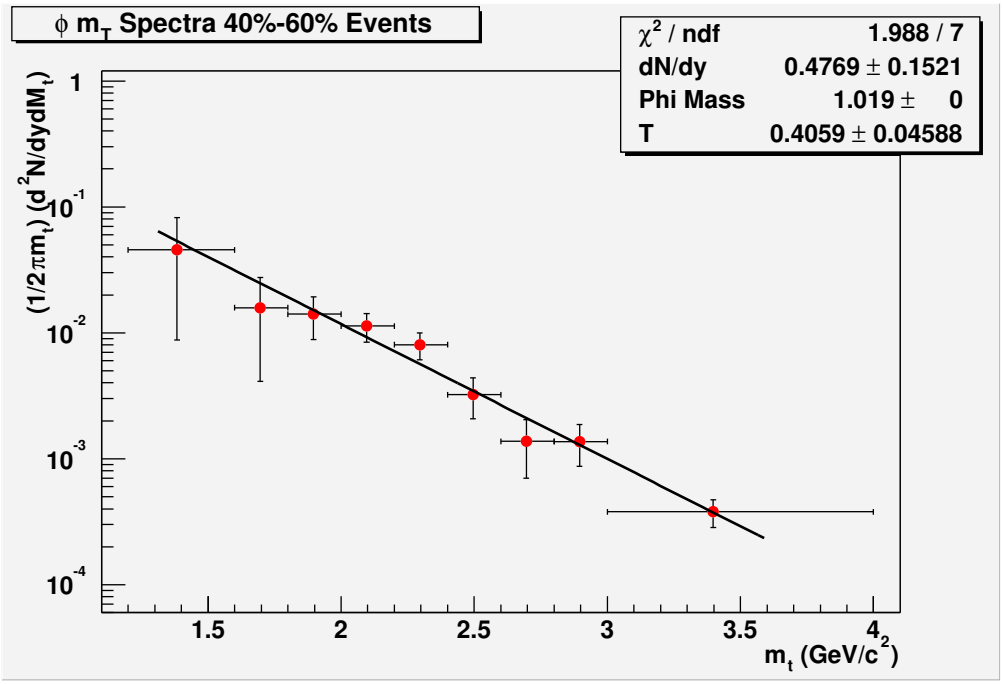

Figure 52: Yield in TOF–TOF extracted by the UCR group for the 40–60% centrality class

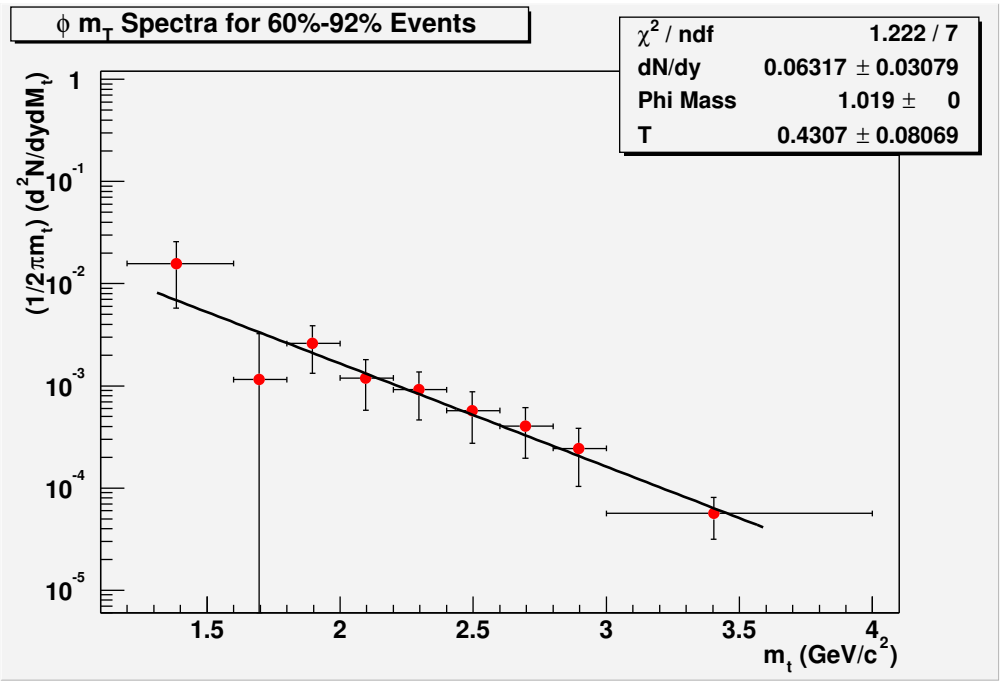

Figure 53: Yield in TOF–TOF extracted by the UCR group for the 60–92% centrality class

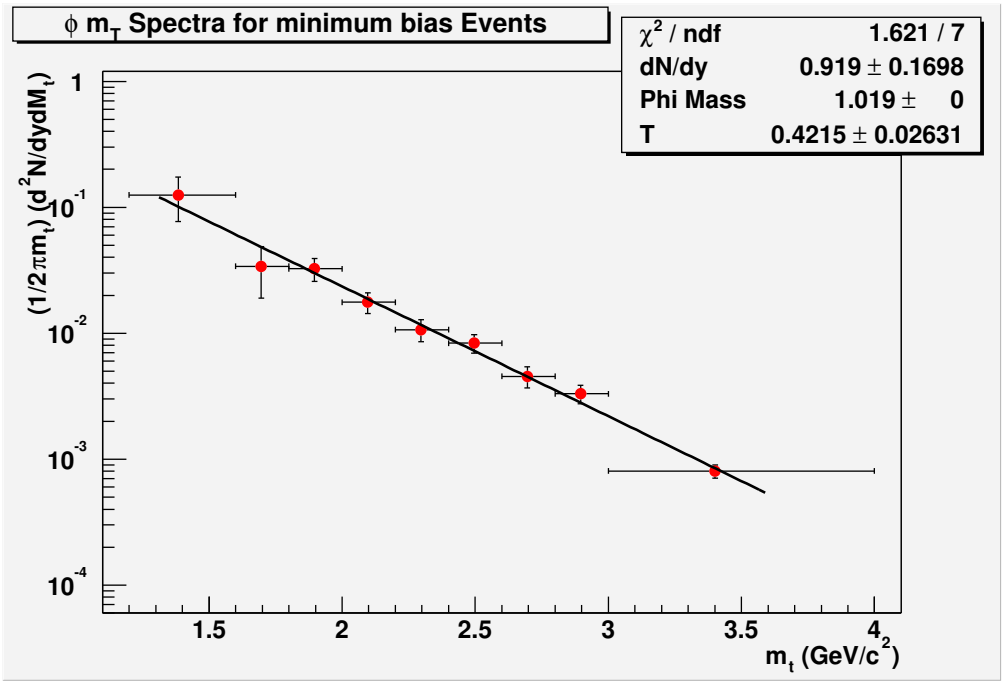

Figure 54: Yield in TOF–TOF extracted by the UCR group for the minimum bias events

H.3 Centrality dependence of dN/dy and T for TOF-TOF Pairs

We measured dN/dy and T by fitting the m_T spectra for five different centrality bins, 0 - 10%, 10 - 40%, 40-60%, and 60 - 92%.

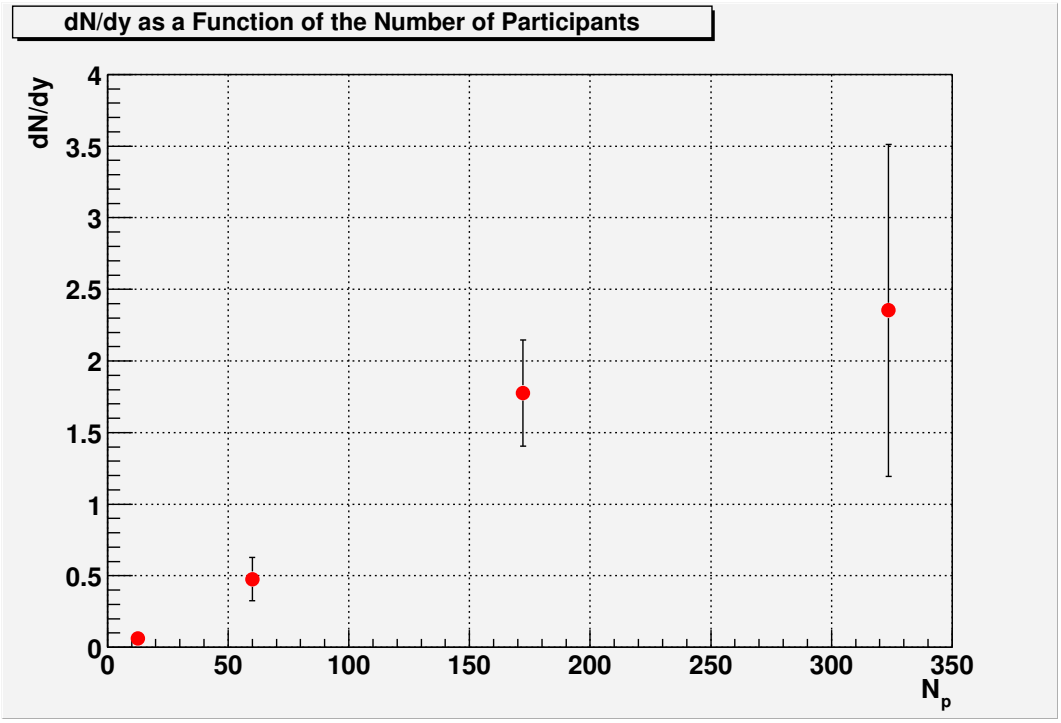

Figure 55: dN/dy vs. number of participants

H.4 Invariant mass spectra for TOF–EMCal pairs analyzed by UCR

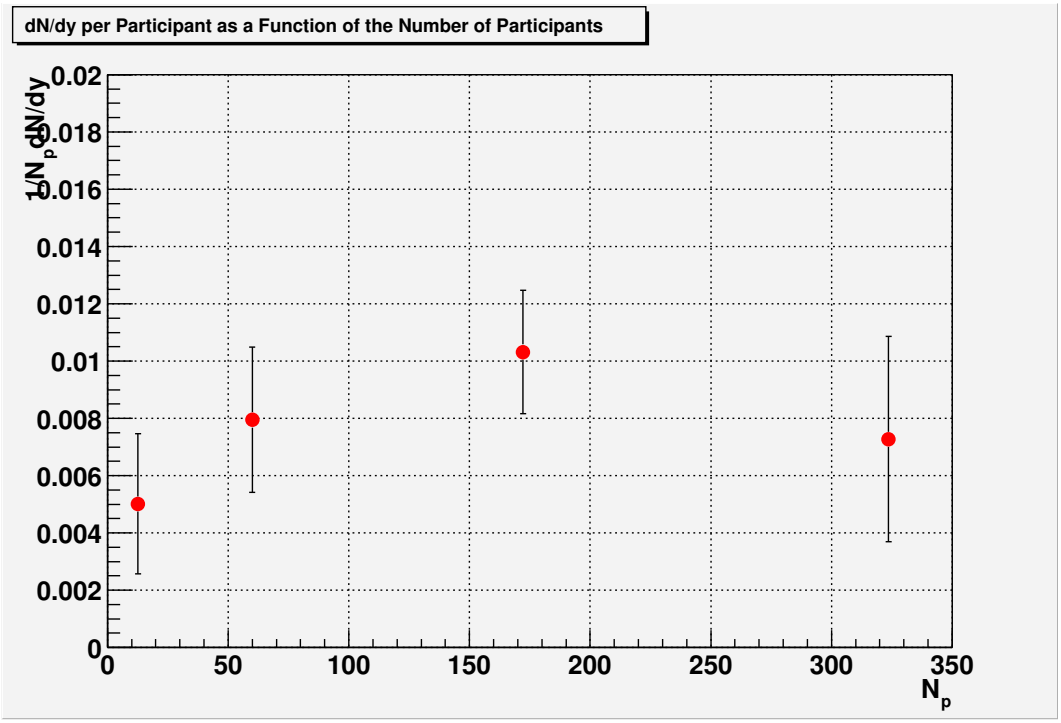

Figure 56: $(1/N_{part})$ (dN/dy) vs. number of participants

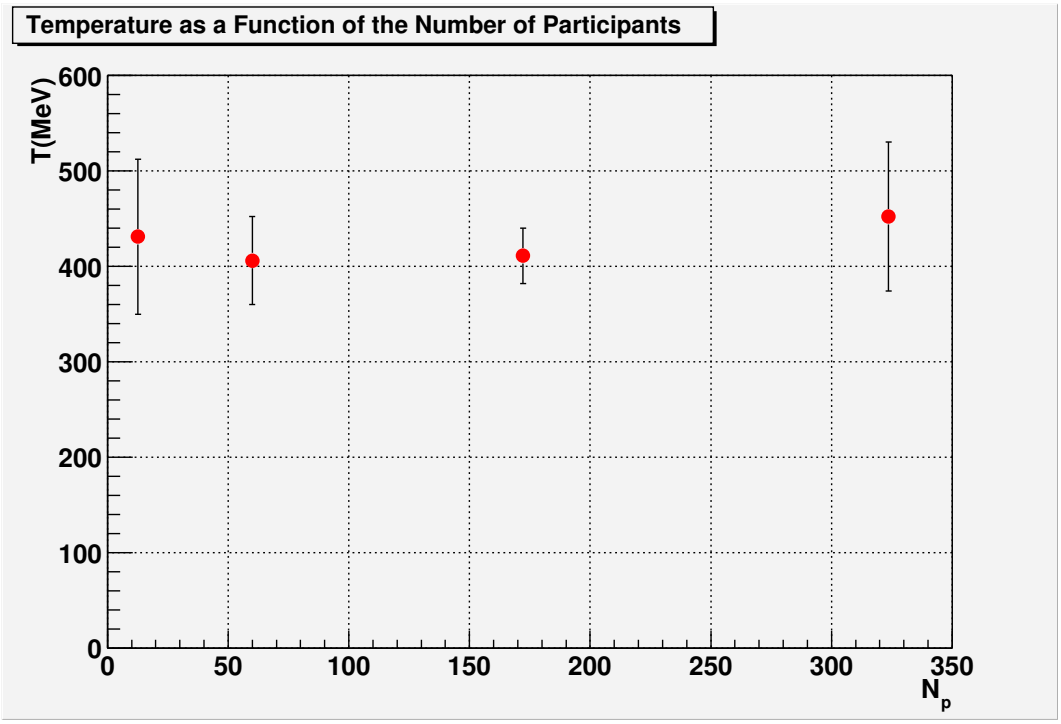

Figure 57: Temperature vs. number of participants

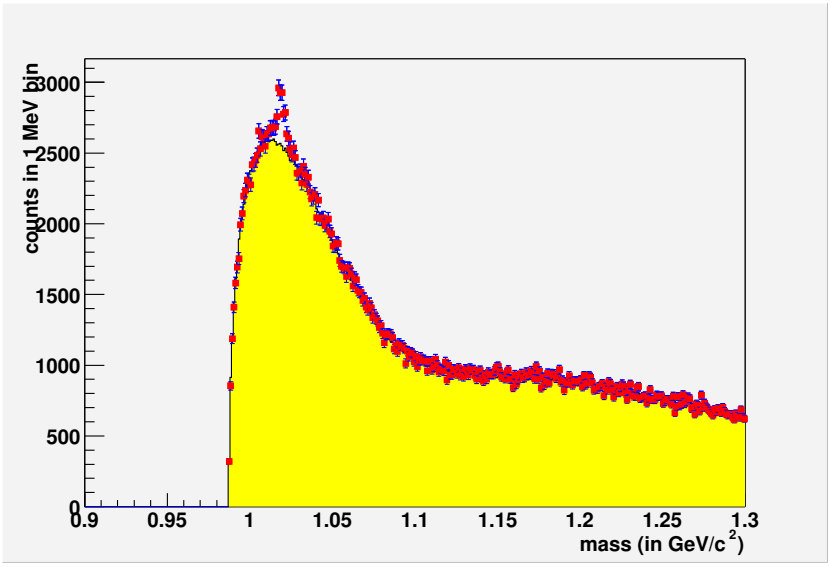

Figure 58: Signal and Combinatoric mass spectra in TOF–EMCal extracted by the UCR group for the minimum bias events

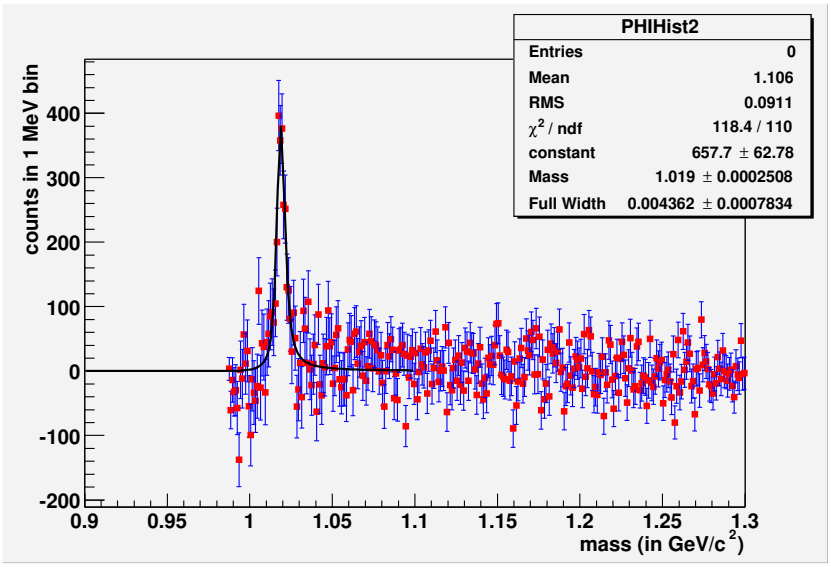

Figure 59: Invariant mass spectra in TOF–EMCal extracted by the UCR group for the mininum bias events

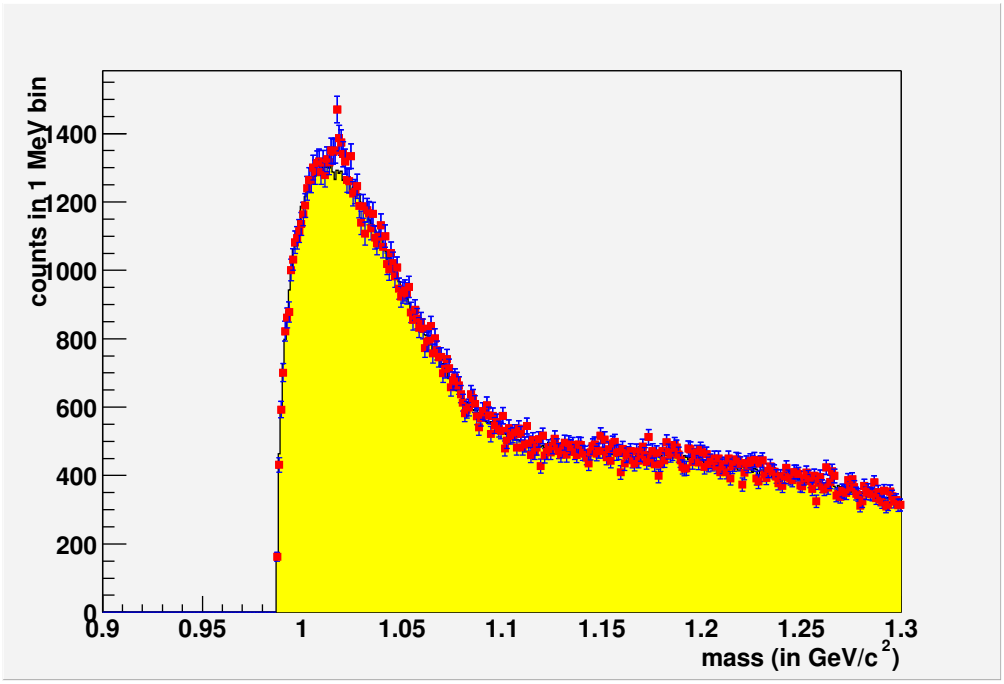

Figure 60: Signal and Combinatoric mass spectra in TOF–EMCal extracted by the UCR group for the 0–10% centrality class

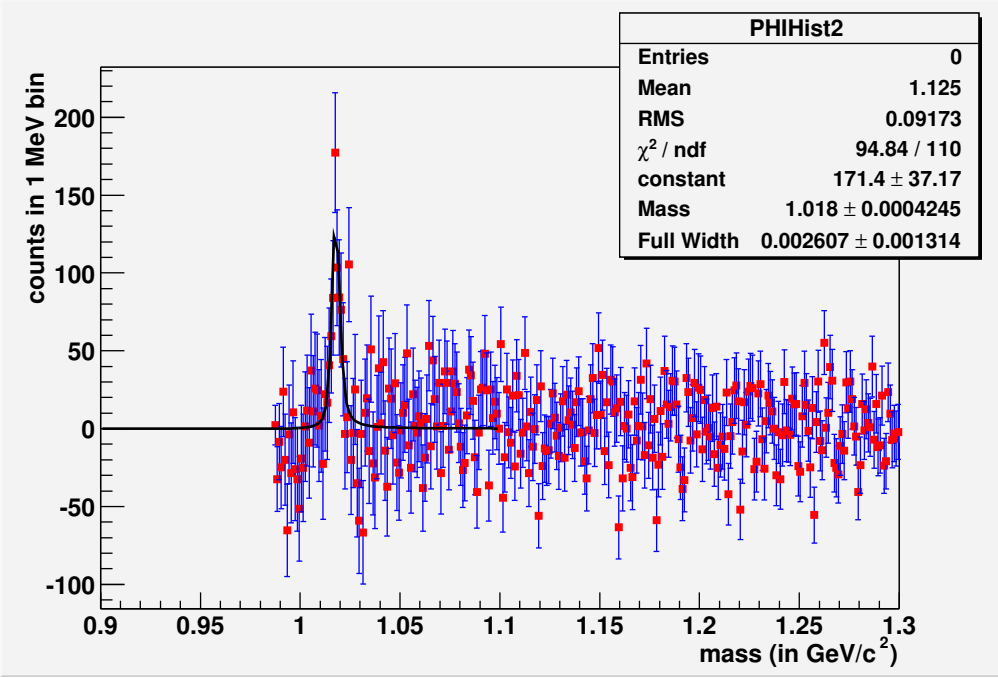

Figure 61: Invariant mass spectra in TOF–EMCal extracted by the UCR group for the 0–10% centrality class

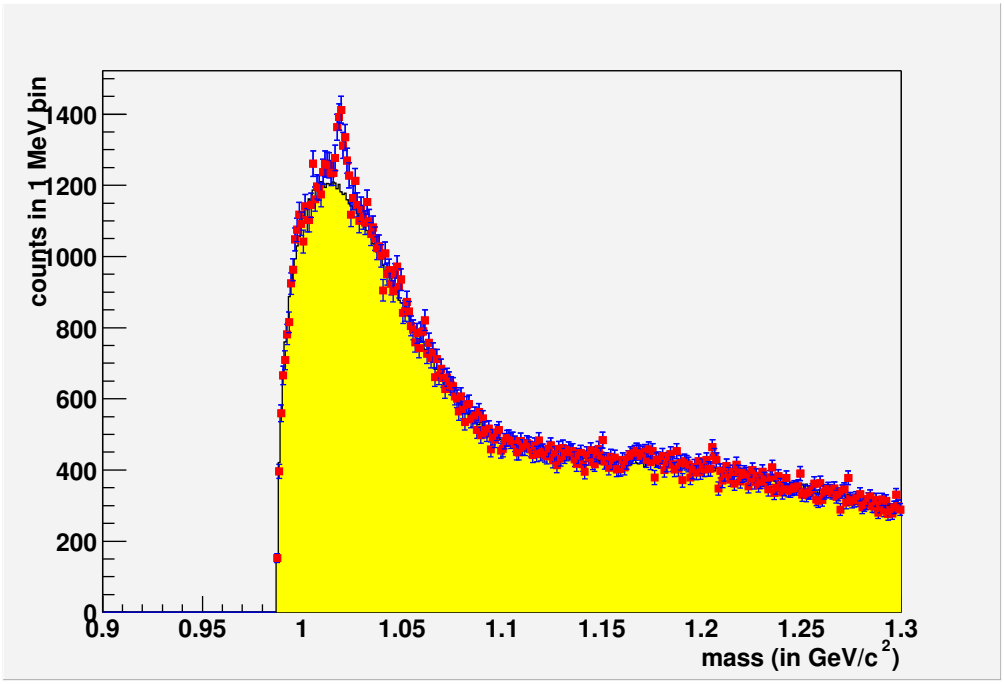

Figure 62: Signal and Combinatoric mass spectra in TOF–EMCal extracted by the UCR group for the 10–40% centrality class

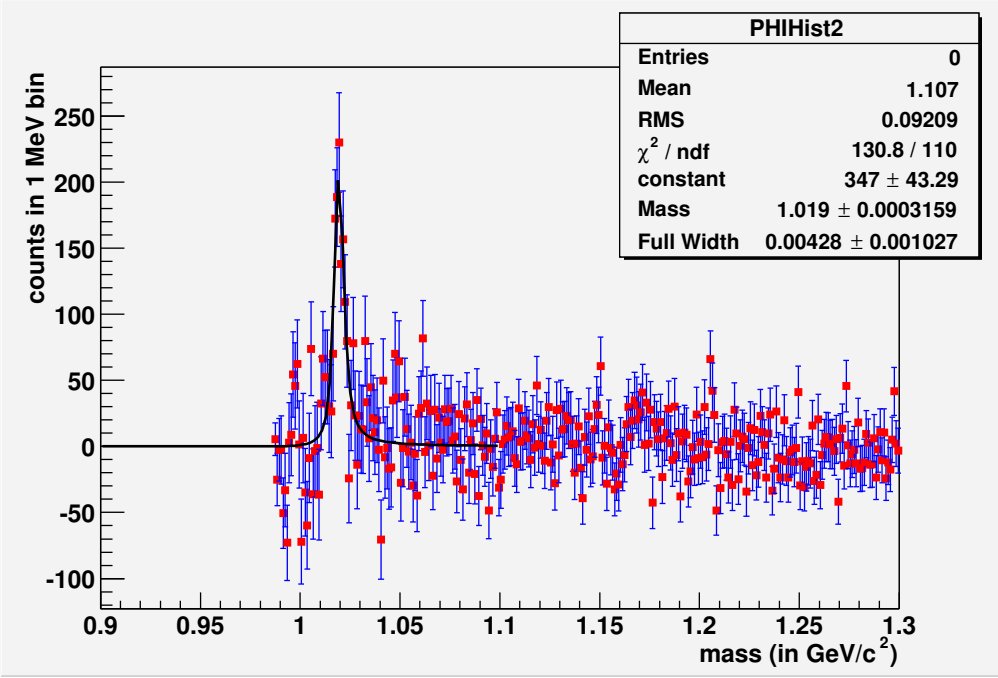

Figure 63: Invariant mass spectra in TOF–EMCal extracted by the UCR group for the 10–40% centrality class

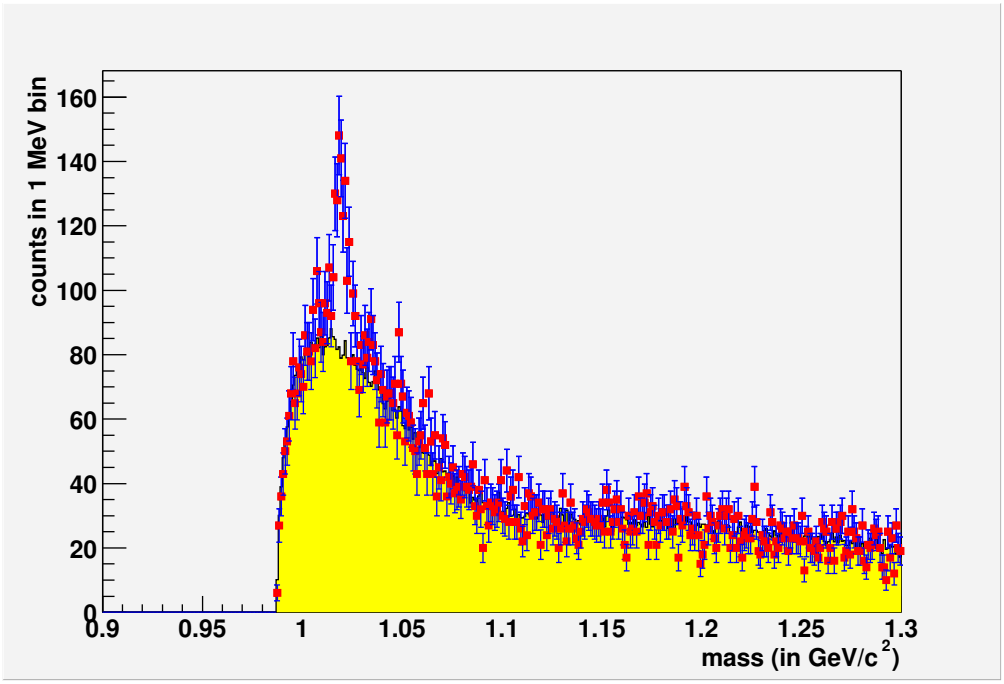

Figure 64: Signal and Combinatoric mass spectra in TOF–EMCal extracted by the UCR group for the 40–92% centrality class

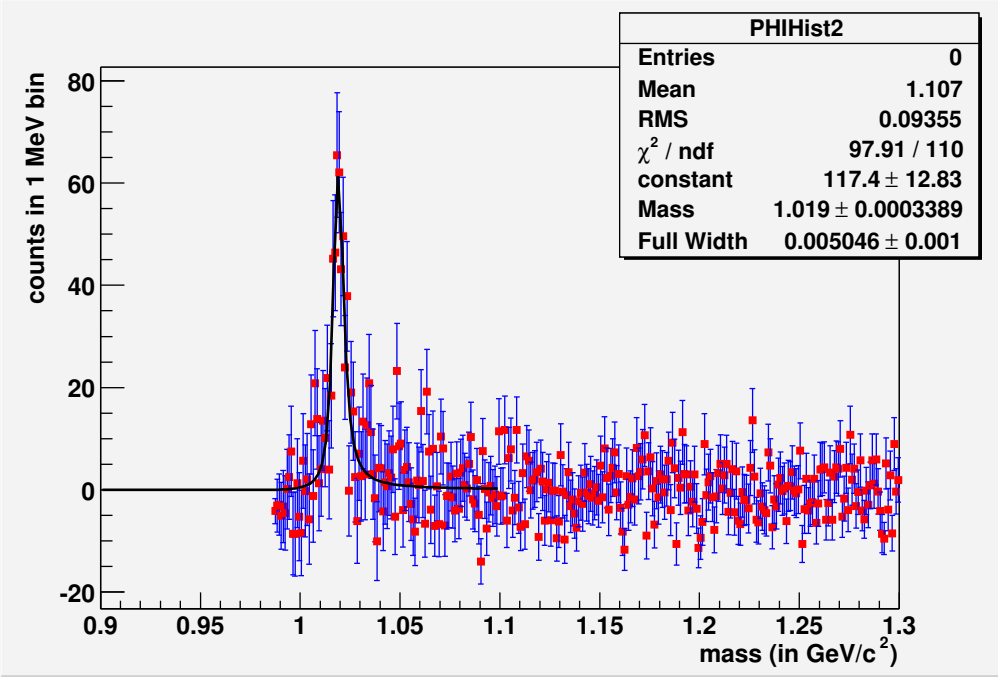

Figure 65: Invariant mass spectra in TOF–EMCal extracted by the UCR group for the 40–92% centrality class

H.5 Yield $dN/dy\,dm_T$ for TOF–EMCal pairs analyzed by UCR

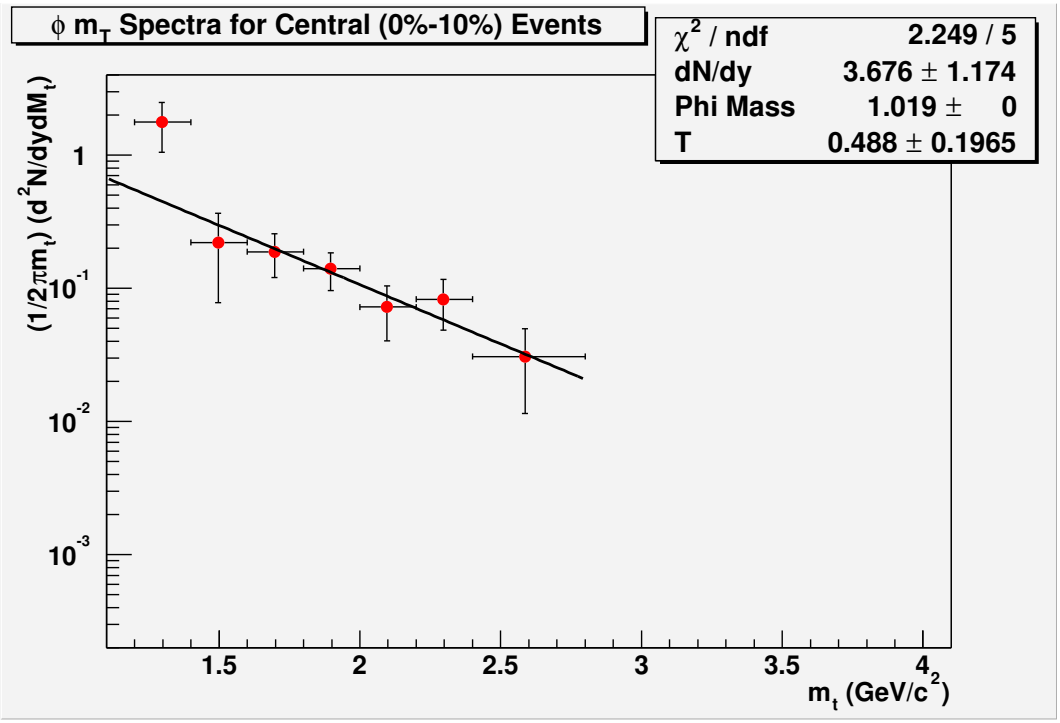

Figure 66: Yield in TOF–EMCal extracted by the UCR group for the 0–10% centrality class

H.6 Invariant mass spectra for EMCal–EMCal pairs analyzed by UCR

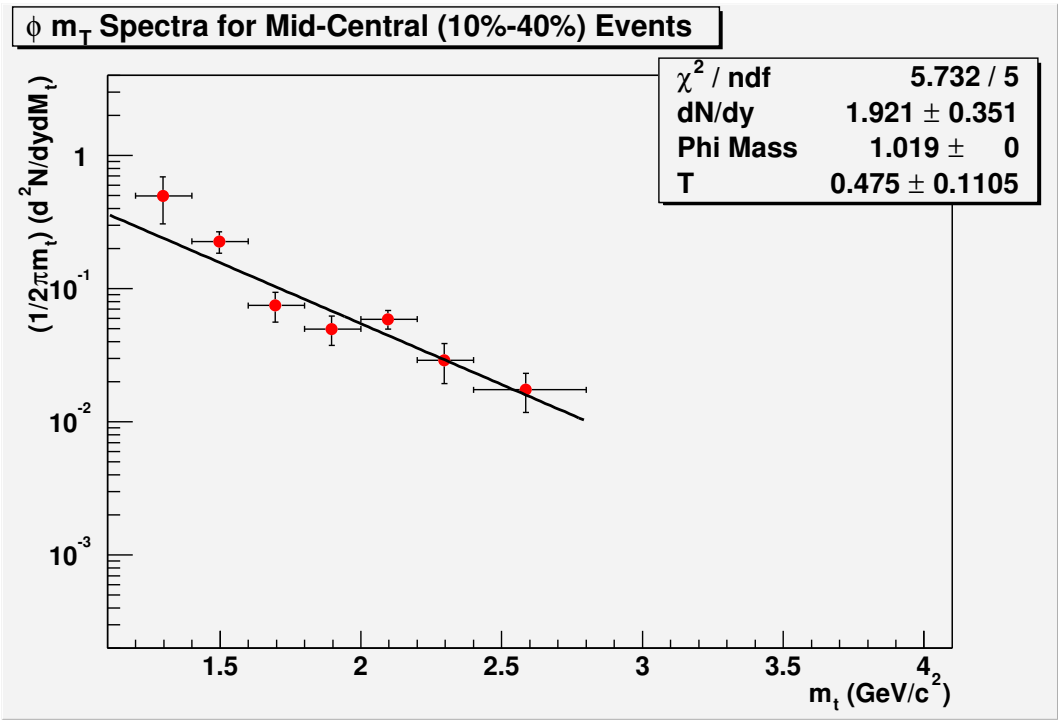

Figure 67: Yield in TOF–EMCal extracted by the UCR group for the 10–40% centrality class

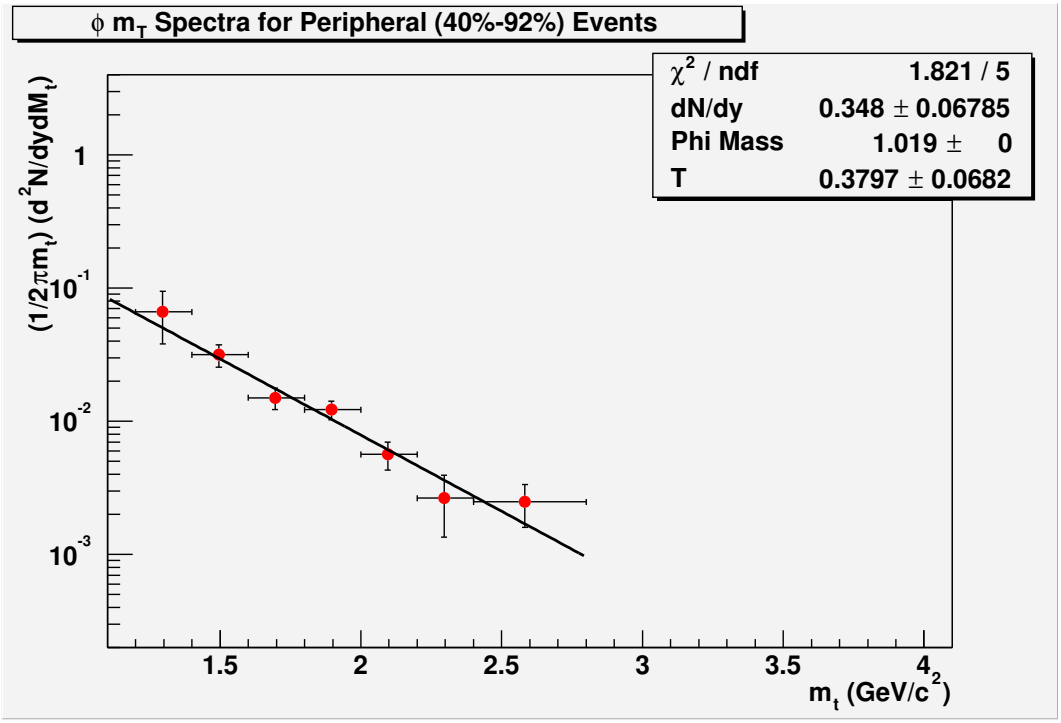

Figure 68: Yield in TOF–EMCal extracted by the UCR group for the 40–92% centrality class

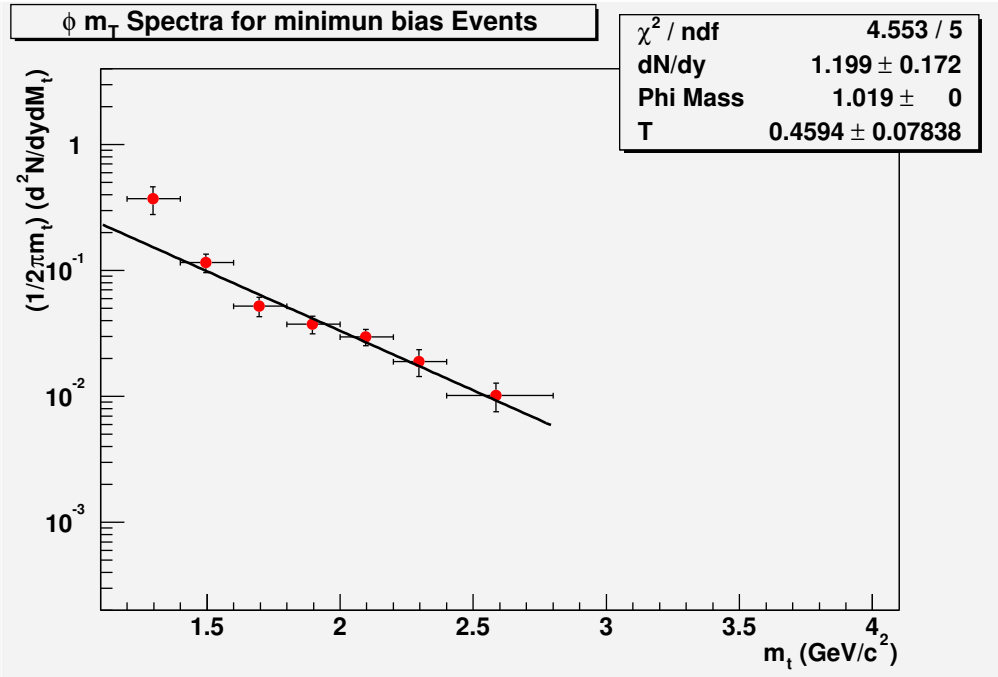

Figure 69: Yield in TOF–EMCal extracted by the UCR group for the minimum bias events

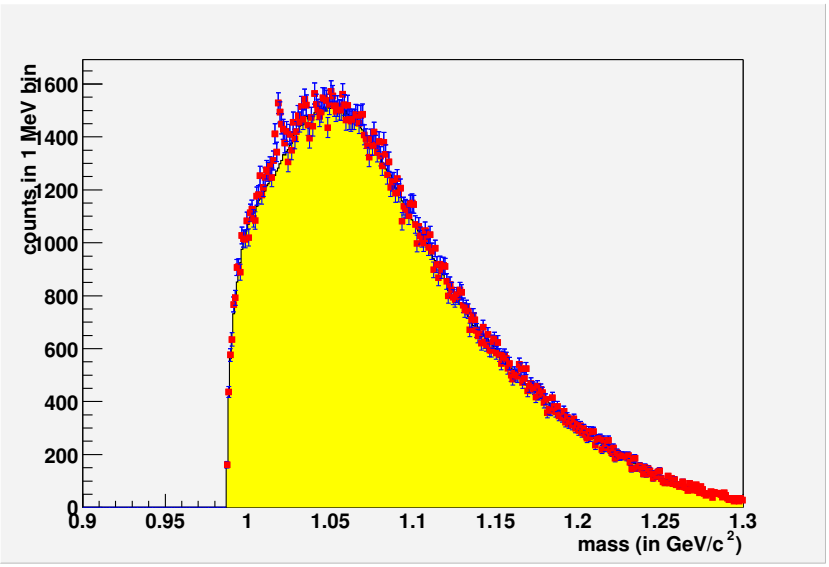

Figure 70: Signal and Combinatoric mass spectra in EMCal–EMCal extracted by the UCR group for the minimum bias events

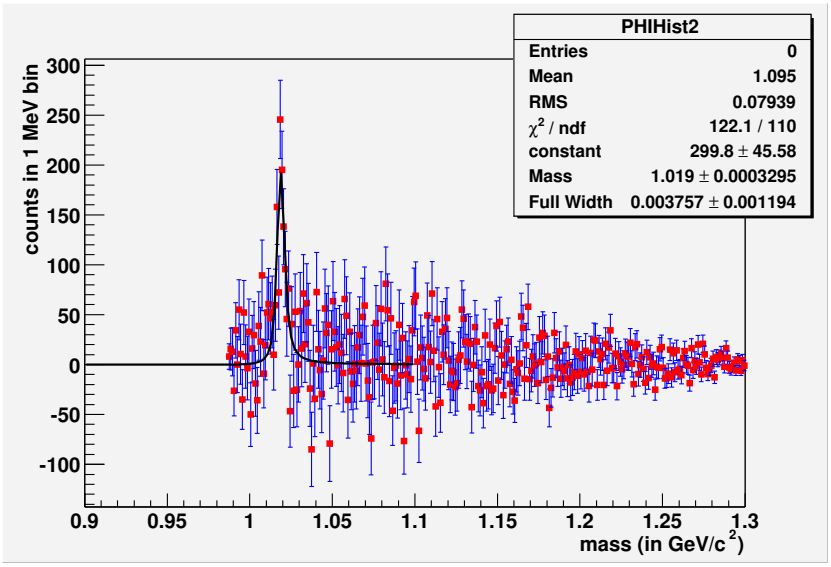

Figure 71: Invariant mass spectra in EMCal–EMCal extracted by the UCR group for the minium bias events

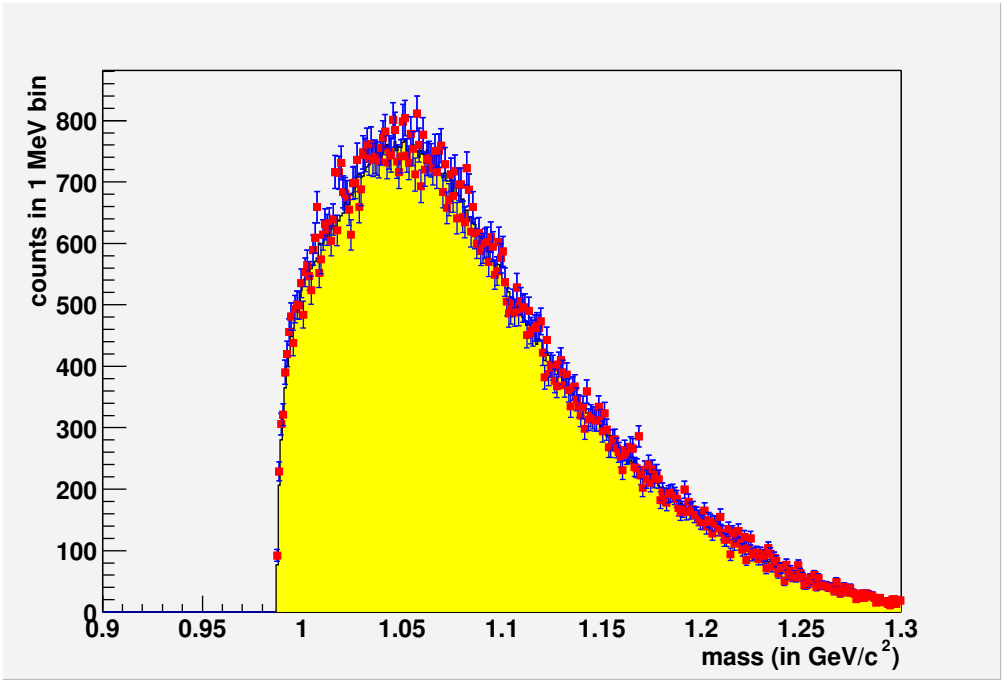

Figure 72: Signal and Combinatoric mass spectra in EMCal–EMCal extracted by the UCR group for the 0–10% centrality class

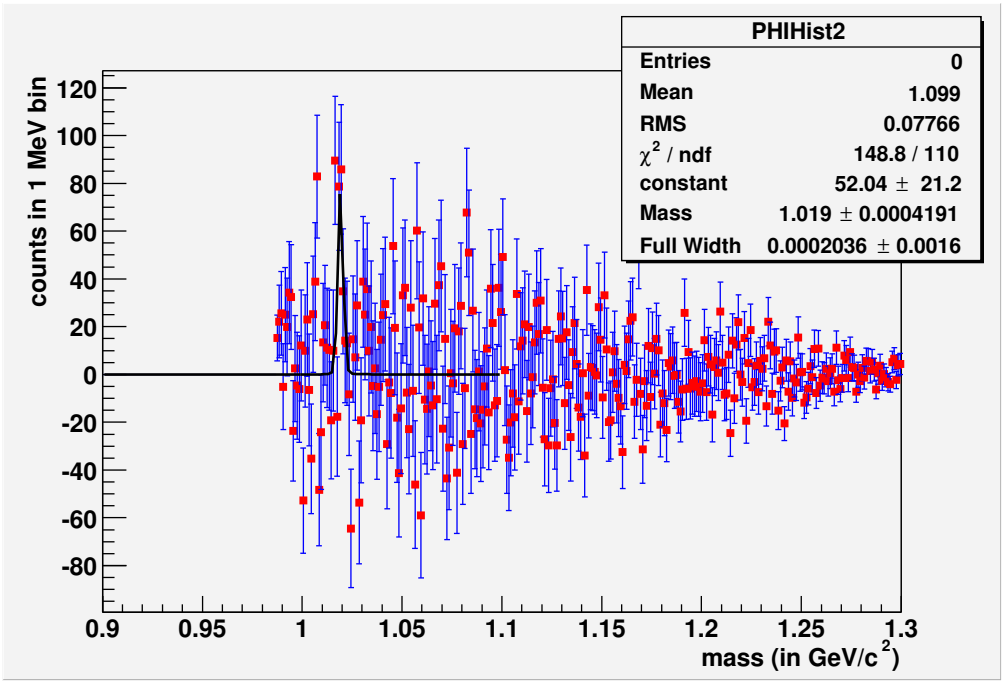

Figure 73: Invariant mass spectra in EMCal–EMCal extracted by the UCR group for the 0–10% centrality class

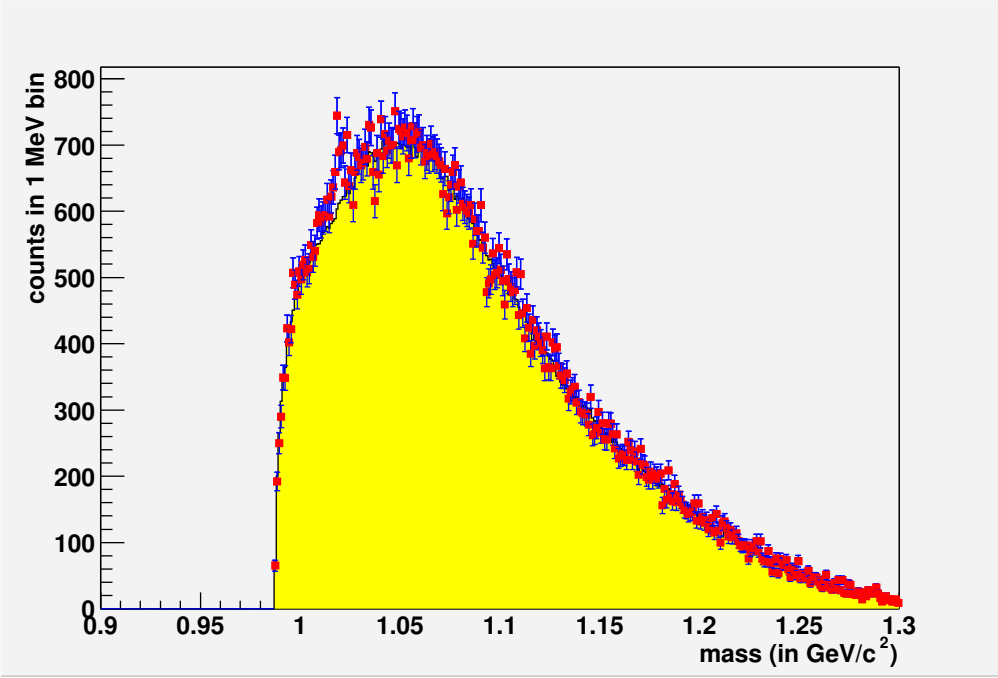

Figure 74: Signal and Combinatoric mass spectra in EMCal–EMCal extracted by the UCR group for the 10–40% centrality class

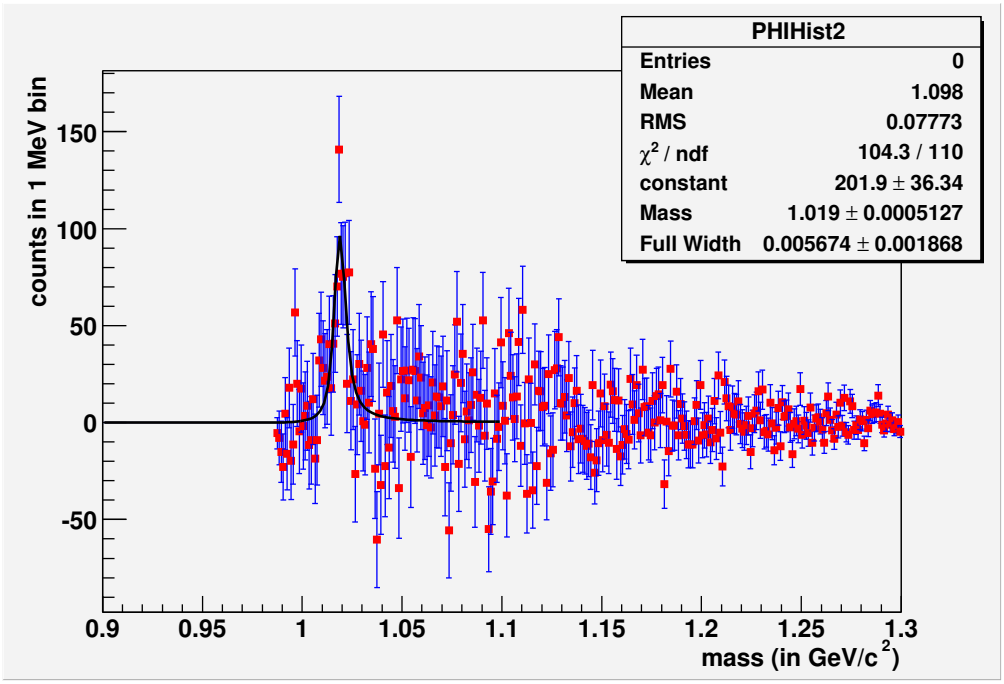

Figure 75: Invariant mass spectra in EMCal–EMCal extracted by the UCR group for the 10–40% centrality class

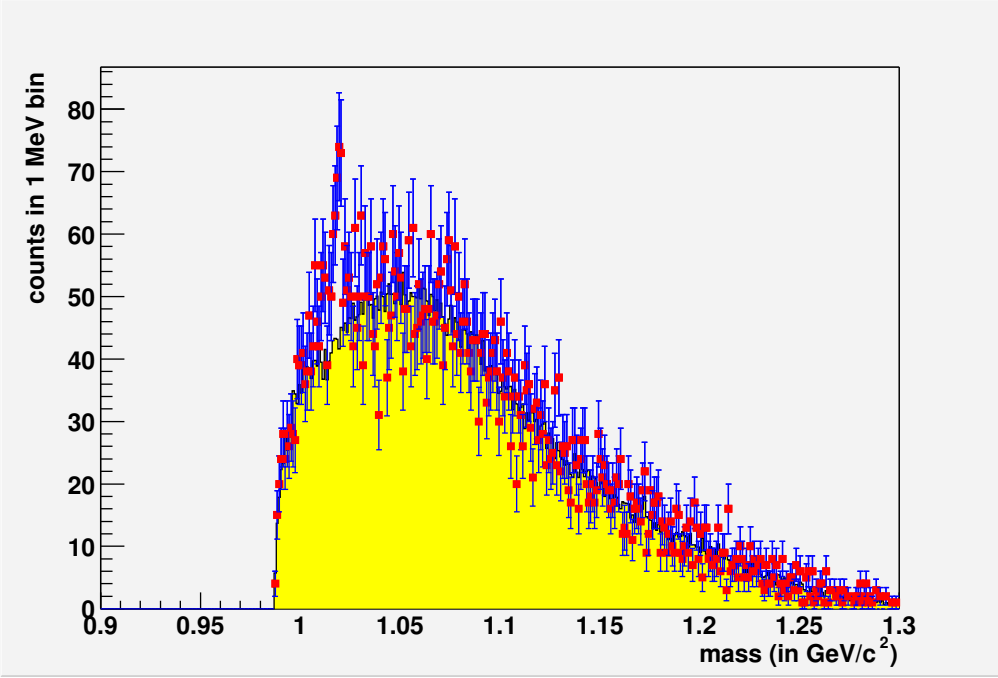

Figure 76: Signal and Combinatoric mass spectra in EMCal–EMCal extracted by the UCR group for the 40–92% centrality class

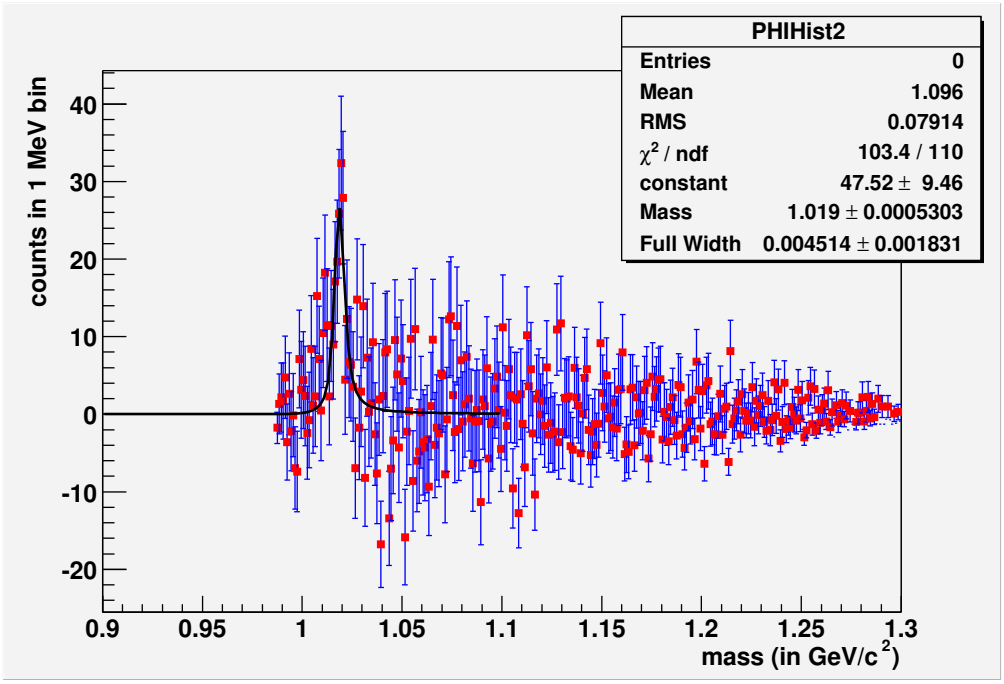

Figure 77: Invariant mass spectra in EMCal–EMCal extracted by the UCR group for the 40–92% centrality class

H.7 Yield $dN/dy\,dm_T$ for EMCal–EMCal pairs analyzed by UCR

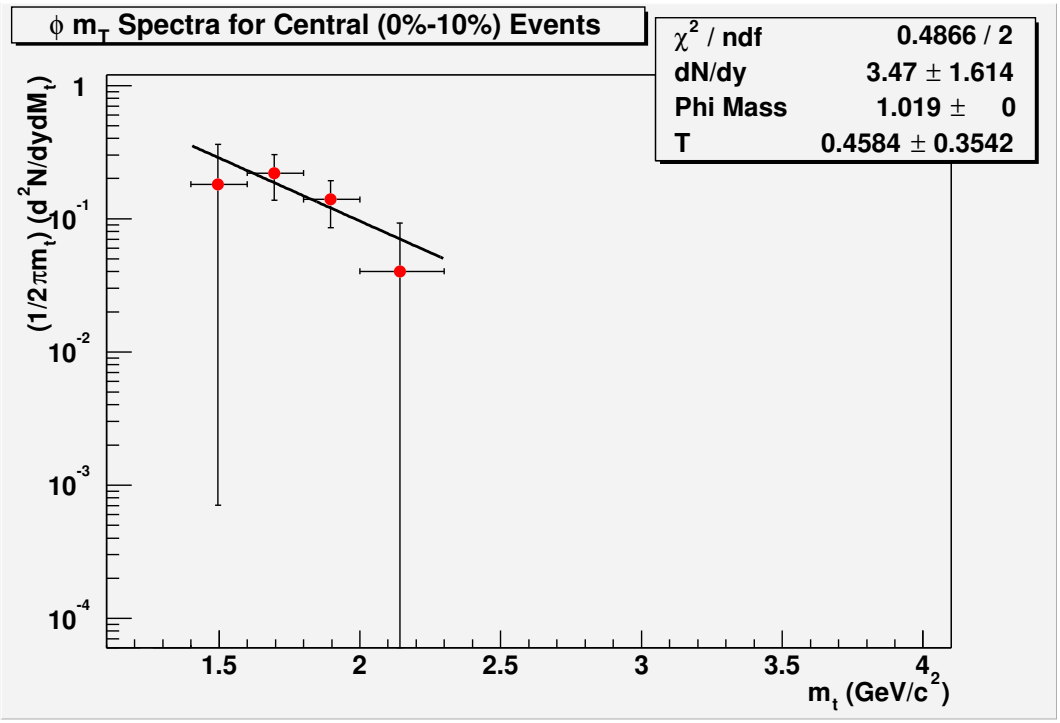

Figure 78: Yield in EMCal–EMCal extracted by the UCR group for the 0–10% centrality class

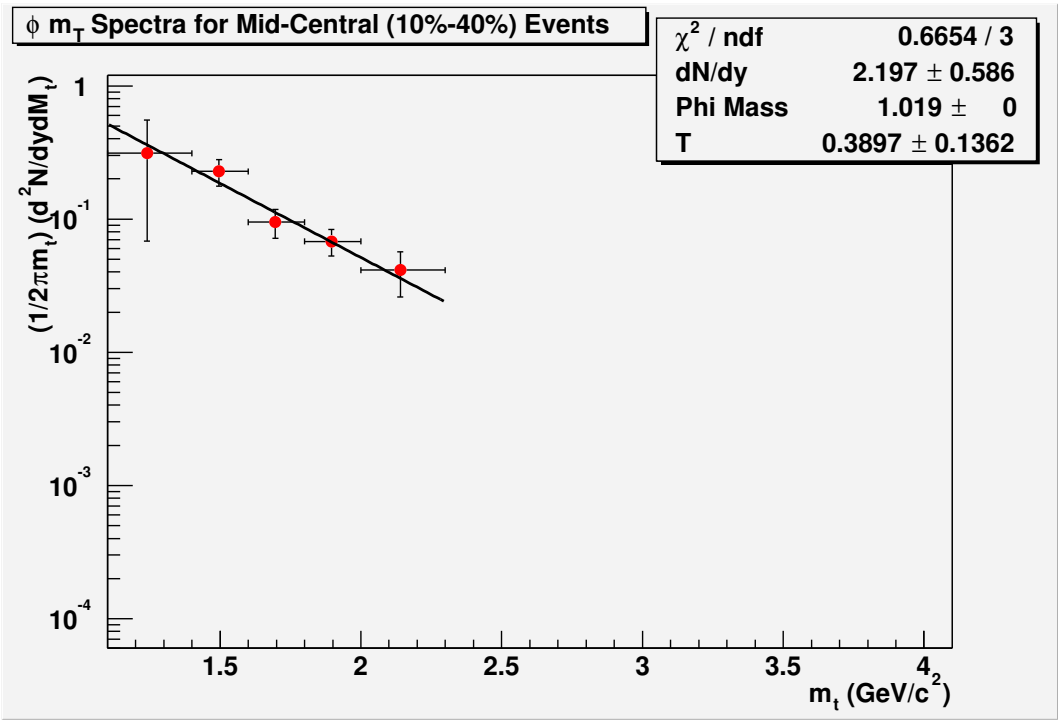

Figure 79: Yield in EMCal–EMCal extracted by the UCR group for the 10–40% centrality class

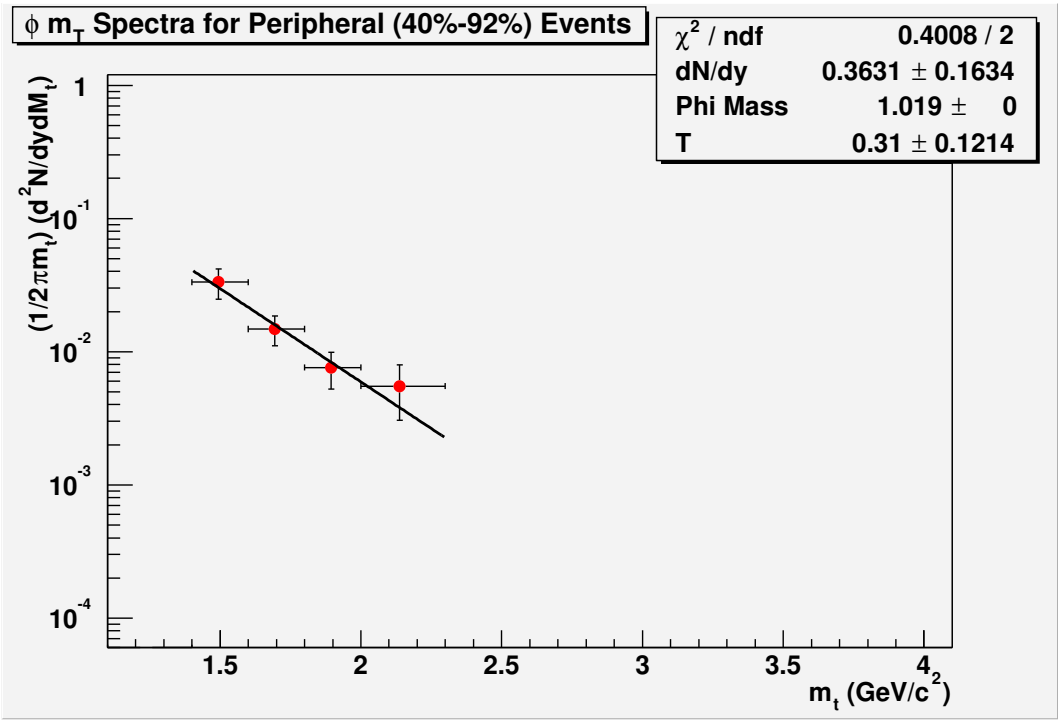

Figure 80: Yield in EMCal–EMCal extracted by the UCR group for the 40–92% centrality class

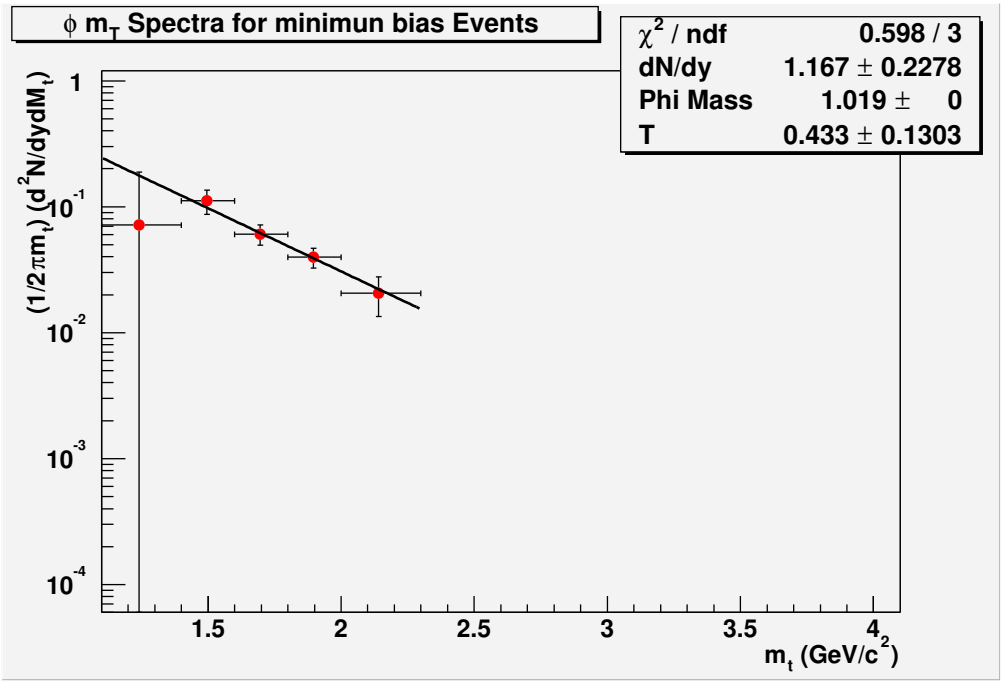

Figure 81: Yield in EMCal–EMCal extracted by the UCR group for the minimum bias events

I Analysis Results for the ϕ from the WIS group

I.1 Invariant mass spectra in TOF–TOF analyzed by WIS

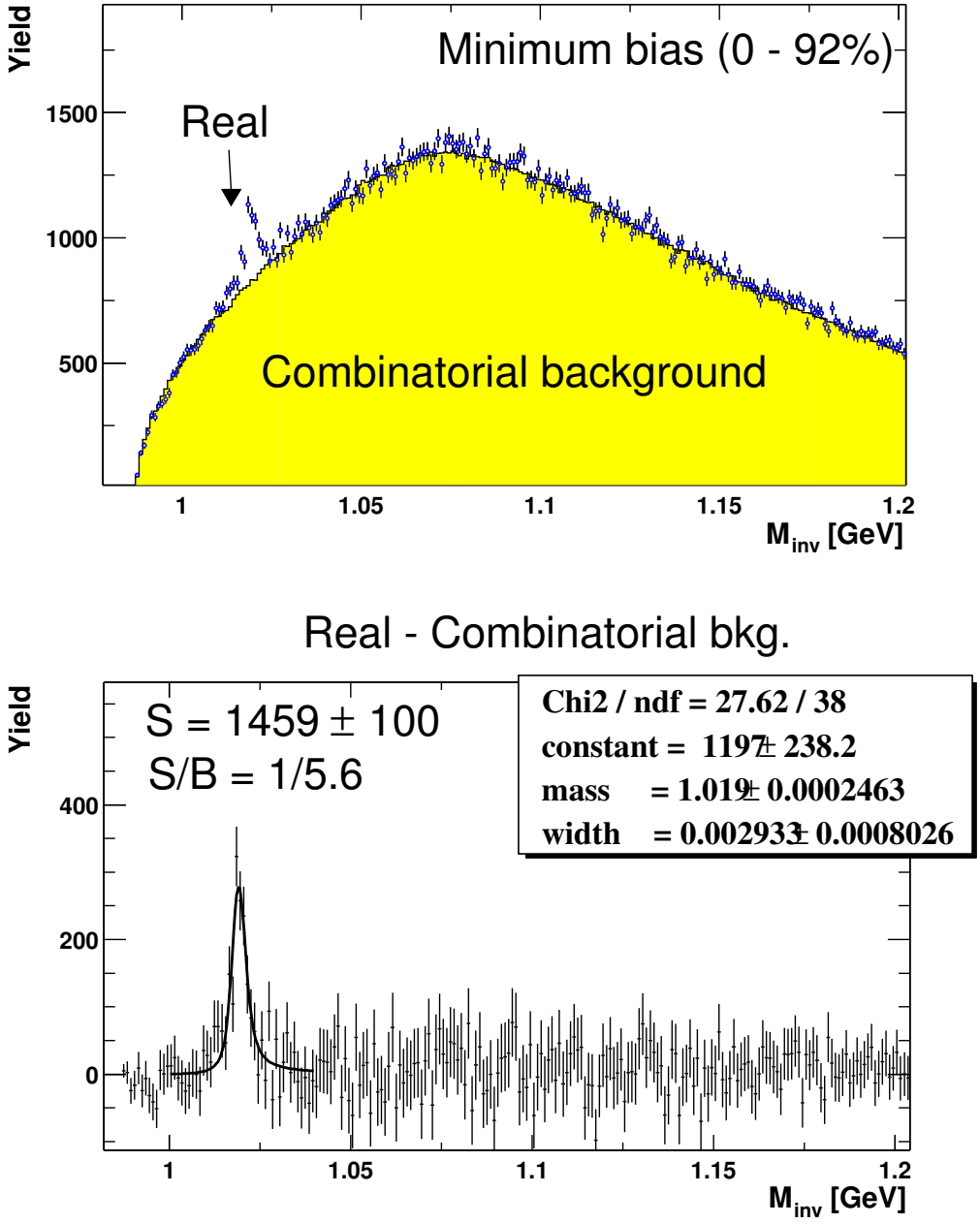

Figure 82: Invariant mass spectra in TOF–TOF extracted by the WIS group for the minimum bias events

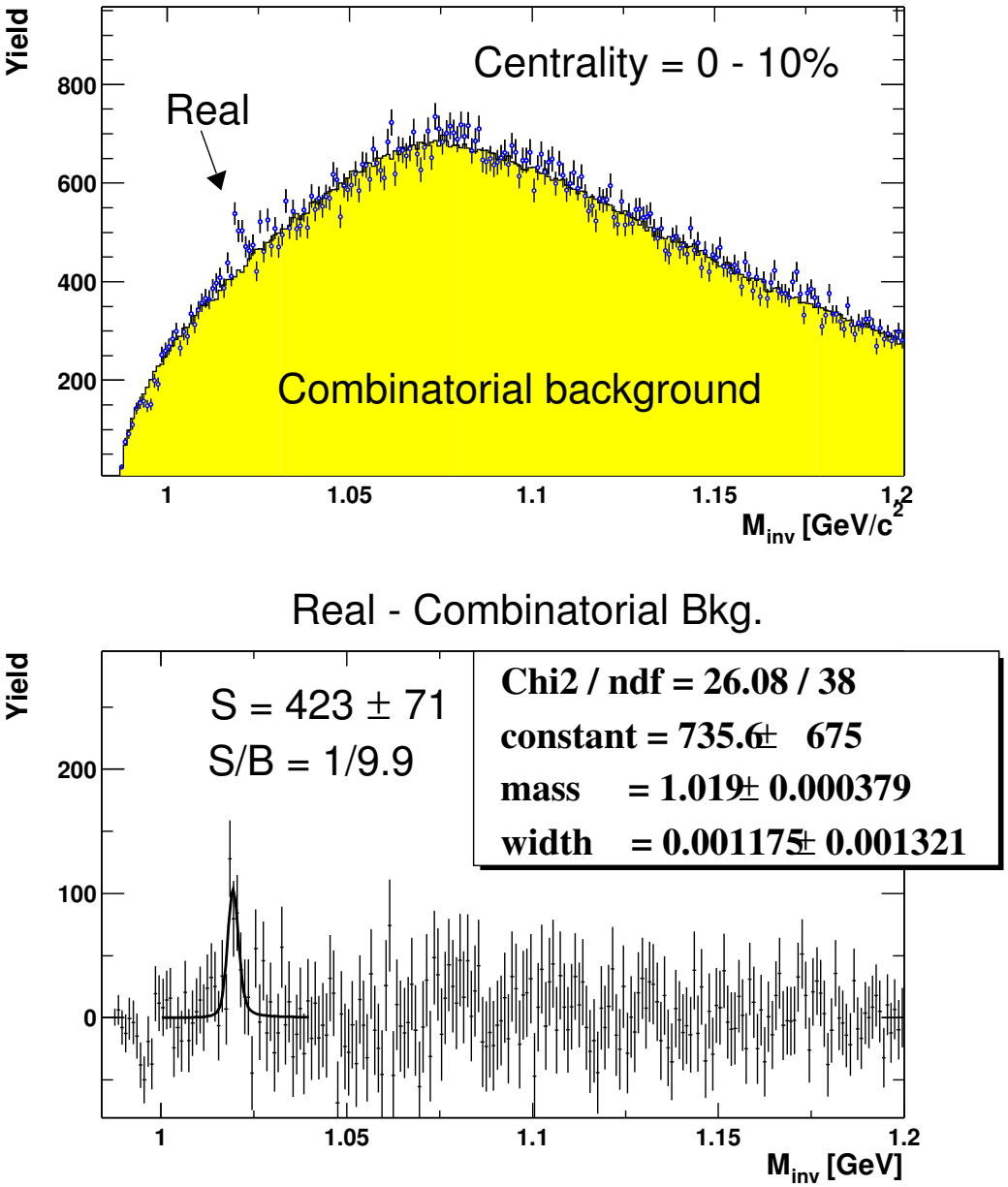

Figure 83: Invariant mass spectra in TOF–TOF extracted by the WIS group for the 0–10% centrality class

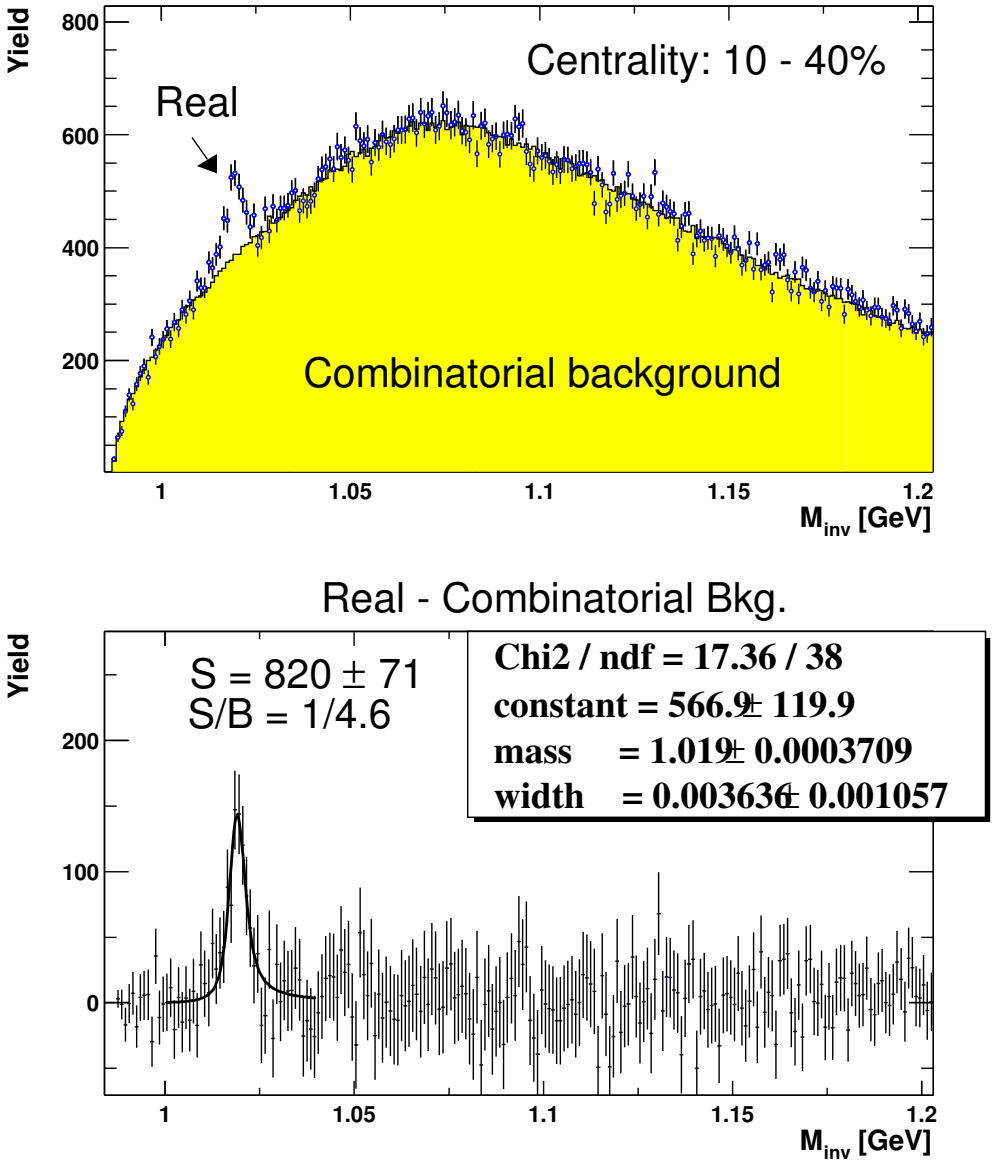

Figure 84: Invariant mass spectra in TOF–TOF extracted by the WIS group for the 10–40% centrality class

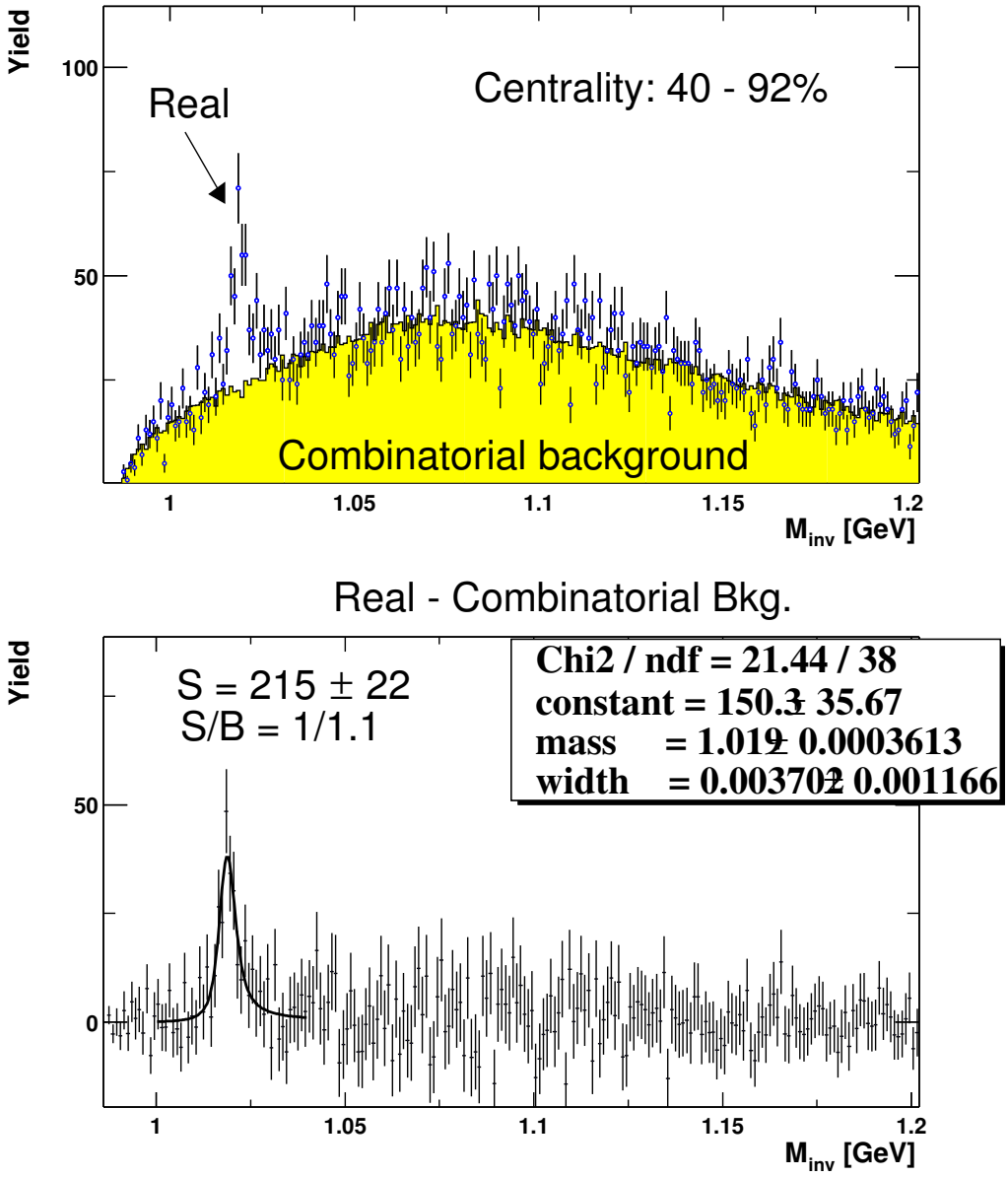

Figure 85: Invariant mass spectra in TOF–TOF extracted by the WIS group for the 40–92% centrality class

I.2 Yield $dN/dy\,dm_T$ in TOF–TOF analyzed by WIS

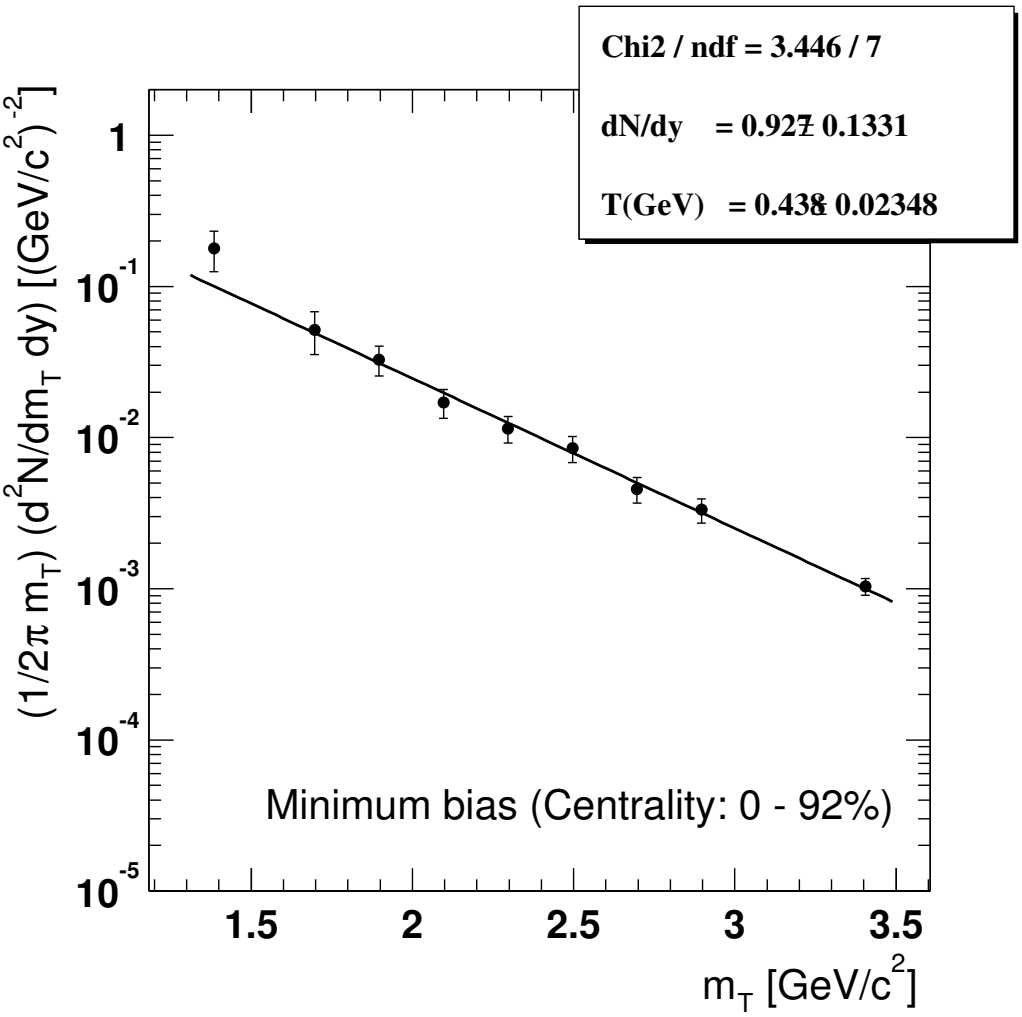

Figure 86: Yield in TOF–TOF extracted by the WIS group for the minimum bias events

I.3 Centrality dependence of dN/dy and T

We measured dN/dy and T by fitting the m_T spectra for five different centrality bins, 0 - 10%, 10 - 20%, 20 - 40%, 40-60%, and 60 - 92%.

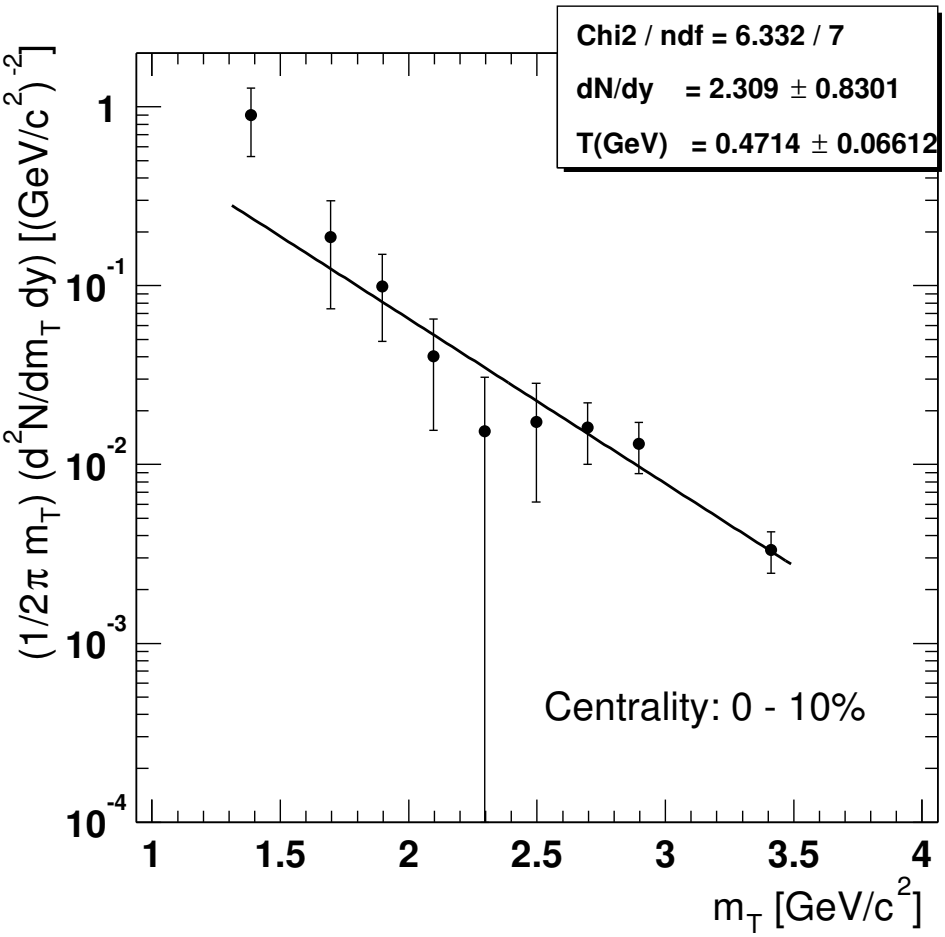

Figure 87: Yield in TOF–TOF extracted by the WIS group for the 0–10% centrality class

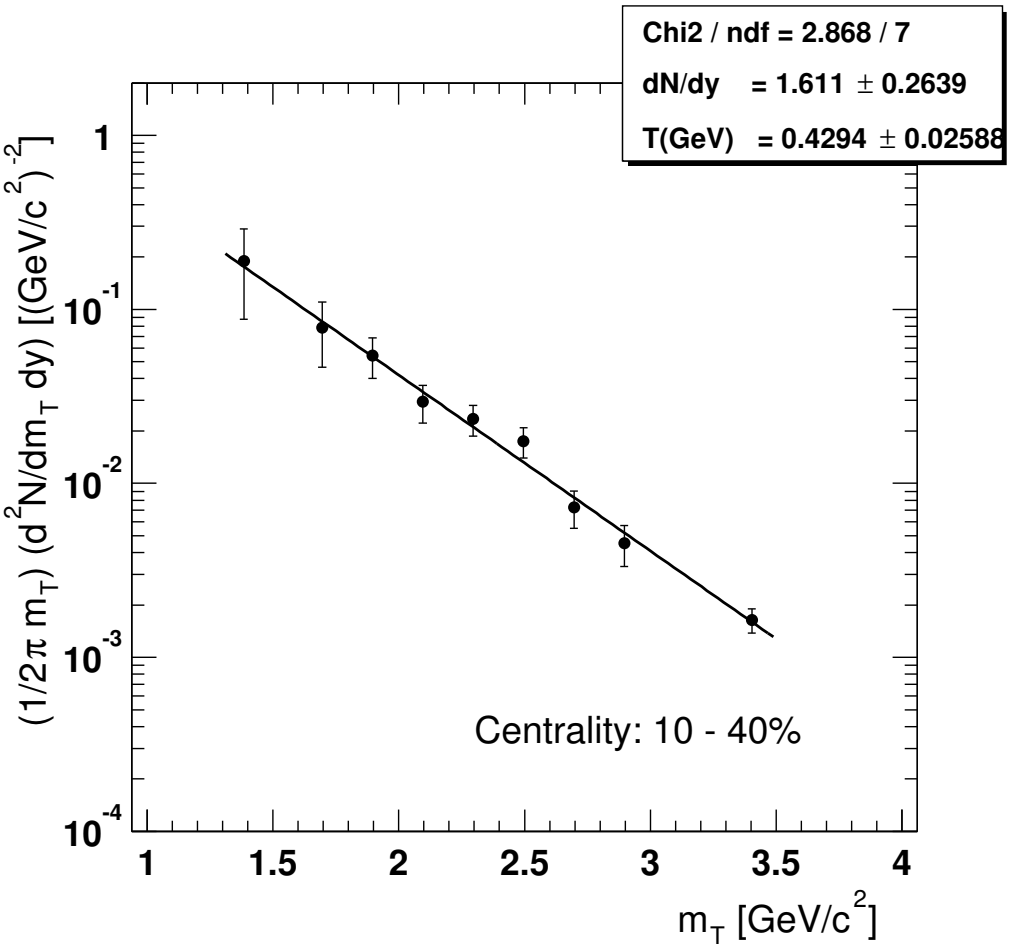

Figure 88: Yield in TOF–TOF extracted by the WIS group for the 10–40% centrality class

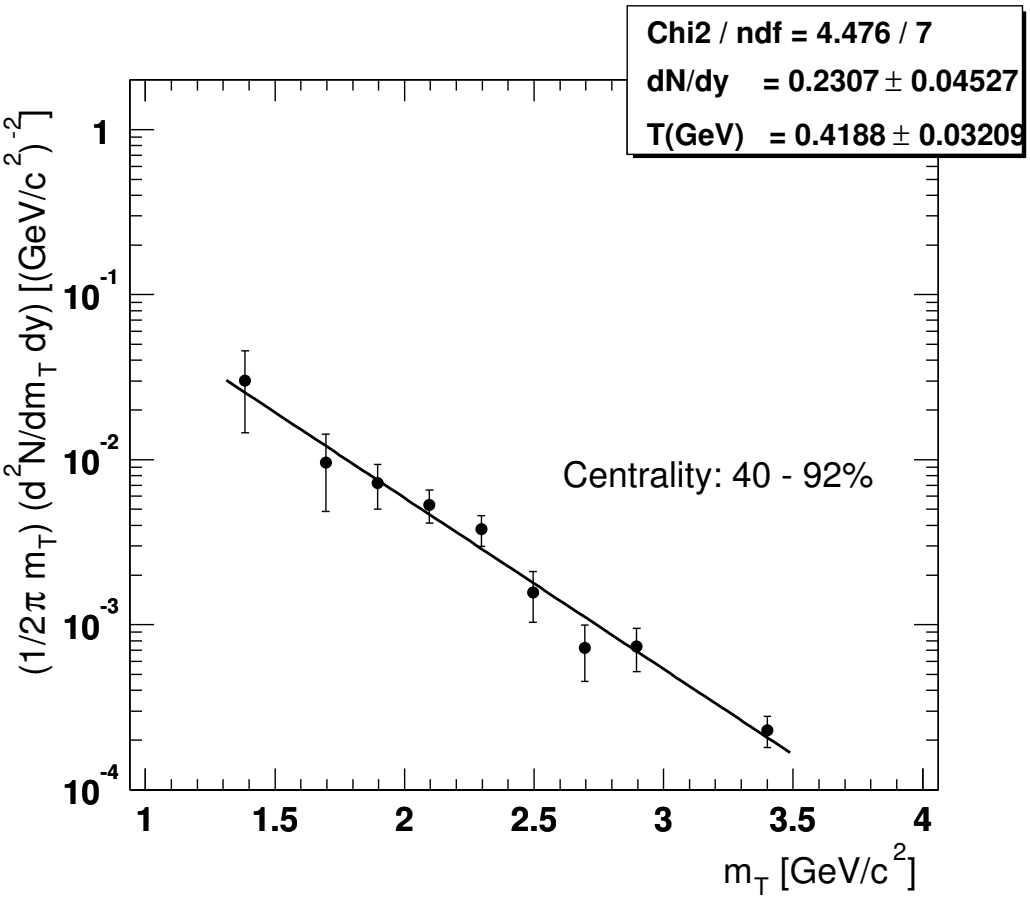

Figure 89: Yield in TOF–TOF extracted by the WIS group for the 40–92% centrality class

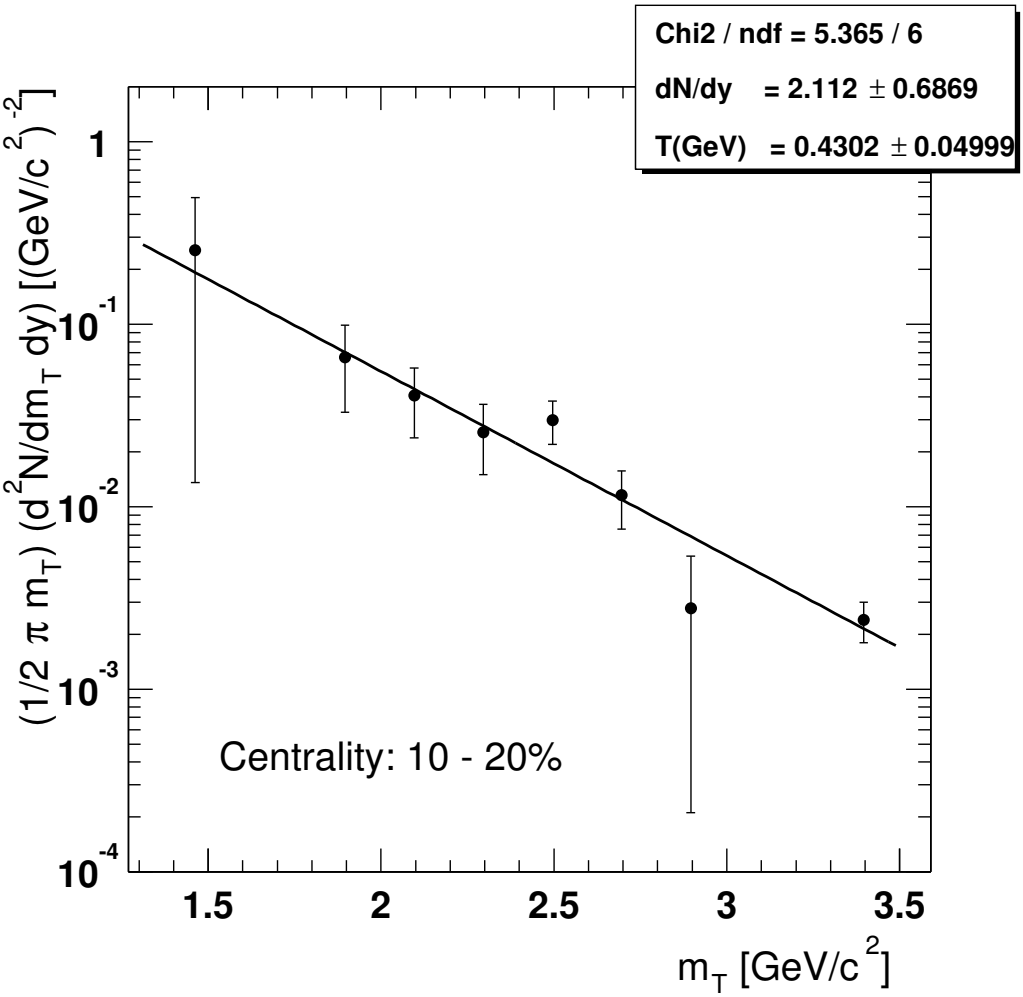

Figure 90: Yield in TOF–TOF extracted by the WIS group for the 10–20% centrality class

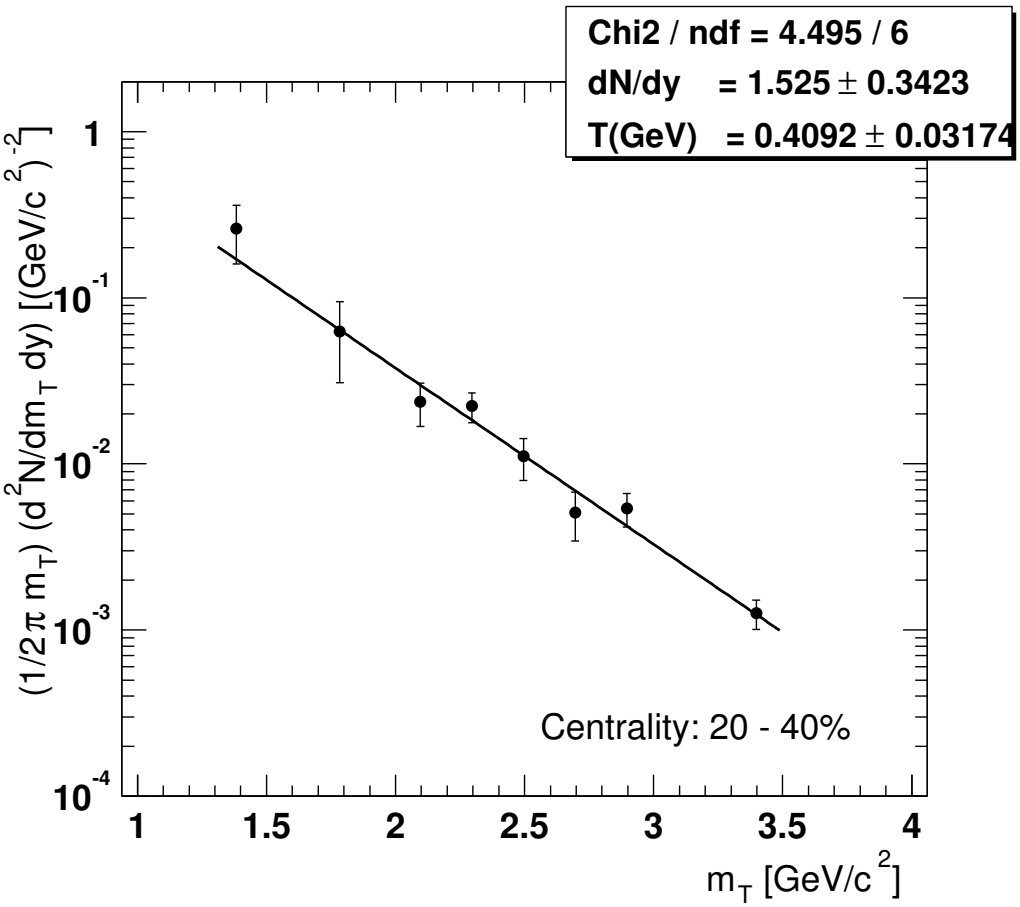

Figure 91: Yield in TOF–TOF extracted by the WIS group for the 20–40% centrality class

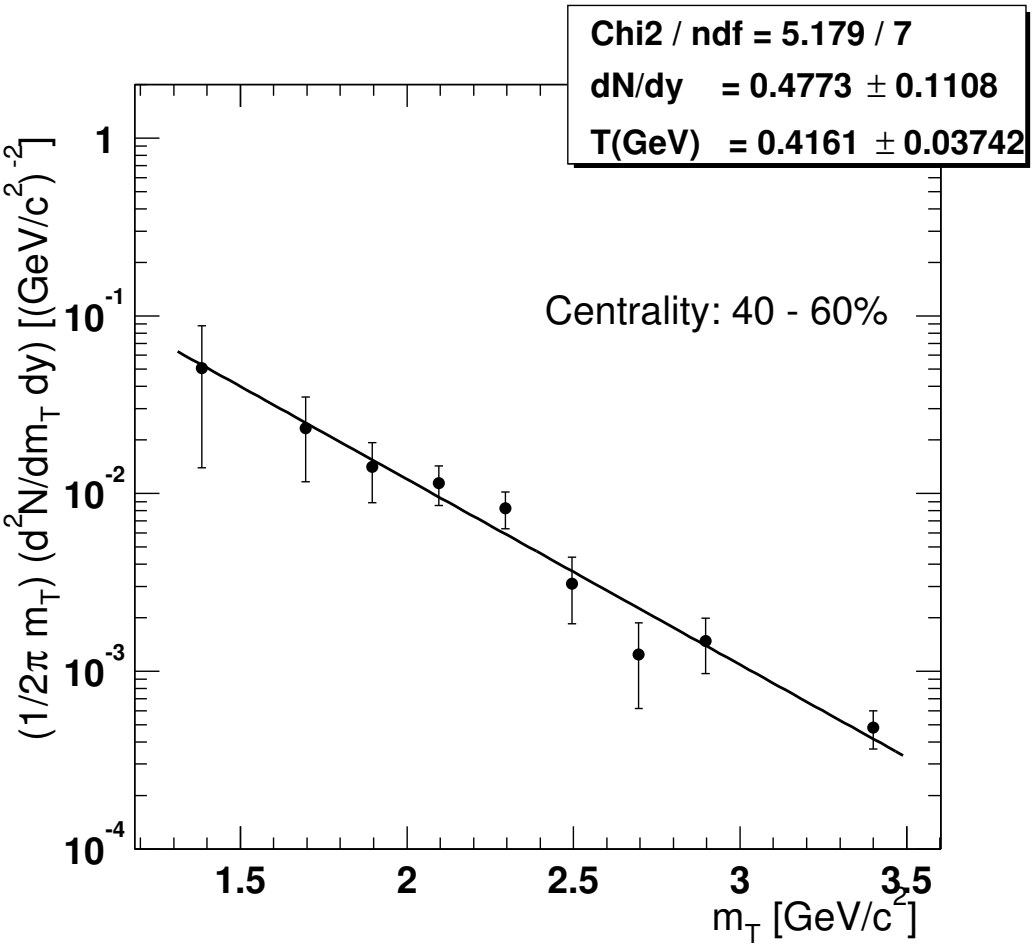

Figure 92: Yield in TOF–TOF extracted by the WIS group for the 40–60% centrality class

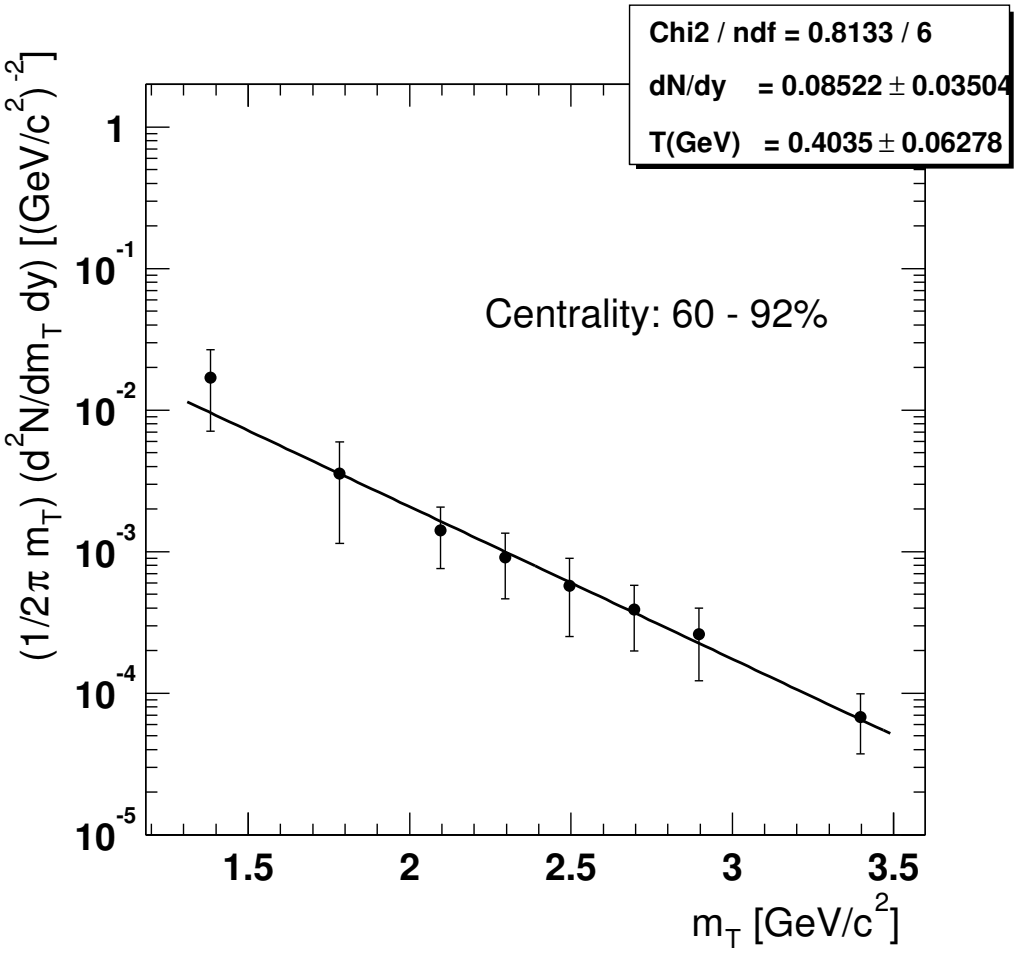

Figure 93: Yield in TOF–TOF extracted by the WIS group for the 60–92% centrality class

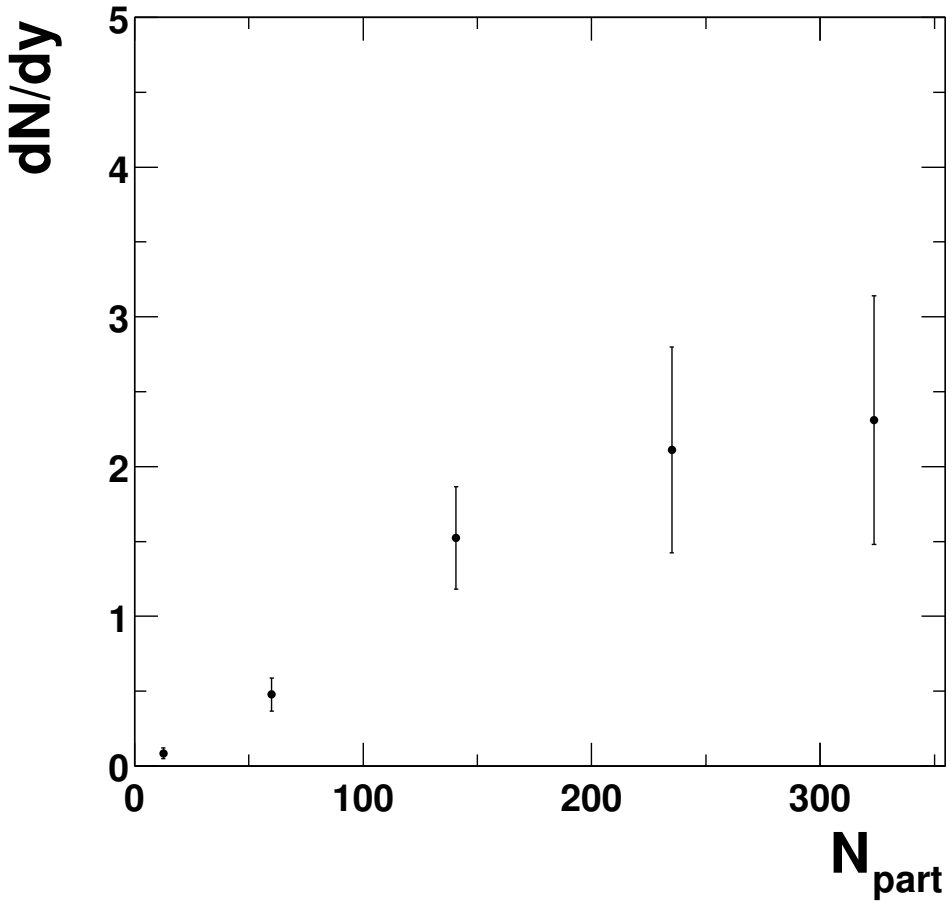

Figure 94: dN/dy vs. number of participants

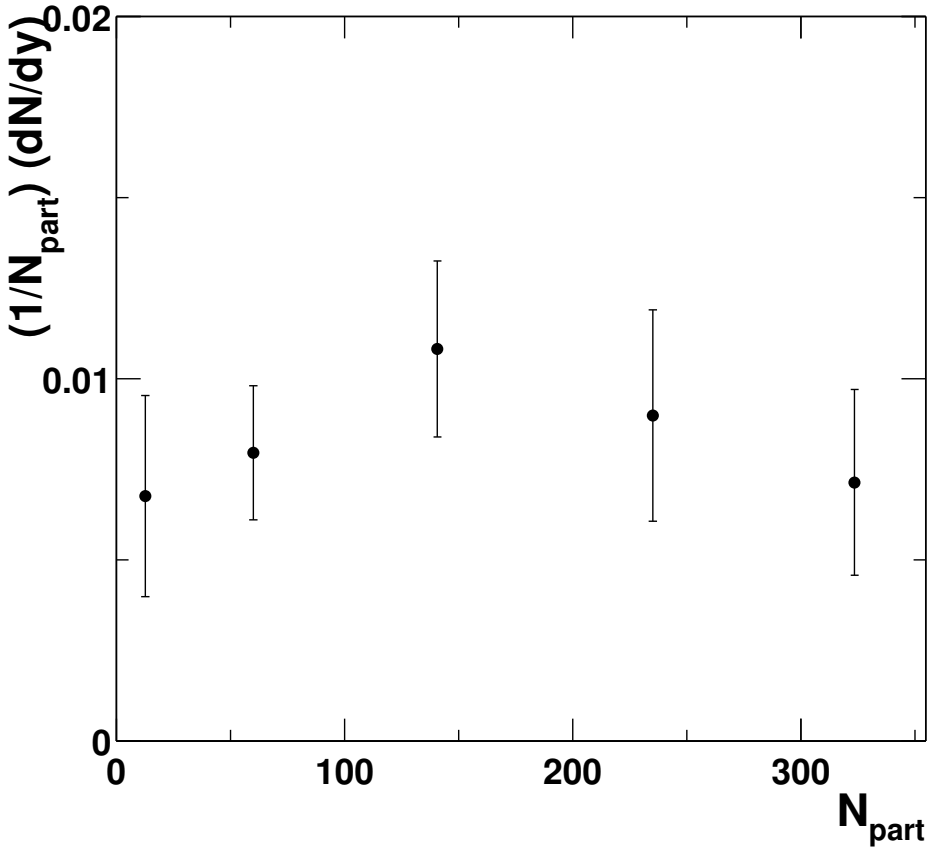

Figure 95: $(1/N_{part})$ (dN/dy) vs. number of participants

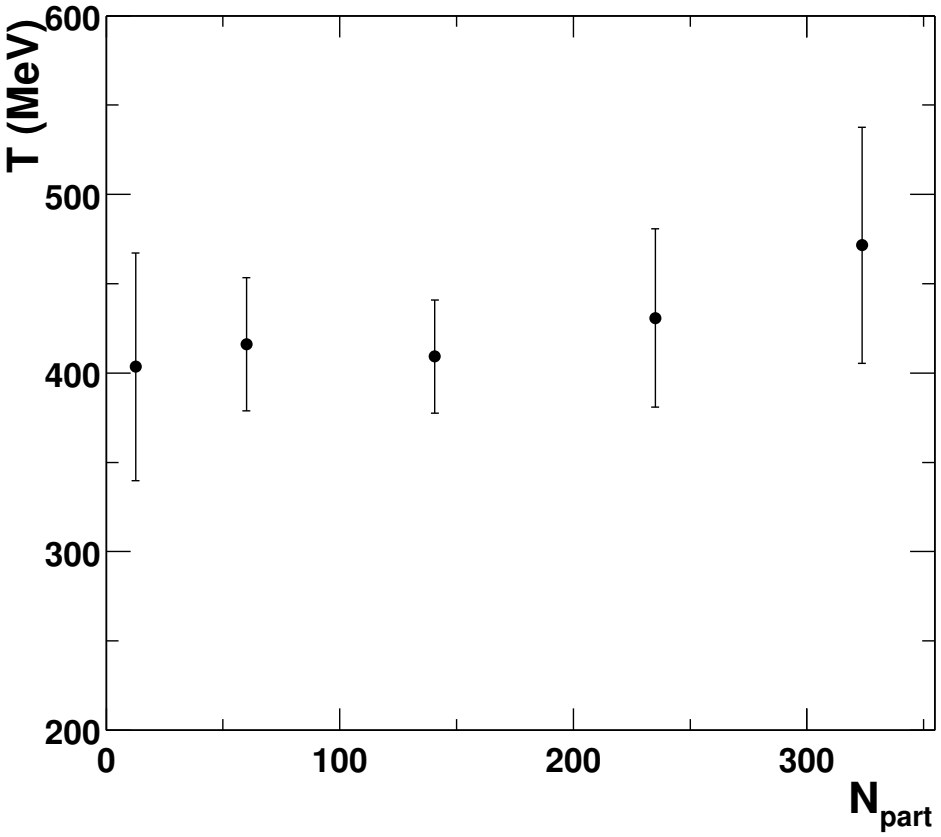

Figure 96: Temperature vs. number of participants

I.4 Invariant mass spectra in East - East analyzed by WIS

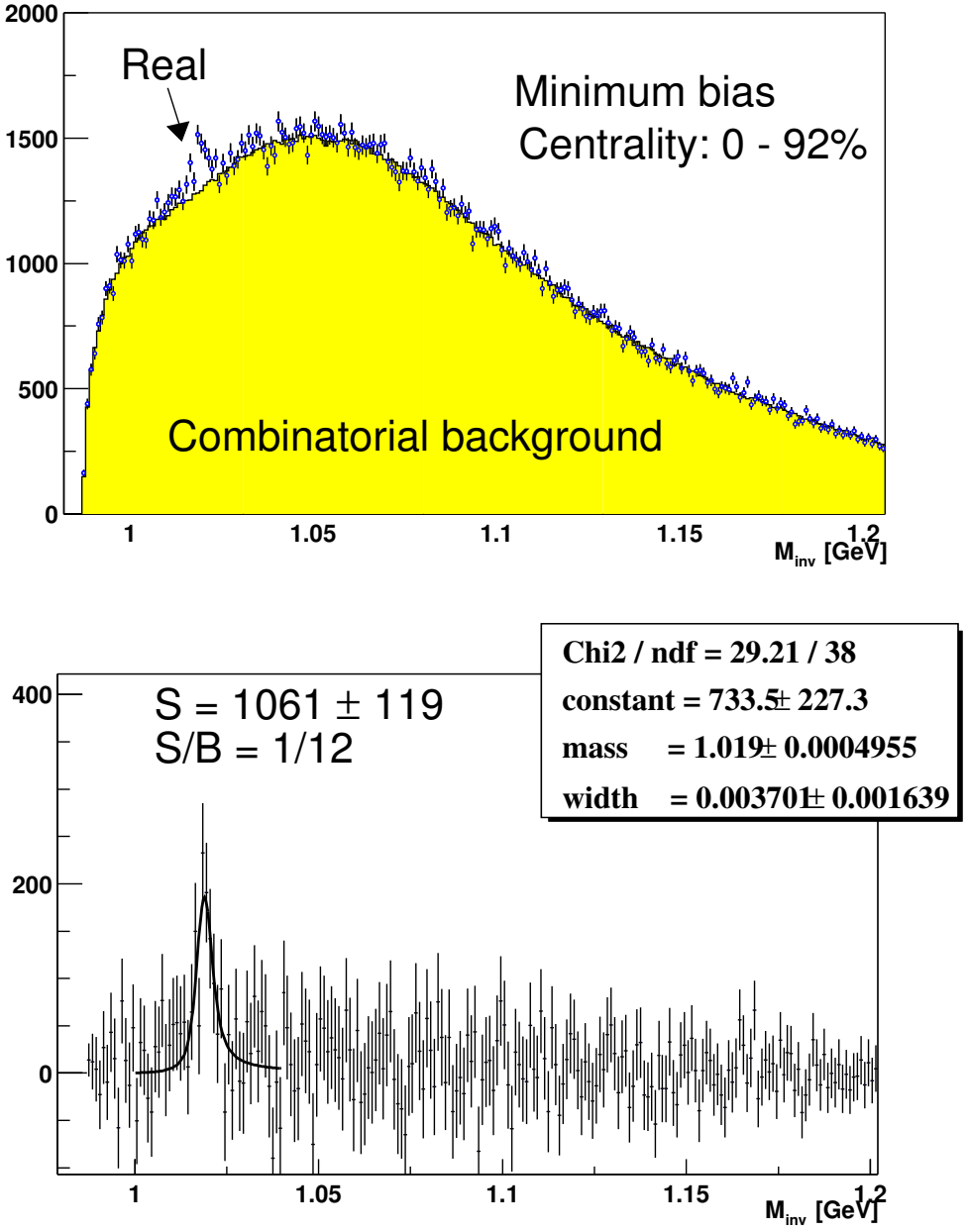

Figure 97: Invariant mass spectra in East-East extracted by the WIS group for the minimum bias events

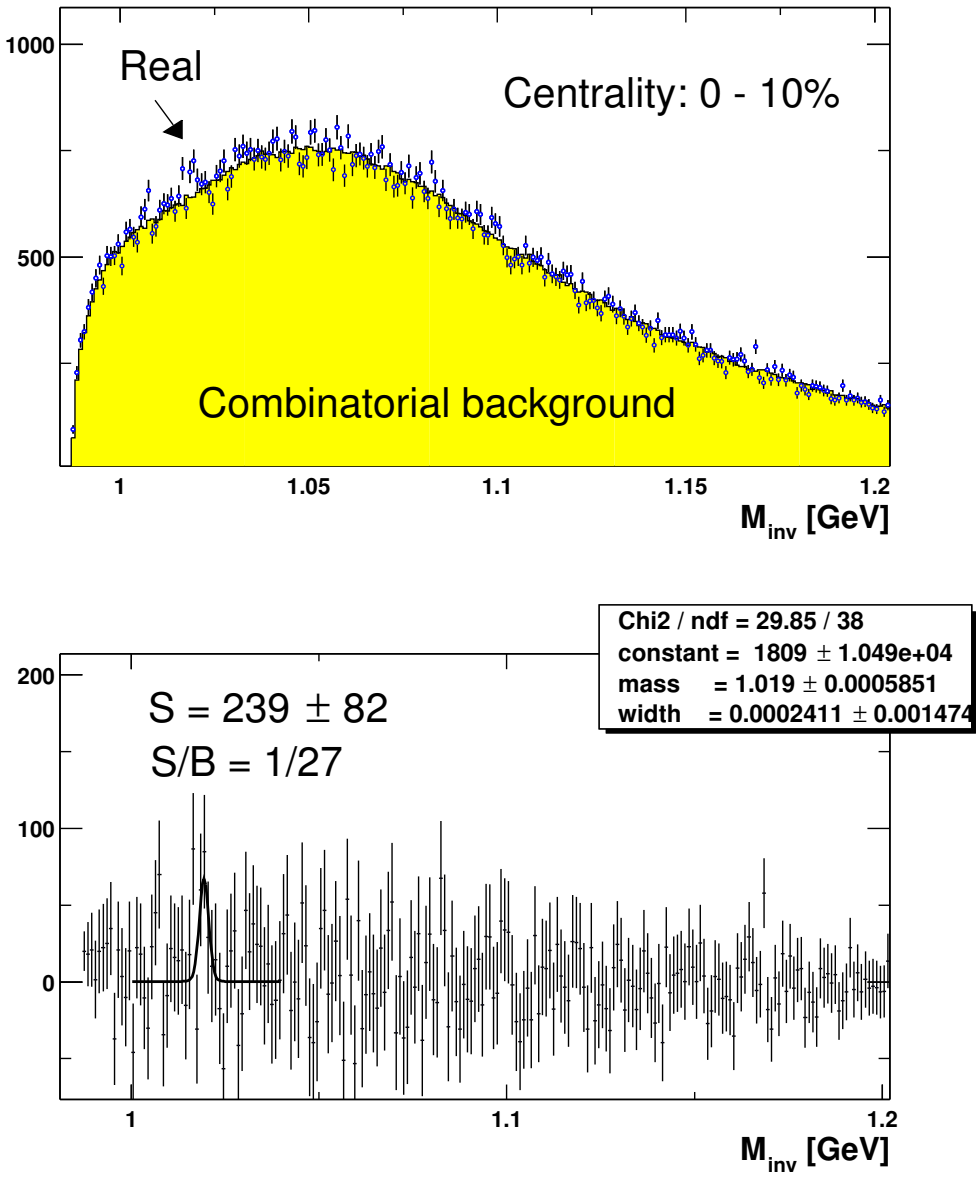

Figure 98: Invariant mass spectra in East-East extracted by the WIS group for the 0–10% centrality class

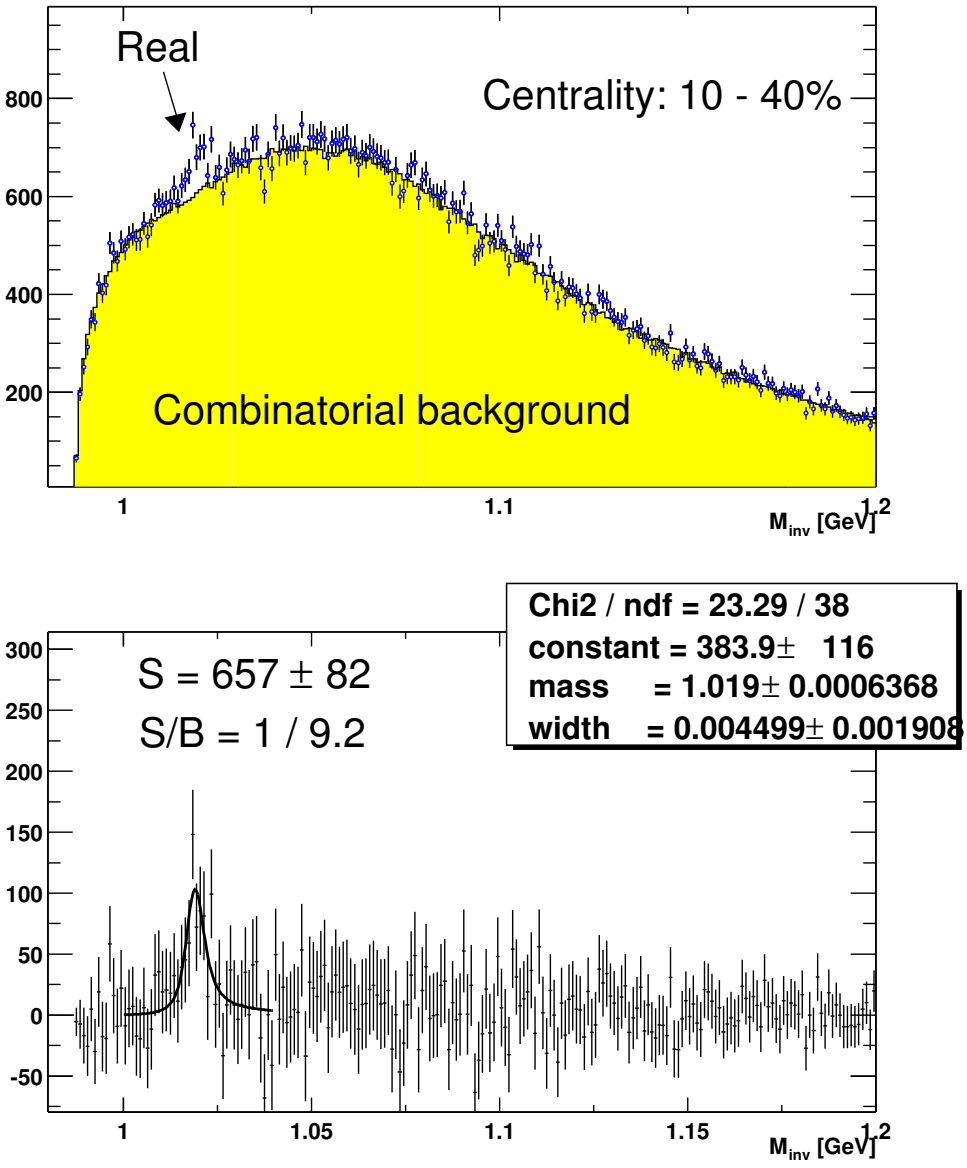

Figure 99: Invariant mass spectra in East-East extracted by the WIS group for the 10–40% centrality class

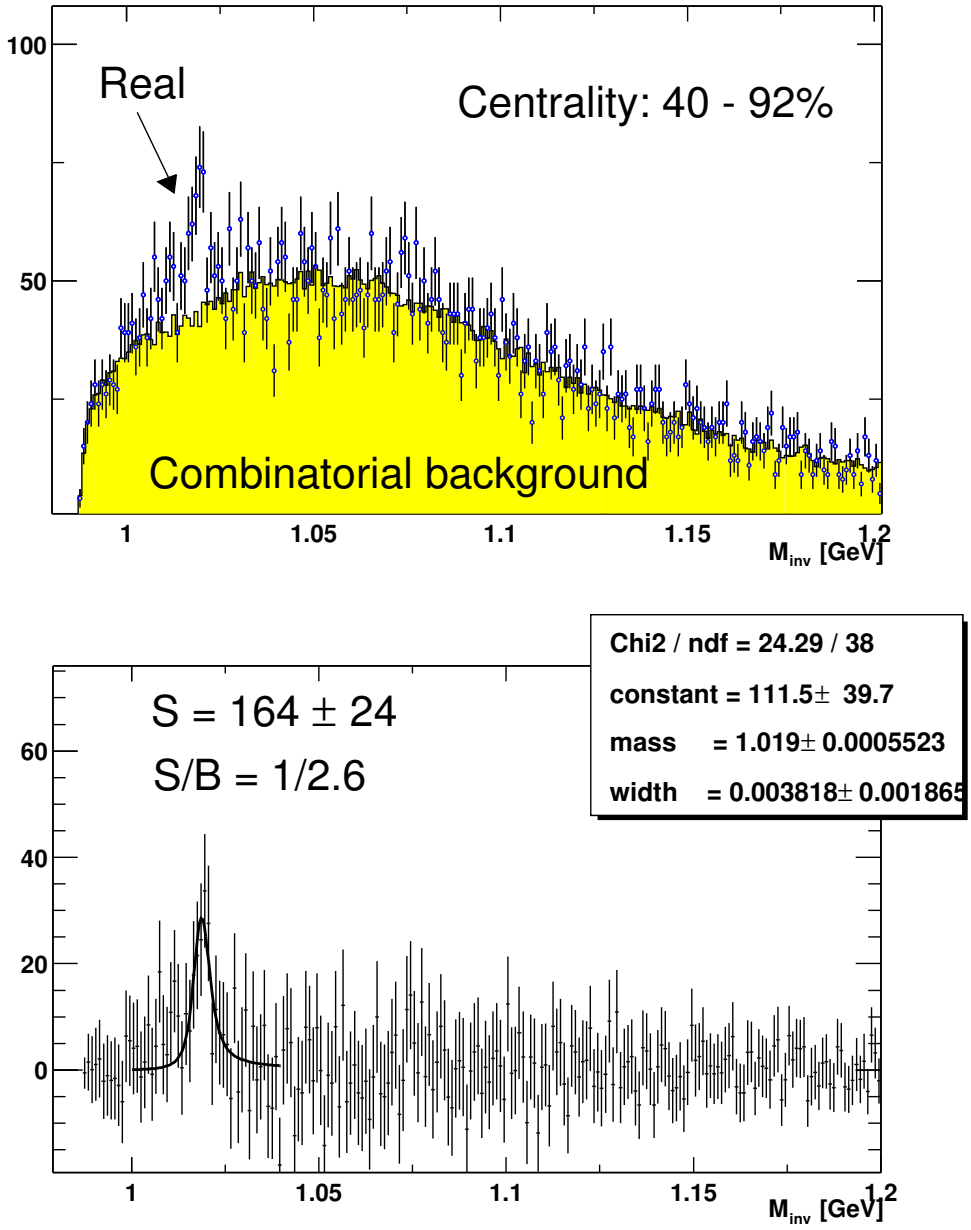

Figure 100: Invariant mass spectra in East-East extracted by the WIS group for the 40–92% centrality class

J Systematic Effects for the Yield and Temperature Extraction

J.1 Effect of the Signal Extraction Window on Yield and the Inverse Slope Parameter

We have extracted ϕ signal and background within the mass window of $1.014 < M_{k^+K^-} < 1.024$ GeV/c^2, where $M_{k^+K^-}$ is the pair invariant mass. Let us look at different signal extraction window and find how it affects the dN/dy and T. We use $1.004 < M_{k^+K^-} < 1.034$ GeV/c^2 and $1.009 < M_{k^+K^-} < 1.029$ GeV/c^2 in addition to our selected window $1.014 < M_{k^+K^-} < 1.024$ GeV/c^2. We tabulate the ϕ signal, background and the simulated ϕ within the specified windows for three different centralities in Tables 19-21:

m_T GeV/c^2	$\pm$5 MeV Window $1.014 < M < 1.024$			$\pm$10 MeV Window $1.009 < M < 1.029$			$\pm$15 MeV Window $1.004 < M < 1.034$		
	Sig	Bkg	MC	Sig	Bkg	MC	Sig	Bkg	MC
1.2 - 1.6	43.25	531.75	310	55.50	1111.50	366	50.21	1665.8	384
1.6 - 1.8	22.46	668.55	419	21.60	1389.40	498	14.14	2053.86	519
1.8 - 2.0	74.90	747.10	555	76.25	1572.75	666	87.58	2306.42	697
2.0 - 2.2	46.43	703.57	580	66.92	1446.08	693	63.055	2104.95	727
2.2 - 2.4	20.43	537.57	435	64.53	1114.47	513	85.21	1625.79	537
2.4 - 2.6	37.38	379.62	298	23.56	780.45	342	10.57	1141.43	359
2.6 - 2.8	40.97	249.03	217	55.81	516.19	246	55.45	755.55	258
2.8 - 3.0	45.11	157.89	145	71.29	328.71	181	79.97	477.03	190
3.0 - 4.0	67.56	212.44	213	74.95	433.05	246	54.30	635.70	258

Table 19: ϕ signal, background and simulated ϕ in $\pm$5MeV,$\pm$10MeV and $\pm$15MeV pair invariant mass window for 0%-10% events

J.2 m_T Spectra for Different Window

The transverse mass spectra of ϕ for $1.014 < M < 1.024$ is shown before. We here show the m_T spectra of ϕ for $\pm$10 MeV and $\pm$15 MeV windows in Fig. 101 through Fig. 106. We also summarize the dN/dy and T extracted for different mass windows and centralities in Table 22. From Table 22 we see that the dN/dy and T are consistent with each other for different mass windows.

J.3 Effect of Fitting Function on the Yield

One component of the systematic error of dN/dy comes from the choice of the fitting function of the transverse mass spectra. To see the effect of the fitting function on the yield, we fit with

m_T GeV/c^2	±5 MeV Window $1.014 < M < 1.024$			±10 MeV Window $1.009 < M < 1.029$			±15 MeV Window $1.004 < M < 1.034$		
	Sig	Bkg	MC	Sig	Bkg	MC	Sig	Bkg	MC
1.2 - 1.6	36.71	478.29	310	54.25	997.75	366	61.52	1502.48	384
1.6 - 1.8	57.82	617.18	419	50.84	1278.16	498	62.89	1876.11	519
1.8 - 2.0	104.82	691.18	555	124.60	1441.40	666	110.48	2113.52	697
2.0 - 2.2	134.68	630.32	580	138.46	1318.54	693	128.67	1921.33	727
2.2 - 2.4	122.70	498.31	435	118.57	1029.43	513	115.89	1496.11	537
2.4 - 2.6	124.96	341.04	298	132.81	706.20	342	118.33	1039.67	359
2.6 - 2.8	76.59	218.41	217	97.51	458.49	246	120.38	669.62	258
2.8 - 3.0	64.57	140.43	145	89.50	296.50	181	106.98	438.07	190
3.0 - 4.0	113.98	185.02	213	137.07	381.94	246	152.99	567.02	258

Table 20: ϕ signal, background and simulated ϕ in ±5MeV,±10MeV and ±15MeV pair invariant mass window for 10%-40% events

m_T GeV/c^2	±5 MeV Window $1.014 < M < 1.024$			±10 MeV Window $1.009 < M < 1.029$			±15 MeV Window $1.004 < M < 1.034$		
	Sig	Bkg	MC	Sig	Bkg	MC	Sig	Bkg	MC
1.2 - 1.6	11.85	33.15	310	14.66	71.34	366	7.65	108.35	384
1.6 - 1.8	10.66	43.34	419	11.79	88.21	498	9.02	126.98	519
1.8 - 2.0	26.89	42.11	555	28.80	89.20	666	34.28	131.72	697
2.0 - 2.2	38.29	38.71	580	55.81	79.19	693	61.16	117.84	727
2.2 - 2.4	37.60	29.40	435	42.08	58.92	513	36.02	86.98	537
2.4 - 2.6	21.44	20.56	298	32.41	40.59	342	40.13	57.87	359
2.6 - 2.8	13.70	12.30	217	16.28	24.72	246	18.87	37.13	258
2.8 - 3.0	15.80	8.20	145	17.19	16.81	181	24.99	24.01	190
3.0 - 4.0	28.99	11.01	213	44.21	21.79	246	51.55	31.45	258

Table 21: ϕ signal, background and simulated ϕ in ±5MeV,±10MeV and ±15MeV pair invariant mass window for 40%-92% events

cent	dN/dy			T (MeV)		
	W_1	W_2	W_3	W_1	W_2	W_3
0%-10%	2.354±1.16	2.776±1.41	3.051±1.8	452±78	437±75	404±77
10%-40%	1.777±0.37	1.555±0.40	1.415±0.42	411±29	428±37	446±45
40%-92%	0.229±0.06	0.223±0.06	0.209±0.06	408±40	430±45	456±50

Table 22: ϕ yield and inverse slope parameter for ±5MeV,±10MeV and ±15MeV pair invariant mass window for different centralities. W_1 on the table represents ±5MeV window, W_2 represents ±10MeV window and W_3 represents ±15MeV window,

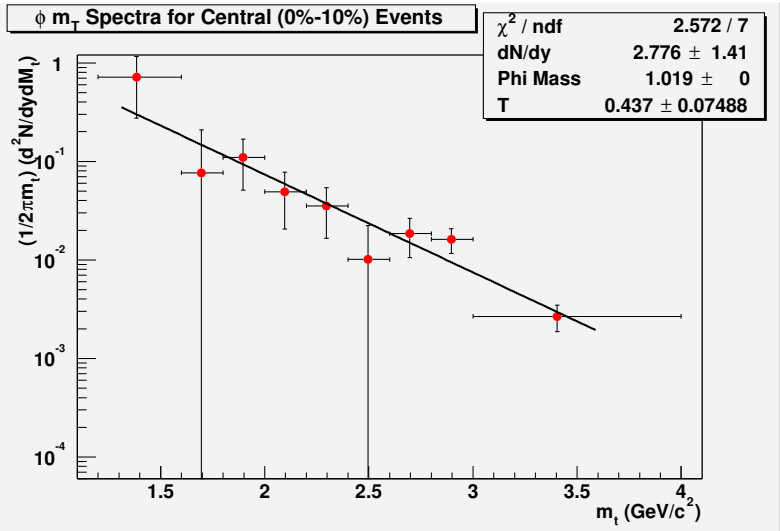

Figure 101: Transverse mass spectra of ϕ for $1.009 < M_{K^+K^-} < 1.029$ ($\pm$10 MeV window) for 0%-10% centrality events

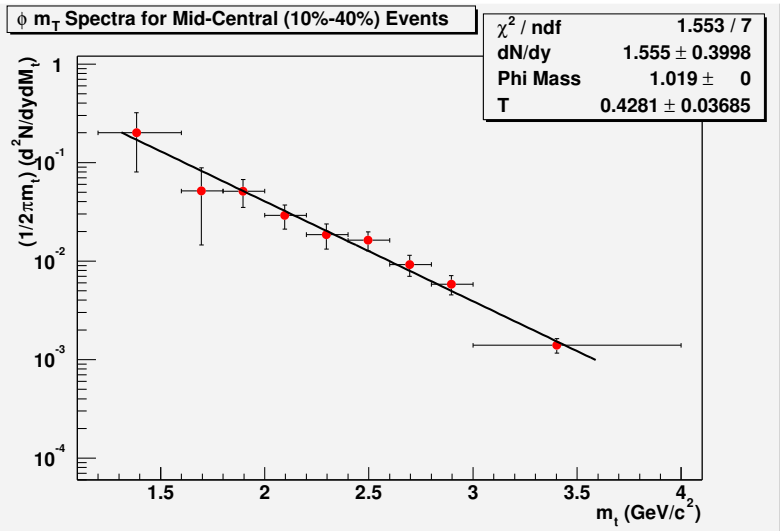

Figure 102: Transverse mass spectra of ϕ for $1.009 < M_{K^+K^-} < 1.029$ ($\pm$10 MeV window) for 10%-40% centrality events

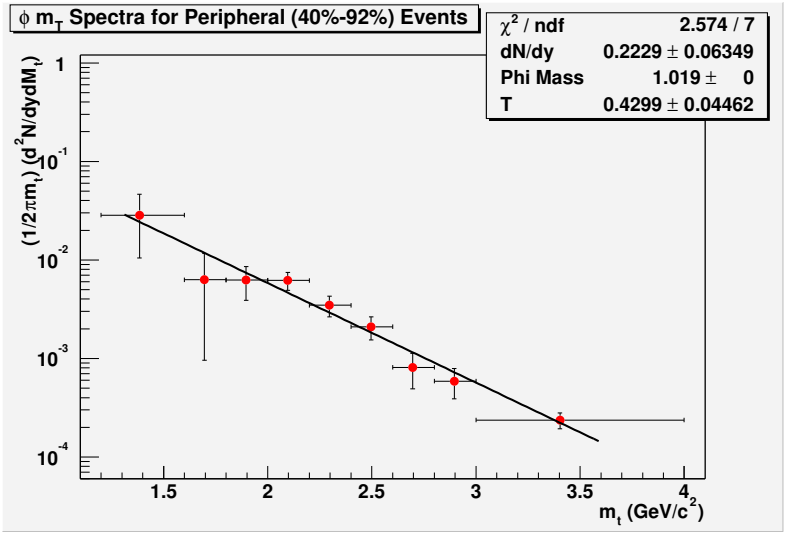

Figure 103: Transverse mass spectra of ϕ for $1.009 < M_{K^+K^-} < 1.029$ ($\pm$10 MeV window) for 40%-92% centrality events

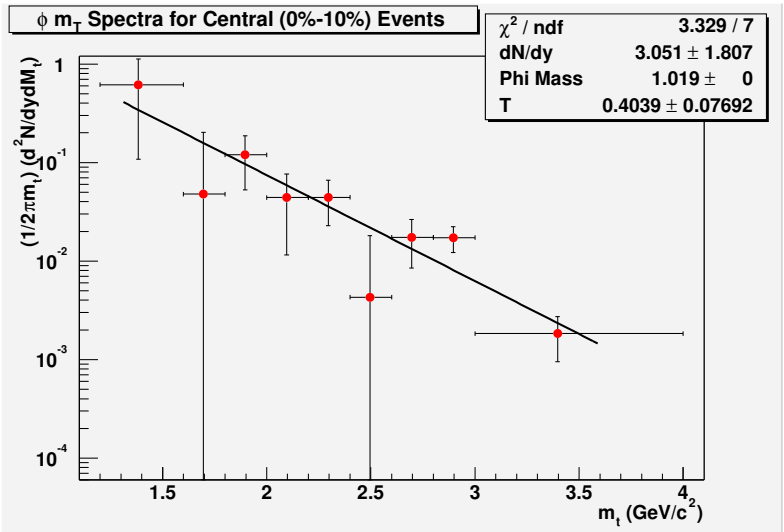

Figure 104: Transverse mass spectra of ϕ for $1.009 < M_{K^+K^-} < 1.029$ ($\pm$15 MeV window) for 0%-10% centrality events

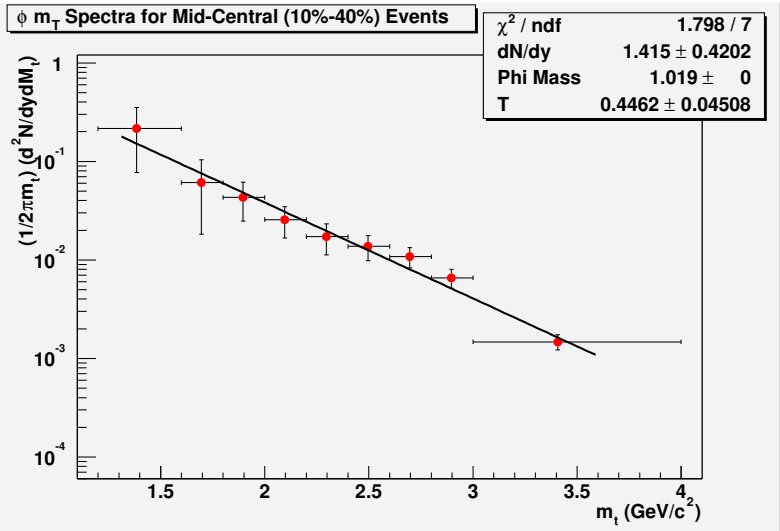

Figure 105: Transverse mass spectra of ϕ for $1.009 < M_{K^+K^-} < 1.029$ ($\pm$15 MeV window) for 10%-40% centrality events

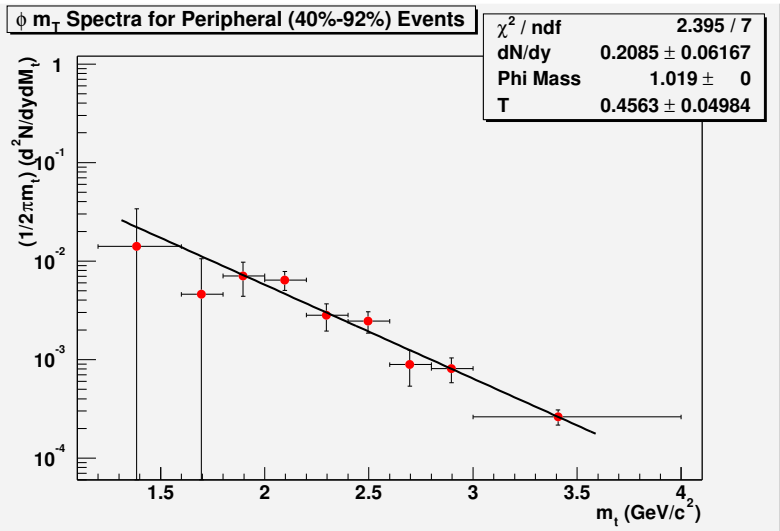

Figure 106: Transverse mass spectra of ϕ for $1.009 < M_{K^+K^-} < 1.029$ ($\pm$15 MeV window) for 40%-92% centrality events

a Boltzmann finction. The yield for different centralities extracted from an exponential fit and the Boltzmann fit is shown in Table 23. The yield as a function of the number of participants is shown in Fig (107). The red circles are from the exponential and the blue circles are from the Boltzmann fit. The blue points are shifted to right for better viewing.

Centrality	dN/dy from Exponential	dN/dy from Boltzmann
0%-10%	2.354±1.16	2.503±1.38
10%-40%	1.777±0.371	1.959±0.455
40%-92%	0.229±0.0623	0.254±0.0775

Table 23: ϕ yield extracted with an exponential and a Boltzmann functionfor different centralities.

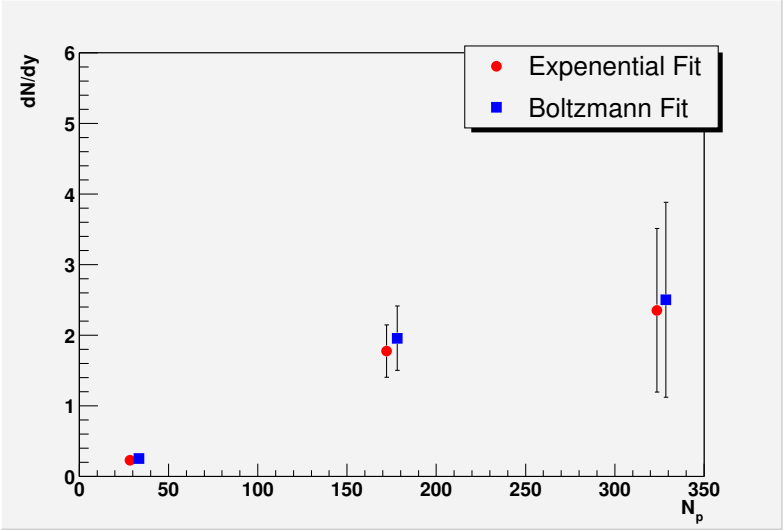

Figure 107: ϕ as a function of number of participants

The systematic errors fitting function are 6% for 0-10% events, 10% for 10-40% events and 11% for 40-92% events.